Chemical Tools for the Control of Biological Systems

Thesis by

John Bryce Jarman

In Partial Fulfillment of the Requirements for the degree of

Doctor of Philosophy

CALIFORNIA INSTITUTE OF TECHNOLOGY

Pasadena, California

2019

(Defended May 30th, 2019)

John Bryce Jarman
ORCID: 0000-0002-7581-686X

For my family.

ACKNOWLEDGEMENTS

Although rife with challenge, my time at Caltech has given me immense opportunities to grow, and for that I will always be appreciative. Dennis Dougherty, I would like to thank you for the opportunity to work in your lab, where you let me design and drive my own projects. I truly appreciate the academic freedom I was given in my time at Caltech. Although, my success rate left something to be desired, in many ways each failure was more informative than a success. I may not have been the best scientist at Caltech, I believe that what I take with me will allow me to be a great scientist going forward. I will leave your lab with as much passion for science as when I entered, something that speaks to your innate curiosity. I hope I can keep this curiosity going for the rest of my life. Ellen Dougherty, I would like to thank you for being such a gracious host and supporting all of us graduate students behind the scenes.

I would like to thank my thesis committee, Peter Dervan, Shu-ou Shan, and Bob Grubbs, for taking the time to explore my science with me. Peter, you give the best introductions; it is always a pleasure to see you on stage hosting a seminar. Shu-ou, your enzyme kinetics class was phenomenal; you are an inspiration when it comes to dissecting biological phenomena at a chemical level. Bob, it has been a pleasure working with you, Dan Schwartz, and Chris Marotta on the myopia project. Although I may be up at Stanford going forward, I hope to remain involved in any way that I can.

To lab mates current and former: you have all been fantastic. I don't think I can do justice with a few words to all the wonderful experiences I have had, but I will try. Ethan Van Arnam, Kristina Daeffler, Ximena da Silva, and Kayla Busby, although our overlap may have been limited, the culture y'all developed in this lab is a big reason why I wanted to join in the first place. Tim Miles, thank you for leaving me with a low key disaster of a project. Joking side, it was a great way to get into the Dougherty lab and think about what we do, and I really appreciate all the ground work you did with the nuclear receptors project. Noah Duffy, it's been awesome having you as a labmate and then as a friend around Pasadena. Wine Wednesday was not always the best idea, but I am glad we were in it together. Betty Wong, I will be honest when I say that we did not see eye to eye on many things, but you have a tenacity

that I respect immensely. Michael Post, the precipitous drop in drinking games after you left the lab is a travesty that I will never have closure for. In all honesty though, I really appreciated the work life balance you brought to the lab; you made it a great community for all. Matt Rienzo, I enjoyed working in lab with you. If I have to be honest, we had some bad ideas. But we also had some good ones, and working alongside you in lab made the experience that much more enjoyable. I am also grateful for the time we spent together outside of lab. Matt Davis, it was awesome teaching Chem 144 with you multiple times, and would jump at the chance to do it again.

Clint Regan, you are honestly so much fun to talk to. I never felt quite as scientifically free as talking to you at one in the morning about a random photochemistry question or some biochemistry technique. You ultimately sent me down the photochemistry route that made me into the scientist I am today, and I am extremely grateful for your company in lab. Oliver Shafaat, your love for lasers was bound to pass on to someone else in the group, and I am lucky that it was me. Spending time down at the laser table, tinkering with the system to get everything working for the SOSDF project was such a gratifying experience, as was getting to know you better along the way. Chris Marotta, I am grateful for the opportunity to work with you, Bob Grubbs, and Dan Schwartz on the myopia project. It is an incredibly challenging problem, and one that I hope to stay involved with as I move to the bay area. You are a great person to work with and a better person to be around.

Paul Walton, desk mate and friend. I appreciate you in so many ways, and meeting you was one of the greatest boons of Caltech, both on a scientific and personal level. Annet Blom, we had quite the adventure together, more or less start to finish. Starting with tough projects that signified difficult roads ahead, we pulled through on nothing but grit. They say misery loves company, but that in no way accounts for how much I have enjoyed yours. Richard Mosesso, you are a righteous dude. It has been a pleasure being with you in lab, getting swole together, and exploring Studio City. I am ecstatic that I will be seeing more of you up north. Lena Parker-Duncan, thank you for joining in festivities when the opportunity arose. Steve Grant, I appreciate your musical taste, fast driving, and extreme dedication. You give your

all to whatever you do, and I think that is such an admirable trait. I know you will find your own way, but never hesitate to reach out as you continue your scientific journey. Catriona Blunt, best of luck in the world of consulting. I am sure you will put your scientific background to good use; we need analytical, forward thinking people in the business world.

I would like to thank my friends outside the lab. Too many people to count have kept me sane during long weekends working in Pasadena and short getaways to San Diego and San Francisco, but I want to thank Ada Li and Max Trejo in particular for facilitating my adventures in the Bay Area. My two best friends from undergrad, their support has meant a lot to me throughout the years. Also, a very special thanks to Samuel Ho, a member of the Tirrell lab with whom I regularly explored the San Gabriel Valley in search of outstanding Asian food. I am grateful that I have gotten to know you here over the years, and even teach a Chemistry 101 class with you. I look forward to seeing you back in the bay. Also, I hate to anthropomorphize a whole state, but California you have been wonderful.

I would like to thank Allie Obermeyer and Matt Francis, who helped me to start my academic journey in the Francis group at U.C. Berkeley (also, special shout out to all the Francis group alumni who made the lab such a great place to learn science). Allie, I am truly in awe of you as a scientist, and although I have a lot to work on to live up to the example you set, the support you gave me in undergrad kept me going at times when I felt like failure was inevitable here at Caltech.

There are also quite a few people that keep Caltech running that I would like to thank. Mona Shahgholi it has been a pleasure working with you in the mass spectrometry here at Caltech. You run a fantastic facility, and your knowledge of mass spectrometry and general interest in science are inspiring. Dave VanderVelde, the NMR facility is integral to the success of so many students here at Caltech, and the opportunities provided by the lab have undoubtedly made my time here easier. Jay Winkler, BILRC is a fantastic resource and I really appreciate the opportunities I have had to work with all the laser setups that the facility provides. Scott Virgil, you are a unparalleled resource here on campus, and I appreciate the times you stopped to talk with me about synthetic issues I was facing. Linda Syme, thank you for

helping me to wrangle Dennis and Bob on multiple occasions, no easy task. Camilo Toribio, thank you for taking care of the lab space; you make sure this older building doesn't show its age.

Finally, I would like to thank my family. I could write for pages and never do them justice, so instead I will be brief. My mom, dad, and sister have been extremely supportive throughout this journey. They have given me the opportunity to explore science without fear of failure, and I recognize how lucky I am to have that. This journey would have been nigh impossible without you all around. I am excited to see where my journey takes me, knowing I have your support.

ABSTRACT

This dissertation describes attempts to develop new methodology in the Dougherty lab, ultimately focused on controlling biological systems. It is split between two fields of study. The first is exploring new ways to utilize noncanonical amino acids. The second is development of new photochemistry based on NIR chromophores.

The first chapter describes attempts to use noncanonical amino acids to study nuclear receptors in *Xenopus laevis* oocytes. Nuclear receptors are vital to cell regulation, however, due to a lack of structural information, are still poorly understood. Structure-function studies, similar to those performed in ligand-gated ion channels in the Dougherty lab, would provide significant insight into the function of these proteins. Methodology was developed for analyzing the activity of a specific nuclear receptor, the retinoic acid receptor, based on a quantitative reverse transcriptase polymerase chain reaction.

The second chapter discusses attempts to introduce noncanonical amino acids into mammalian cells using the chemical acylation methodology. Successful incorporation of noncanonicals would allow ion channels to be evaluated in their native environment, expanding on the work previously done by the Dougherty lab. A number of different transfection methods were explored, as well as ways to increase tRNA stability post transfection.

The third chapter bridges the gap between chemical biology and photochemistry, and focuses on the exploration of singlet oxygen-sensitized delayed fluorescence (SOSDF) as a potential tool for visualizing biological systems. An experimental set-up was devised for evaluating the weak fluorescence produced by SOSDF and a number of SOSDF systems were characterized. The effect of sensitizer and emitter concentrations on SOSDF were evaluated, both as a function of fluorescence intensity and lifetime. Progress towards the practical application of SOSDF is described.

The fourth chapter focuses on the development of phenothiazine derivatives for use as NIR singlet oxygen generators and photoremovable protecting groups. A range of derivatives were characterized, and their applications explored. An updated series of singlet oxygen-sensitize protecting groups based on the

anthracene backbone are also described, as is their attempted introduction into a phenothiazine derivative.

The fifth chapter describes the development of long wavelength triplet sensitizers based on heptamethine dyes. These sensitizers provide access to the triplet state and consequently singlet oxygen at NIR wavelengths, making them a valuable addition to the limited NIR photochemistry tool set. The synthesis and analysis of these dyes is discussed, as is their application for the generation of singlet oxygen.

PUBLISHED CONTENT AND CONTRIBUTIONS

Jarman, J.B. et al. (2019). "Charge-transfer heptamethine dyes for NIR singlet oxygen generation". In : Chemical Communications, 55, pp 5511-5517. doi:10.1039/C9CC01096C

J.B.J. Conceived of project, collected data, and helped write manuscript.

TABLE OF CONTENTS

LIST OF FIGURES

Chapter 1: Exploration of the Use of Noncanonical Amino Acids to Study Nuclear Receptors in the *Xenopus laevis* Oocyte Model System

Chapter 2: Further Work on the Use of Chemical Acylation for Noncanonical Amino Acid Mutagenesis in Mammalian Cells

Chapter 3: Exploration of Singlet Oxygen-Mediated Upconversion as an Upconversion Phenomenon with Potential Applications in Biological Systems

Chapter 4: Exploration of Phenothiazine Derivatives as Singlet Oxygen-Mediated Photoremovable Protecting Groups

Chapter 5: Development of Heptamethine-Based Charge-Transfer Dyes for Long-Wavelength (NIR I/II) Photochemistry

Chapter 1: Exploration of the Use of Noncanonical Amino Acids to Study Nuclear Receptors in the *Xenopus laevis* oocyte Model System

1.1 Abstract

The *Xenopus laevis* model system has been used extensively in the Dougherty lab to study ion channels containing noncanonical amino acids. Introduced via a chemical acylation methodology, these noncanonical amino acids have provided a mechanistic understanding of ion channel function, generating insights that transcend the static world of crystallography. Despite the utility of this technique, it has found little use beyond ion channels, as the method requires a stoichiometric amount of tRNA for protein production. Practically, this means that only systems with significant signal amplification – such as ion channels – can be observed. In an attempt to expand this technique to a new set of proteins, another system with significant signal amplification was explored: nuclear receptors. This class of proteins is responsible for transcriptional regulation, meaning that mRNA levels within a cell can be correlated with the function of a nuclear receptor. Although transcriptional activation itself does not provide enough signal amplification to explore the mechanistic subtleties introduced by noncanonical amino acid mutagenesis, the mRNA can be amplified and quantified using a reverse transcriptase quantitative polymerase chain reaction (RT-qPCR). Described herein are initial attempts at using *Xenopus laevis* oocytes, noncanonical amino acids, and RT-qPCR to explore transcriptional activation in the nuclear receptor RARα, as well as subsequent attempts made in HEK-293T cells.

1.2 Introduction

1.2.1 Noncanonical Amino Acids

Life has achieved incredible biochemical diversity based on a simple suite of 20 amino acids. Although these building blocks have proven a sufficient basis for the complexity of the world around us, they are still lacking in the eyes of the modern chemist. The discovery of selenocysteine in the early 1970s[1] suggested that the proteinogenic code was not as strict as originally thought, and by 1989 the first noncanonical amino acid had been incorporated into a protein *in vitro*.[2] Schultz contributed heavily to this field, rapidly developing an array of noncanonical amino acids. By 1995, the first unnatural amino acid had been incorporated into a protein expressed in a vertebrate cell via a collaboration between the Schultz,

Lester, and Dougherty labs.[3] Since this time, three methods for the incorporation of unnatural amino acids have become predominant, each with their own strengths and weaknesses.

Noncanonical amino acid incorporation can be broken down into two different types: residue-specific and site-specific. In residue-specific noncanonical amino acid incorporation, a residue is exchanged for a noncanonical counterpart throughout the cell; for instance, a methionine could be exchanged for an azidohomoalanine (Figure 1).[4,5] This does not mean that each methionine in a cell would be an azidohomoalanine, but rather each methionine could be an azidohomoalanine. In the most basic systems, this is done by taking an auxotrophic organism and depriving it of an essential amino acid. As protein synthesis continues, the pool of tRNA acylated with the essential amino acid is depleted, leaving unacylated tRNA and halting protein synthesis.[4] At this point, a noncanonical amino acid is introduced, which the cell uses to charge unacylated tRNA using the standard cellular machinery.[4] Without additional mutagenesis, only noncanonical amino acids that closely resemble a canonical amino acid can be used. Despite this limitation, a variety of functional amino acids have been introduced, enabling a wide array of proteomic studies and protein-based materials.[6] This technique has also found use in crystallography labs, where cysteine is exchanged for selenocysteine, enabling easier crystallographic analysis.[7]

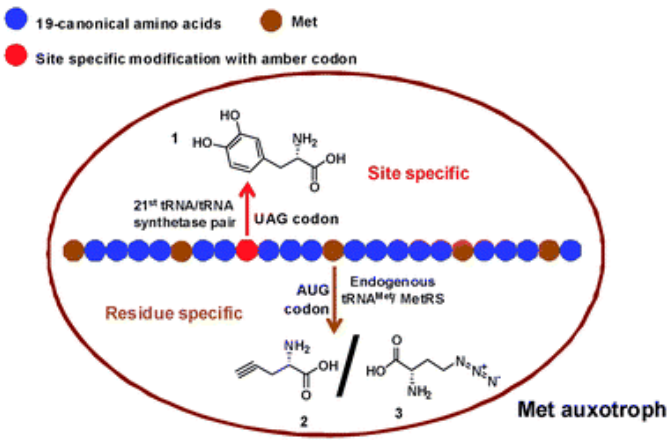

Figure 1: Comparison of residue specific and site specific incorporation. Adapted from Yun et al.[5]

In site-specific noncanonical amino acid incorporation, a specific residue in a specific protein is substituted for a noncanonical residue, one which is not limited by homology (Figure 1).[5,8] To achieve this, a tRNA is developed that recognizes a codon that is orthogonal to the host organism's translation system. Typically, these tRNA are evolved from those found in organisms that encode greater than 20 amino acids. They often recognize stop codons such as TAG, and, to ensure orthogonality, are evolved

to be incompatible with tRNA synthetases endogenous to the host organism.[8] These tRNAs can be charged in two different manners. The first, known as enzymatic acylation, relies on the development of tRNA synthetases capable of enzymatically acylating tRNA with novel amino acid substrates.[8] These synthetases must be completely orthogonal to the organism they are introduced into and require significant effort to evolve. Once generated, however, they are extremely robust and capable of producing high protein yields. This methodology leads to efficient site-specific incorporation of noncanonical amino acids, but is ultimately somewhat restricted in substrate scope due to limitations on synthetase orthogonality and enzymatic evolution. Enzymatic acylation has found widespread use, from basic biochemistry to protein-drug conjugates.[9]

Chemical acylation exists as a foil to enzymatic acylation; it gives nearly limitless flexibility in terms of the amino acid incorporated, but requires a stoichiometric amount of tRNA for protein production, resulting in low yields.[10] In chemical acylation, the amino acid of interest is attached through a set of synthetic steps that culminate in the ligation of a truncated tRNA to an oligonucleotide containing an amino acid of interest.[10] This tRNA is then introduced into a host system, where it can interact with an orthogonal codon in the same way an enzymatically labeled tRNA would. Despite the wide range of noncanonical amino acids that can be accessed with the methodology, chemical acylation has found much more limited use than the aforementioned methods, primarily being used *in vitro* and in the study of ion channels in *Xenopus laevis* oocytes.[10]

Starting with the incorporation of phenylalanine and tyrosine derivatives in the muscle type nicotinic acetylcholine receptor in 1995, the Dougherty lab has used the *Xenopus laevis* model system to perform extensive chemical scale analyses on ligand-gated ion channels (Figure 2), a class of proteins that lend themselves to the chemical acylation methodology due to the signal amplification they provide. A single ion channel controls the flow of millions of ions, allowing even small amounts of protein to be observed through electrophysiology.[10] In two decades of electrophysiology, a number of binding interactions have

been probed and a vast array of noncanonical amino acids have been incorporated. Especially unique are alcohol analogs of amino acids, residues that cannot be done with any other methodology (Figure 3).[10] Ideally, it would be possible to expand the strengths of the chemical acylation methodology to a different set of proteins or a different model system all together. One particularly interesting set of proteins are transcription factors.

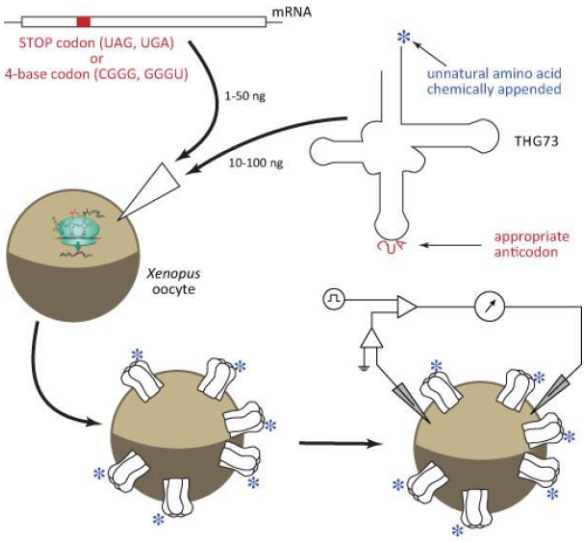

Figure 2: Methodology for chemical scale analysis of ligand-gated ion channels. Adapted from Dougherty et al.[10]

Transcription factors, are proteins that regulates a cell's response to stimuli by controlling the process of RNA generation. By producing multiple transcripts of RNA, a single transcription factor is capable of producing a substantial amplification event. Although significant, it is unlikely that this event alone would be capable of producing sufficient signal amplification for evaluation. However, RNA production can be paired with another amplification event, reverse transcriptase quantitative polymerase chain reaction (RT-qPCR). In RT-qPCR, primers are used to transcribe RNA to DNA using a reverse transcriptase. At this point, a set of

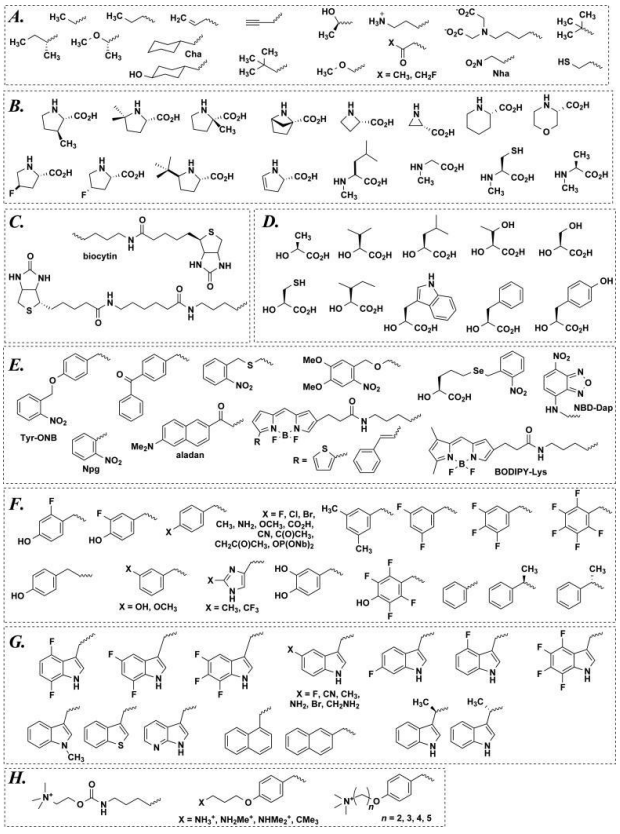

Figure 3: A selection of noncanonical amino acids incorporated by the chemical acylation method. Adapted from Dougherty et al.[10]

traditional PCR cycles is carried out, and a dye that intercalates DNA is incorporated to give a quantitative readout with regards to the amount of DNA that is produced (Figure 4).[11,12] By evaluating the number of cycles required to attain a certain fluorescence threshold, it is possible to determine the amount of RNA initially present. By combining these two types of amplification, it may be possible to observe changes in transcription factor activity mediated by chemically acylated tRNA.

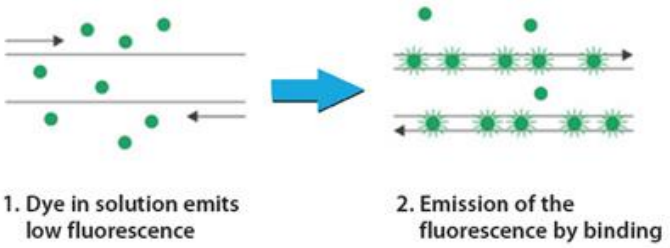

Figure 4: qPCR fluorescence readout. Adapted from Sigma Aldrich.[12]

Transcription factors are regulated by a number of processes, from ligand binding to post-translational modification. As our lab's previous research has focused heavily on binding interactions, we chose to focus initial studies on ligand-regulated transcription factors known as nuclear receptors.

1.2.2 Nuclear Receptors

Nuclear receptors are a specific subset of ligand gated transcription factors. With 48 unique nuclear receptors identified in humans, they play a prominent role in gene regulation.[13] They are responsible for the detection of sterols, fatty acids, and retinoids, and have been implicated in diverse physiological processes, from metabolism to immunity.[13,14] The family of nuclear receptors is defined by its conserved evolutionary template.[14] Each nuclear receptor has two domains – a ligand-binding domain and DNA-binding domain – linked by a flexible hinge region, as well as a functionally important N-terminal region.[13,14] Nuclear receptors are generally grouped into three classes: those that act as monomers, those that act as homodimers, and those that act as heterodimers with the retinoid X receptors.[13] A number of examples exist for all three classes, and some nuclear receptors have been shown to stimulate transcription in more than one manner.[13,14]

Each nuclear receptor binds to a unique six base DNA consensus sequence, and dimer pairs require specific distances between these individual consensus sequences.[13] The two consensus sequences along with the bases in between constitute a response element for a given heterodimer.[13] This rigid spatial

requirement suggests the otherwise flexible hinge region plays an integral role in controlling the relative orientation of the ligand-binding domain and the DNA-binding domain upon formation of a dimer.[13] In addition to the hinge region, it is thought that interactions with co-activators, of which there are over 150 for nuclear receptors, play a large role in controlling the relative positioning of the two DNA-binding domains.[13] These co-activators are thought to bind at one of two distinct sites: the activation function 1 surface (AF1) in the N-terminal region and the activation function 2 surface (AF2) in the ligand-binding domain.[13]

Given the complexity of transcriptional regulation in the nuclear receptor family, analysis of nuclear receptors – particularly the relationship between structure and function – has proven far from trivial.[14,15] Although the crystallization of nuclear receptors, particularly dimeric complexes, has provided some functional insight, structure based analyses are complicated by the high level of disorder intrinsic to many transcription factors.[15–18] This disorder is often associated with regions involved in transcriptional activation and complex formation, and thus poor crystallographic resolution is obtained in functionally interesting regions. Precise structure-function studies, which could be performed using noncanonical amino acids, would drastically improve current knowledge of nuclear receptor function. Of particular interest among these receptors are the retinoic acid receptors.

1.2.3 Retinoic Acid Receptors

In humans, there are three unique retinoic acid receptors (RARα, RARβ, and RARγ) and three unique retinoid X receptors (RXRα, RXRβ, and RXRγ).[19] Each of these receptors is encoded by a distinct gene, and a number of RAR/RXR dimers have been described.[19] These dimers regulate gene expression by recruiting transcriptional complexes to retinoic acid response elements (RAREs) in DNA, and have been implicated in cell cycle regulation.[19] The RARα/RXRα heterodimer is of particular interest due to the role RARα plays in promyelocytic leukemia, where a fusion protein consisting of domains from the promyelocytic leukemia protein and RARα has been shown to activate oncogenes.[19] This dimer has been

well characterized biochemically, however, only limited structural data exists.[20,21] As is common for transcription factors, significant portions of available structures – such as the N-terminal domain and hinge region – are not resolved.

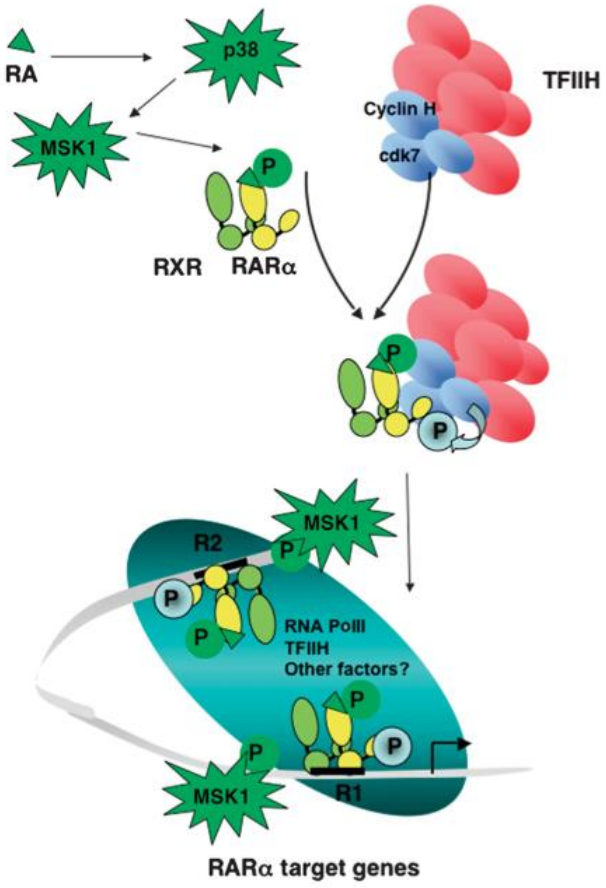

Figure 5: Proposed Activation Pathway for RARα/RXRα Heterodimer. Adapted from Rochette-Egly et al.[22]

It is believed that, in the absence of ligand, the RARα/RXRα dimer interacts with a corepressor complex that suppresses transcription at RAREs.[19] The binding of all-*trans* retinoic acid (ATRA) alters the activity of the heterodimer, increasing its affinity for coactivator proteins while decreasing its affinity for the corepressor complex.[19] This process of receptor activation involves a number of events (Figure 5). In addition to binding RARα, ATRA activates the p38MAPK signaling pathway.[22] This allows the kinase MSK1 to phosphorylate RARα at serine 369, a residue in the ligand binding domain adjacent to AF2.[22] Following this initial phosphorylation, a secondary phosphorylation – mediated by cyclin H and the kinase CDK7 – can occur at serine 77 (S77), a residue in the RARα N-terminal domain near AF1.[23] This second phosphorylation results in RARα activation, and leads to increased nuclear localization of the transcription factor.[23,24] The importance of phosphorylation at this site has been corroborated

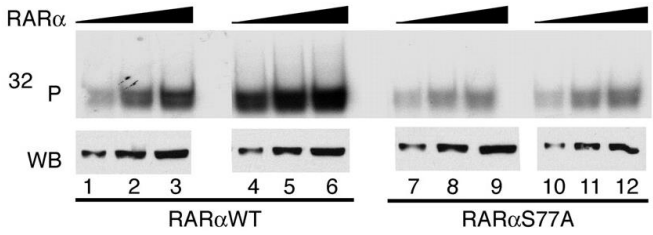

Figure 6: Differential DNA binding for WT and S77A RARα/RXRα heterodimers. Adapted from Rochette-Egly et al.[23]

through an alanine mutation (S77A), which greatly reduces the ability of RARα to bind DNA at RAREs (Figure 6).[23] How phosphorylation at S77 mediates binding is still unclear. One possibility is through interaction with the proceeding residue, proline 78 (p78), as a phosphorylated serine residue adjacent to a proline residue constitutes the minimum motif required for interaction with the phospho-directed prolyl isomerase Pin1.[25] Although a relationship between Pin1 mediated isomerization and transcriptional activation has yet to be established, isomerization at P78 is known to occur, and is well documented in another context.[26] It has previously been shown that degradation of RARα is dependent on both interaction with Pin1 and phosphorylation at S77, implying that isomerization occurs at P78 and is integral to degradation of the protein (Figure 7).[26]

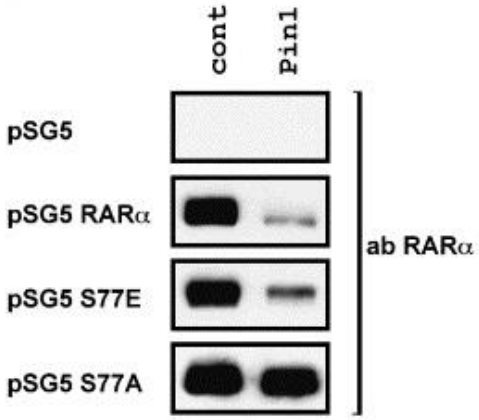

Figure 7: Regulation of RARα concentration by phosphorylation at serine 77. Adapted from Klimkait et al.[26]

1.2.4 Prolyl Isomerization and Pin1

Of the canonical amino acids, proline is the only residue to adopt a *cis* conformation to an appreciable extent (about five percent).[27] Although the *cis* conformation is heavily disfavored and spontaneous isomerization between the two forms is slow, prolyl isomerases make isomerization events relevant on a biological time scale.[27] In fact, prolyl isomerization has been shown to play a regulatory role in a number of biological systems.[27] Four structurally distinct classes of prolyl isomerases have been identified, three of which have similar substrate specificity.[27] The fourth, which includes Pin1 and Pin1 like enzymes, is unique in that members of the class are phosphorylation dependent: they catalyze prolyl isomerization for prolines adjacent to phosphorylated serine and threonine residues.[19] The other three classes are incapable of catalyzing such isomerizations.[27] Pin1 and similar enzymes are particularly important in regulation because of this orthogonal substrate scope.[27]

Of the Pin1 like enzymes, Pin1 is the most studied. Pin1 catalyzes both *trans-cis* and *cis-trans* isomerization, and therefore does not bias the conformational equilibrium; if the intrinsic *cis* bias is only

five percent, this will not be altered by the isomerase.[25] However, in the event that one isoform is depleted by biological activity, this rapid isomerization allows it to be replaced on a biologically relevant time scale.[25] Given that isomerization is often linked to subsequent events that preclude further isomerization – such as complex formation – this allows substrate to be funneled towards an active conformation.[25] It is worth noting that catalysis via Pin1 is significant; uncatalyzed isomerization of phosphorylated serine/threonine-proline bonds is significantly slower than other *cis-trans* isomerizations, essentially locking the backbone in place.[27]

Despite the prevalence of Pin1 mediated processes in biology, few assays exist for detecting Pin1 activity. Although in certain systems – such as Pin1 mediated degradation of RARα – there is a direct functional output, often times this is not the case.[26] For instance, in RARα mediated gene transcription, the effects of isomerization at proline 78 cannot easily be differentiated from the effects of phosphorylation at serine 77. In systems that lack a direct functional output, mutagenesis can be used to probe the importance of Pin1 isomerization, albeit a significant caveat limits the utility of the technique. Although prolyl mutation implies a lack of functional importance when protein activity is unaffected by mutation, the converse is not true. Proline can play an integral structural role independent of isomerization, therefore a lack of protein activity following prolyl mutation can not necessarily be attributed to a functionally important isomerization. This ambiguity greatly limits the utility of traditional mutagenesis, however, noncanonical amino acid mutagenesis can be used to differentiate between these scenarios.

Noncanonical amino acid mutagenesis offers a compelling means by which to explore Pin1 mediated isomerization, as noncanonical residues could be used to uncouple the roles of phosphorylation and isomerization at a given site. By incorporating proline analogs with a diverse range of *cis* preferences in a phosphorylation incompetent mutant, it would be possible to directly observe the effect of altered c*is-trans* biases on protein activity, and thus infer the importance of prolyl isomerization. In the case of the

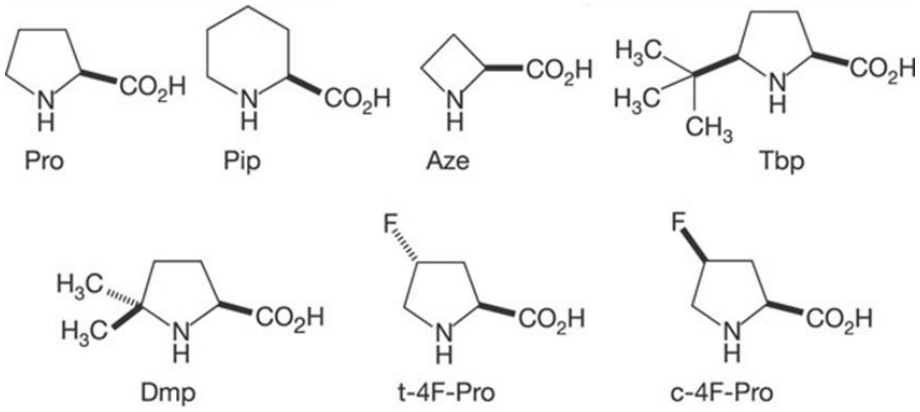

Residue	Per cent *cis**	EC_{50} (μM)†	$\Delta\Delta G(c\text{-}t)$ (kcal mol^{-1})‡	$\Delta\Delta G(EC_{50})$ (kcal mol^{-1})§
Pro	5	1.29 ± 0.07	0	0
Pip	12	0.75 ± 0.06	−0.54	−0.32
Aze	18	0.42 ± 0.03	−0.85	−0.66
Tbp	55	0.030 ± 0.024	−1.86	−1.73
Dmp	71	0.021 ± 0.009	−2.28	−2.47

Figure 8: Various Proline Analogs and their *Cis-Trans* Preferences. Adapted from Lummis et al.[30]

RARα/RXRα heterodimer, if *cis*-biased proline analogs could rescue transcriptional activity in a phosphorylation incompetent mutant (S77A), it would suggest that isomerization at P78 is crucial for activation.

Selection of a library of amino acids to probe the role of a proline requires significant thought. Of the 20 canonical amino acids, proline is the only residue with a secondary backbone amine. This additional nitrogen-carbon bond prevents hydrogen bond formation at the backbone amide, and thus has significant implications for secondary structure.[28] Additionally, the cyclic nature of proline introduces a number of steric constraints, which manifest as a significant *cis*-bias (about 5%).[29] Alpha hydroxyl acids, *N*-methyl alanine, and a number of proline analogs have all previously been used to explore the structural role of proline.[28] Among these, the proline analogs are of particular interest in cases where a *cis-trans* isomerization is predicted. These analogs exhibit a range of conformational preferences, as predicted by model peptides, and therefore can be used to probe isomerization (Figure 8).[30] For example, in the 5HT-3 receptor – a ligand gated ion channel whose natural agonist is serotonin – receptor activation scales as a function of

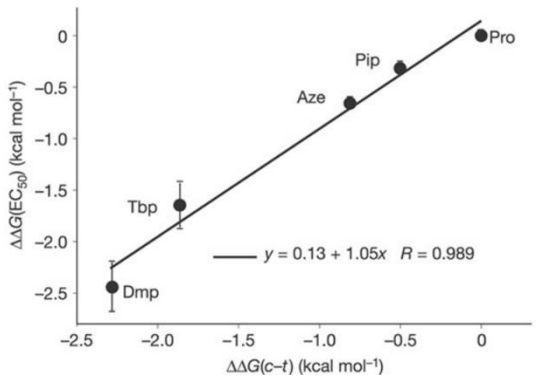

Figure 9: EC50 as a function of conformational preference. Adapted from Lummis et al.[30]

conformational preference at a specific proline (Figure 9), suggesting isomerization played a key role in channel activation.[30] Given the precedent set by this analysis, a similar set of residues was selected for studying the role of *cis-trans* isomerization in proline 78 of RARα. In this work, we discuss the development of an assay for analyzing nuclear receptors in *Xenopus laevis* oocytes using unnatural amino acids, with a focus on mutating serine 77 and proline 78.

1.3 Results and Discussion

1.3.1 Selection of an Appropriate Model System

To probe the nature of S77 and P78 in RARα using noncanonical amino acids, a new assay had to be developed to evaluate transcription in *Xenopus laevis* oocytes. Towards this end, former lab member Tim Miles obtained plasmids containing RARα and RXRα, as well as a previously described reporter plasmid containing a retinoic acid response element linked to a luciferase gene (RARE-Luc). This reporter plasmid was chosen for a number of reasons. First, the plasmid was designed with three retinoic acid response elements, ensuring selective expression only in the presence of active RARα/RXRα heterodimer (Figure 10). Second, the plasmid had previously been used in *Xenopus laevis* oocytes for a luciferase luminescence assay, making it a good starting point for experiments utilizing a qPCR readout.[31] Finally, in the event of issues with the RT-qPCR readout, the plasmid offered the possibility of a chemiluminescence read out.

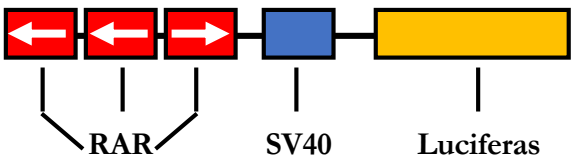

Figure 10: Cartoon representation of RARE-Luc. An SV40 promoter serves as the base promoter, with RAREs (one forward and two reverse, as denoted by the arrows) regulating the expression of luciferase.

Tim also designed luciferase specific primers for the qPCR readout and selected *Xenopus laevis* reference genes for the assay: glyceraldehyde 3-phosphate dehydrogenase (GAPDH) and ornithine decarboxylase (ODC). [32,33]

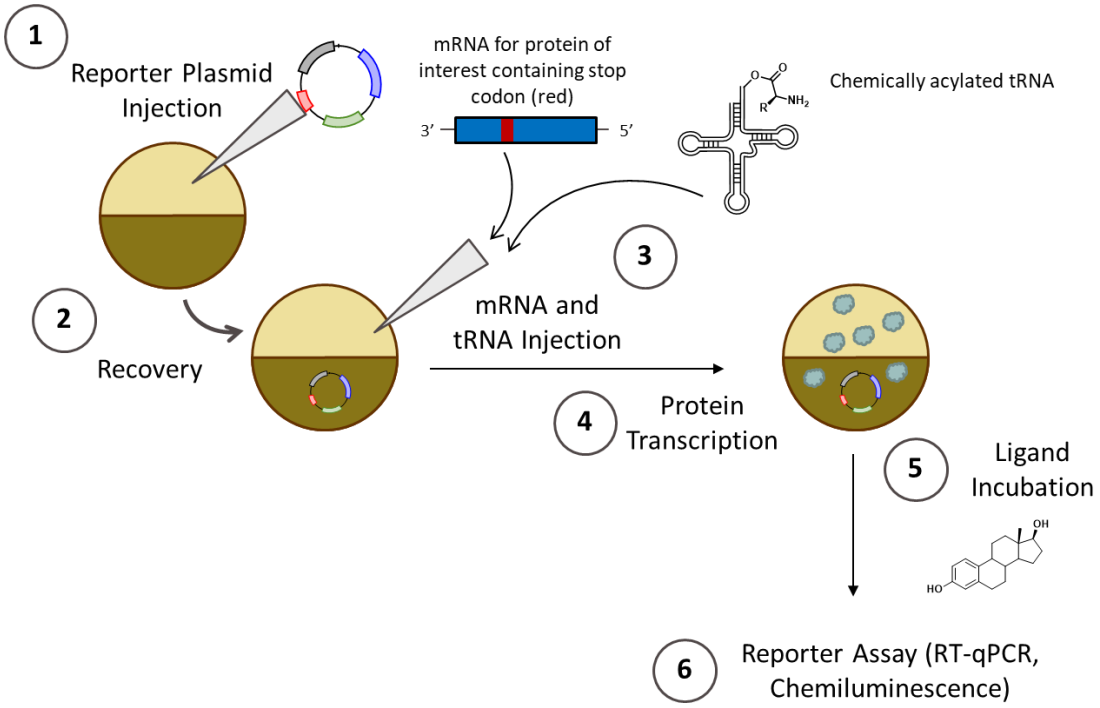

Figure 11: Experimental workflow in *Xenopus* oocytes.

To assay luciferase transcript production using native RARα, the following experiment was performed by Tim Miles.[34] Oocytes were injected internuclearly with the RARE-Luc reporter plasmid, given a 24-hour recovery period, and then injected cytoplasmically with RARα/RXRα mRNA. Following the second injection, cells were given another 24-hour recovery period to produce transcription factor, at which point they were incubated with or without all-trans retinoic acid (a transcriptional activator) overnight (Figure 11). Cells were then lysed and the RNA isolated for use in RT-qPCR experiments. The efficiency of transcript generation was evaluated by determining the number of cycles required to reach a specific fluorescence threshold (C_q). To account for differences in RNA production and isolation, this value was normalized against a reference gene to produce the value ΔC_q (where $\Delta C_q \equiv C_q$(Luciferase) – C_q(Reference Gene)).[32] Using this methodology, the results obtained in previous luciferase assays could not be reproduced. Signal was unaffected by incubation with all-trans retinoic acid (ATRA), as each set of oocytes had a similar fluorescence threshold when normalized against the reference gene. To probe the cause of the constant luciferase signal, an analogous experiment was run, but receptor mRNA (RARα/RXRα) was not injected. A similar result was obtained, suggesting that either endogenous RARα

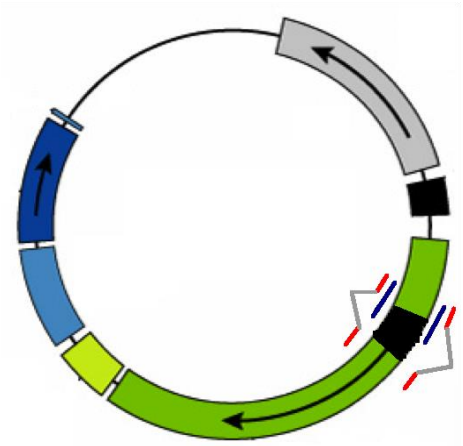

Figure 12: Intron containing gene and associated qPCR primers. The red primers will selectively bind to processed RNA.

activity was responsible for the observed signal or that isolated RNA was contaminated with plasmid DNA. To differentiate between these two possibilities, qPCR was performed on isolated RNA prior to reverse transcription. Since single stranded RNA would not be amplified, signal would only be observed if significant amounts of contaminating DNA were present. Although the reference gene (GAPDH) was not amplified in this control, luciferase was, demonstrating that background contamination of DNA was a significant issue. As a work around, Tim attempted to introduce native luciferase introns back into the luciferase gene (Figure 12). Ultimately he was able to introduce an intron (intron-3) back into the gene RARE-Luc construct, but was subsequently unable to produce an RT-qPCR signal.

Taking over from this point, I decided to reevaluate the RARα and RXRα constructs to ensure that the lack of signal was a result of the luciferase gene and not some other component of the assay. RARα expression was initially analyzed by western blot using a His-6 tag that was previously incorporated into the construct. No expression was observed, suggesting that RARα expression was at least as much of an issue as the RARE-Luc construct. To determine the source of expression issues, the RARα DNA and RNA were analyzed by gel electrophoresis. Observing no issue with the quality of either, the construct was sequenced again, and a mutation was found (P403Q). Restoring the mutant to wild type led to clean expression of the protein in oocytes (Figure 13).

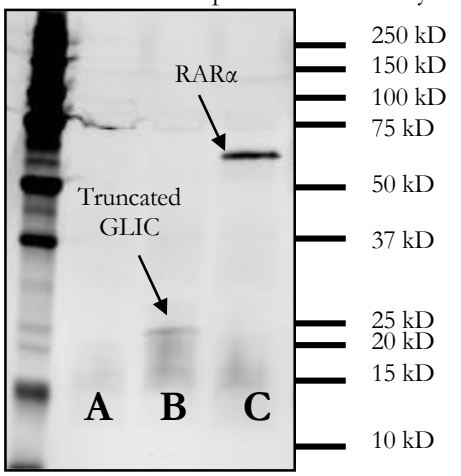

Figure 13: RARα expression blot. Lane A contains naïve oocytes (a negative control), lane B contains GLIC-expressing oocytes (a positive control) and lane C contains RARα expressing oocytes, which contain a mass which matches RARαs MW.

At this point, complete sequencing was performed for the RXRα and intron-3 RARE-Luc constructs to ensure there were no other issues with the plasmids obtained from Tim. Although the RXRα construct contained no mutations, the intron-3 RARE-Luc construct had multiple intron-3 insertions, rendering it useless. While new RARE-Luc intron constructs were generated using newly designed primers, the original assay was reevaluated using functional RARα.

The first experiments were designed to reproduce previous observations. This time, transcriptional activation was observed, although not to the extent previously reported using a luciferase assay (Figure 14).[31] After normalization to either of two reference genes, a $\Delta\Delta C_q$ of approximately 3.5 cycles was observed, a value which can be used to estimate a 10-fold shift in transcription (since each cycle leads to a doubling in the amount of DNA). Despite the success of this experiment, such a small cycle difference posed a significant issue for subsequent experiments. Since noncanonical RARα mutants are expected to express at significantly lower levels than wild-type RARα, the observed cycle difference would be expected to be even smaller for RARα mutants, essentially at the level of noise. To complicate matters further, the results obtained were inconsistent. Even when oocytes from the same batch of cells were compared, the ΔC_q values for the exact same experimental setup often varied by a couple of cycles. Comparisons between batches of oocytes were worse; ΔC_q values ranging from 2 to 7 were obtained.

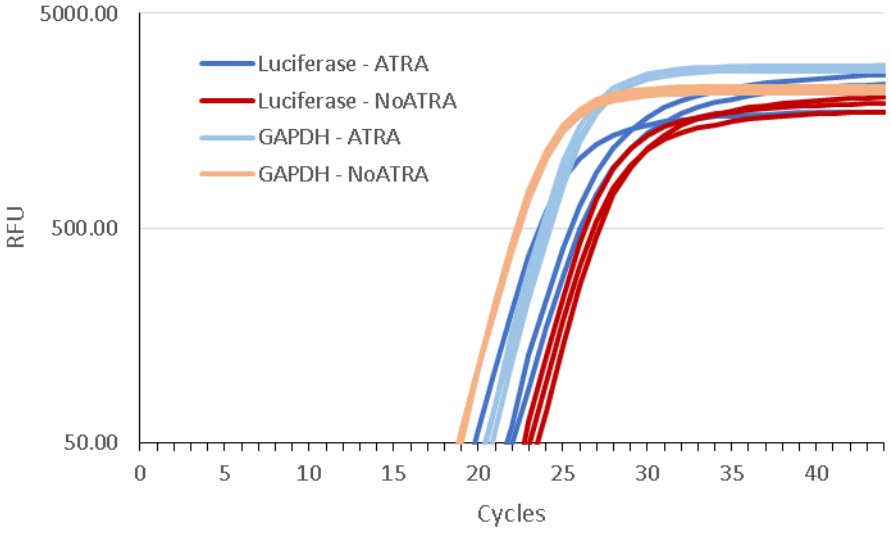

Figure 14: RARα expression and transcriptional activation in the presence of ATRA. RT-qPCR results demonstrating successful RARα expression and transcriptional activation in the presence of ATRA. Each condition was run in triplicate to obtain a more accurate ΔC_q.

Whether or not this was a characteristic inherent to the oocyte model system or the result of an unoptimized protocol was unclear. To differentiate between the two, a number of steps were taken to optimize the entire assay.

1.3.2 Assay Development

To frame discussions regarding optimization of the RT-qPCR assay, the protocol as it was originally performed will be described in greater depth.[34] To begin each experiment, the reporter plasmid was injected internuclearly, at which point the oocyte was given 24 hours to rest. RARα and RXRα mRNA was then injected cytoplasmically, and the oocyte given another 24 hours to produce the nuclear receptors. After this second 24-hour period, oocytes were incubated overnight in a blacked-out container, either in media containing ATRA or media containing the ATRA vehicle, DMSO. Following this incubation, the cells were lysed and the RNA isolated using a QIAGEN RNEasy kit. On column DNASE I digestion was performed to increase the purity of the isolated RNA. Upon elution of the sample, the quantity and quality of isolated RNA was analyzed by UV-Vis. The concentration of the sample as well as the ratio of the 260 nm absorbance to the 280 nm absorbance – a rough approximation of RNA purity known as the A260/280 – were then obtained.[35] If the concentration or A260/280 value was anomalously low, the sample was not subjected to further analysis.[35] Following UV-Vis characterization, isolated RNA was added to a solution containing a polythymine (poly-T) primer – which selectively reverse transcribes mRNA – and this solution was melted to ensure denaturation of any secondary structure that might interfere with polymerization.[34] Polymerization was then carried out, and DNA isolated from the reaction used to seed triplicate RT-qPCR reactions for each of the three genes evaluated (luciferase and the two reference genes). To facilitate later comparison to the intron-3 RARE-Luc plasmid, intron-3 spanning primers were used to evaluate luciferase expression.

Discussion of the parameters evaluated will be broken into three categories: injection conditions, purification conditions, and RT-qPCR parameters. Before this discussion, however, two aspects of the optimization experiments should be noted. First, the two reference genes – GAPDH and ODC – repeatedly gave analogous results while exploring the reproducibility of the system, therefore, GAPDH

was used exclusively for most of the optimization experiments to increase throughput. Second, creation of a genuine intron-3 RARE-Luc reporter plasmid proved difficult, thus most optimization experiments were run using the standard RARE-Luc reporter plasmid, before a genuine intron-3 reporter plasmid was generated.

Injection conditions were screened first, and since any increase in experimental throughput would allow for increased efficiency in screening other conditions, the requirement for two 24-hour rest periods was the first aspect of the assay to be evaluated. This was done by comparing oocytes injected on a single day to oocytes that were injected over two days. Results were similar between the two populations, suggesting that a single injection period could be used. Taking advantage of this higher throughput, a number of injection and incubation conditions were screened. Although altering the amount of injected reporter plasmid affected the amount of background observed – with high levels of reporter plasmid drowning out RARα mediated signal – no other parameter significantly affected $\Delta\Delta C_q$ values or the consistency of the results.

Given that different injection conditions seemed to have a negligible effect on the final results, RNA purification conditions were next screened (Table 1). The purpose of these screens was twofold. In a general sense, these screens were used to evaluate the ability of the A260/280 value to predict the quality of the qPCR outcome. The A260/280 value is often used as a rough measurement of nucleotide purity – with a DNA enriched sample giving a value near 1.8 and an RNA enriched sample giving a value near 2.0 – and therefore was used by a former group member as a way to predict and comment on the quality of the qPCR results.[35] However, given that a number of factors, such as pH and chemical contamination, can have significant effects on the A260/280 value, the degree to which such analysis was appropriate was unclear.[35] After screening a number of conditions, it became apparent that the A260/280 value was at best a binary assay. Although values below 1.90 gave poor qPCR results, values above could not effectively be distinguished in terms of clustering and absolute cycle number, suggesting that assigning significant stock in the assay was inappropriate. Beyond evaluation of the A260/280 value, conditions were screened in an attempt to reduce DNA contamination. Although some conditions, such as running

DNASE Used	First Purification	Second Purification	Relative A260/280	Change in qPCR
Roche	On column digestion	None	(2.03-2.10)	-
Roche	On column digestion	In solution digestion	Decreased	Not Noticeable
Roche	In solution digestion	None	Decreased	Poor Precision
Qiagen	On column digestion	None	Similar	Not noticeable
Qiagen	Column purification	In solution digestion	Decreased slightly	Not noticeable
Qiagen	Column Purification	On column Digestion	Decreased slightly	Absolute C_q altered, $\Delta\Delta C_q$ unchanged

Table 1: Screened purification conditions. An in solution digestion was always followed by a column purification to clean-up the sample.

two column purifications on the same sample, resulted in slightly improved DNA degradation, no method resulted in better $\Delta\Delta C_q$ values, suggesting the additional resources and effort required by such purifications were unwarranted.

After exploring purification conditions, a number of aspects of the RT and qPCR steps were optimized. This was facilitated by the fact that the same RNA sample could be used to seed multiple RT-qPCR experiments, simplifying comparisons between conditions. Among the different aspects explored, two sets of experiments are worth mentioning in particular. In the first set of experiments, RT reactions were seeded with consistent amounts of DNA rather than consistent volumes. From these experiments, it was determined that consistently seeding RT reactions with 1 μg of isolated RNA – rather can a consistent volume of inconsistent concentration as had previously been done – resulted in greater precision among the triplicates and enhanced reproducibility. This practice was adapted going forward. In the second set of experiments, different sets of RT primers were explored. Although poly-T primers are commonly used for studying mRNA – as mRNA is the only polyadenylated RNA and thus is selectively amplified by poly-T primer – they are not infallible, and thus two alternatives were evaluated: random hexamer primers and a gene specific primer. The former, which consists of random hexamers that produce nonspecific reverse transcription, is used to amplify RNA when the target is not well characterized.[36] This set of primers produced poor precision and reproducibility, suggesting its use was

inappropriate. The latter, which was designed to produce transcription of only luciferase gene products, produced a more complicated result. Although it amplified the luciferase signal as expected, it also amplified the GAPDH reference gene. To determine the cause of this unexpected signal, two additional RT experiments were run: one without the luciferase primer and one without the reverse transcriptase (Figure 15). Although the luciferase signal differed negligibly in these experiments, the difference in GAPDH signal was substantial. The lack of a primer seemed to have no effect on GAPDH reverse transcription, whereas the lack of a reverse transcriptase produced no signal (as expected). Although a surprising result, it was not unprecedented – primer-independent reverse transcription has previously been reported.[37] A similar phenomenon was observed when the ODC reference gene was evaluated in the same manner. These experiments suggested that other primers offered no specific advantage, and thus the poly-T primer was used exclusively going forward. As an aside, in analyzing the luciferase controls, the value of a no RT control became apparent. Given that DNA would still be detected in a qPCR experiment independent of whether reverse transcription was performed, a no RT control provided a way to determine the amount of background signal due to DNA contamination. This control was run for all subsequent experiments.

Throughout this series of optimization experiments, it became increasingly apparent that inconsistencies observed were inherent to the model system. As a final attempt to work around this

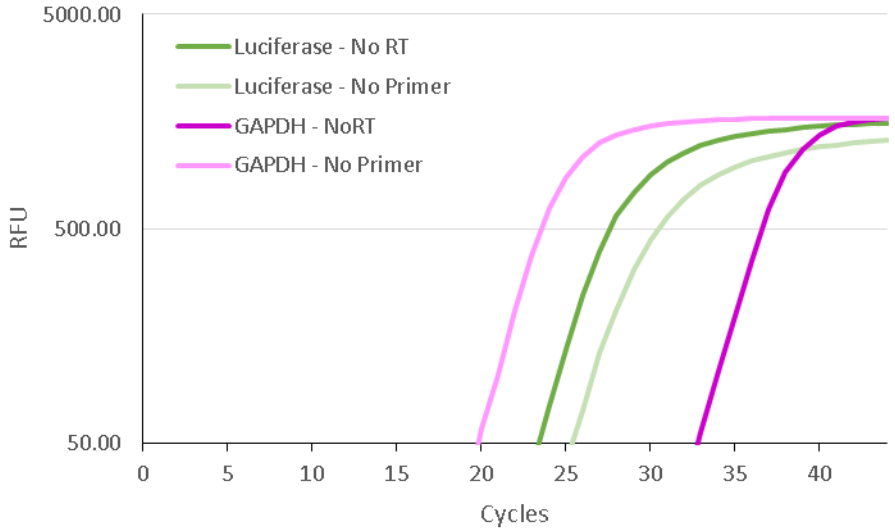

Figure 15: Luciferase specific RT-qPCR.

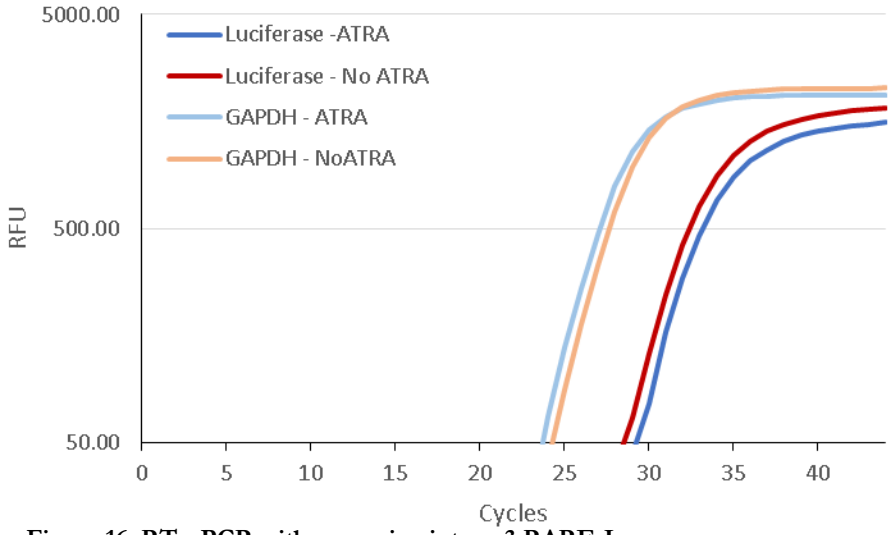

Figure 16: RT-qPCR with a genuine intron-3 RARE-Luc.

limitation, a newly generated intron-3 RARE-Luc gene was evaluated (Figure 16). No signal was observed, suggesting that transcription of the gene did not occur or that the intron was not processed properly in the *Xenopus* oocyte. To determine whether the observed issues were specific to the oocyte model system, a series of experiments were performed in mammalian cells.

1.3.3 Mammalian Cell Experiments

For initial experiments, two different mammalian cell lines were chosen: HEK-293T cells and MDA-MB-231 cells. Although neither of these cell lines has previously been used to study RARα – as much of the work done with RARα had been related to cell cycle regulation and thus done in complicated cell lines such as chondrocytes – each offers distinct advantages in terms of the experimental set up.[38] The HEK-293T cells offer genetic tractability. Given that RARα, RXRα, and the RARE-Luc reporter plasmid must all be present in the same cell (as well as any tRNA that is to be incorporated) if a signal is to be observed, a system which boasts robust transfection efficiency will likely be more effective for the proposed experiments.[39] The HEK-293T cells also offer amenability to noncanonical amino acid incorporation; enzymatic acylation has previously been used to incorporate a number of exogenous amino acids into the cell line.[40] Although chemical acylation in the cell line has yet to be described, previous attempts by the Dougherty group provide a starting point for further investigation.[41] MDA-MB-231 cells lack the high expression efficiencies that characterize the HEK-293T cell line, but they offer

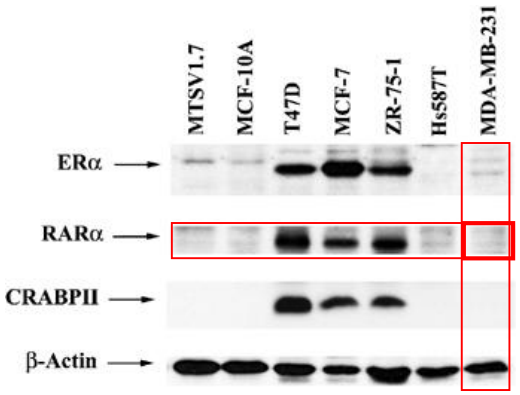

Figure 17: Expression of RARα in different cell lines. Adapted from Lu et al.[31]

low levels of native RARα expression (Figure 17).[31] Given that the inconsistency in the oocyte model system may be due to endogenous RARα activity, having a system with low RARα expression offers a potential experimental advantage. In addition to selecting appropriate cell lines, a new reference gene was selected, ubiquitin C (UBC), as it's use was well characterized in mammalian cells lines.[42]

To probe the ability of each cell line to serve as a potential model system, a number of controls were run. First, RNA from naïve cells was isolated from each cell line, and RT-qPCR performed to ensure that the luciferase qPCR primers did not amplify native genetic material. No amplification was observed in either cell line. This prompted experiments to test the transcriptional activity of native RARα. Although such activity was expected to be negligible in the MDA-MB-231 cell line, the significance of background transcription in the HEK-293T cell line was unclear. Briefly, cells were transfected with the RARE-Luc primer, given 24 hours to recover, incubated with 10 μM ATRA or vehicle overnight, then processed similarly to oocytes for RT-qPCR. Although signal was observed in both cases, the use of no RT controls demonstrated that this was due to DNA contamination, and that true background transcription was negligible for both cell lines (Figure 18). This suggested either cell line could be used for future

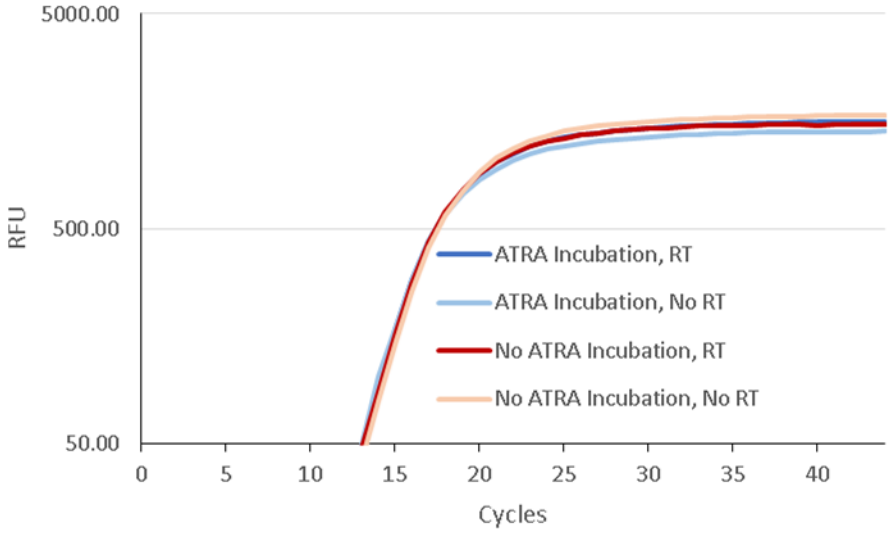

Figure 18: Background RT-qPCR activity in HEK-293T cells.

experiments. Due to the robust nature of HEK-293T cells, from this point forward most optimization was performed in this cell line.

Following demonstration of negligible background signal, a basic transcriptional experiment was performed in each cell line. Both HEK-293T and MDA-MB-231 cells were transfected with pGL3 RARE-Luc, pcDNA6 RARα, and pSV SPORT RXRα (where pXX represents an expression vector). Transcriptional activity was evaluated using qPCR. In both cell lines, no transcriptional activation was observed using these constructs. Although the reasons for this result were unclear, one potential possibility was inefficient transfection. To control for this, an experiment was performed in which HEK-293T cells were incubated with the RARE-Luc reporter plasmid but no transfection reagent. When an RT-qPCR analysis was performed on these cells, no DNA background signal was observed. This suggested that previously observed DNA contamination was present due to transfection of the reporter plasmid into cells, and therefore transfection inefficiency was ruled out as the cause of transcriptional failures.

Another potential possibility was poor expression of the nuclear receptors. To investigate this possibility, a western blot was run using HEK-293T cells transfected with RARα. No expression was observed using either an anti-His6 or an anti-FLAG primary antibody (Figure 19A), suggesting poor RARα expression was at least partially responsible for the lack of transcriptional activation. In an effort to improve expression, the RARα gene was subcloned from the pcDNA6 vector into a new expression vector, pcDNA3.1. This vector has been shown to produce high levels of protein expression in HEK-293T cells.[34] Although an anti-His6 western blot did not

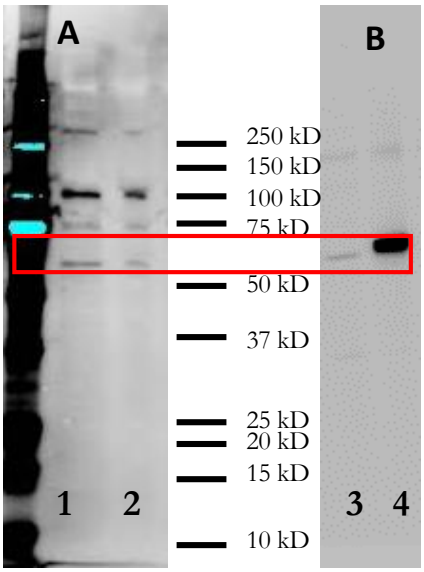

Figure 19: RARα production in HEK-293T cells. A.) Lanes 1 and 2 represent naïve and pcDNA6 RARα-transfected cells. The lack of difference between the lanes suggests RARα is not being expressed. Visualized using an anti-His6 antibody. B.) Lane 3 represents naïve cells probed with anti-FLAG, while lane 4 represents pcDNA3.1 RARα transfected cells.

conclusively demonstrate that this solved expression problems, stripping the membrane and reprobing with anti-FLAG antibody revealed a significant improvement in expression (Figure 19B). Since RXRα lacked an affinity tag to validate expression in the pSV SPORT vector, it was also subcloned into the pcDNA3.1 vector to ensure expression. It is worth noting that although RXRα expression is expected to enhance the observed signal, RXRα was not included in older experimental protocols, therefore the inability to ensure expression, while inconvenient was not debilatating.[43]

Having established RARα expression, basic transcriptional experiments were performed in HEK-293T cells, this time in conjunction with western blot analysis of ATRA-treated and vehicle-treated cells. Once again, transcriptional activation was not observed. However, the results of the western blot were notable. The vehicle treated cells demonstrated significant protein expression, but treatment with ATRA led to a complete ablation of RARα signal (Figure 20). Although the magnitude of this response was somewhat unexpected, it has been previously observed that ATRA can regulate RARα degradation.[44] Given that complete degradation of RARα would preclude any RARα mediated transcription, conditions were screened to determine incubation conditions that did not result in complete degradation of the protein. After screening a number of different incubation times and ATRA concentrations, a one hour incubation using 1μM ATRA was selected for further experiments.

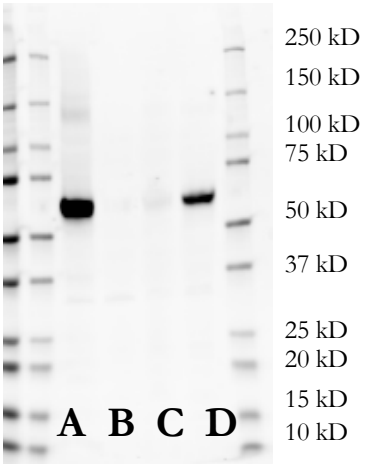

Figure 20: RARα production in the presence of ATRA. Lanes A and B are positive and negative controls, respectively. Lane C contains RARα transfected cells incubated with ATRA and lane D contains RARα transfected cells incubated with vehicle.

With this new set of incubation conditions, basic transcriptional experiments were once again performed, in both HEK-293T cells and MDA-MB-231 cells. Western blots were used to verify protein production in the HEK-293T cells. Despite the revised incubation conditions, transcriptional activity was not observed. This suggested that RARα degradation was not entirely responsible for the lack of observed signal.

As a final attempt to obtain a positive control, the amount of transfected material was doubled. Although this led to decreased cell health (as evidenced by morphology and plate adherence), it ultimately resulted in transcriptional activation and a $\Delta\Delta C_q$ of greater that one (Figure 21). Analogous to the *Xenopus* oocyte experiments, the exact value of the $\Delta\Delta C_q$ was inconsistent between runs. This suggested a more fundamental issue with the RARα/RXRα experimental setup, one that was unrelated to choice of model system.

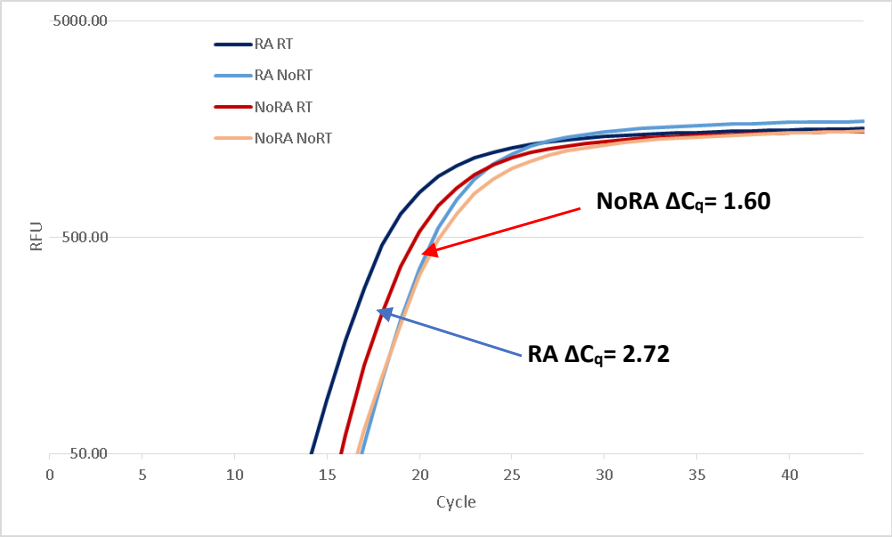

Figure 21: Transcriptional activation in HEK-293T cells. A doubling of transfected material was required to obtain transcriptional activation.

1.3.4 Exploration of the Role of P78

Despite the consistent difficulties of working with the RARα/RXRα model system, an experiment was devised to evaluate the role of proline 78 in regulating RARα transcriptional activation. This experiment was carried out in the *Xenopus* oocyte model system. Serine 77 in RARα was mutated to an alanine (S77A) to test the idea that P78 was a target for Pin1 dependent isomerization. Specifically, it was hypothesized that ablation of the phosphorylation site at S77 would lead to complete interruption of Pin1 isomerization at P78 and disruption of subsequent transcriptional activity. This would lead to a $\Delta\Delta C_q$ of approximately zero. Surprisingly, the S77A mutant produced a negative $\Delta\Delta C_q$, suggesting that S77 itself was regulated by ATRA (Figure 22). This led to an inconclusive result regarding the role of P78 in RARα

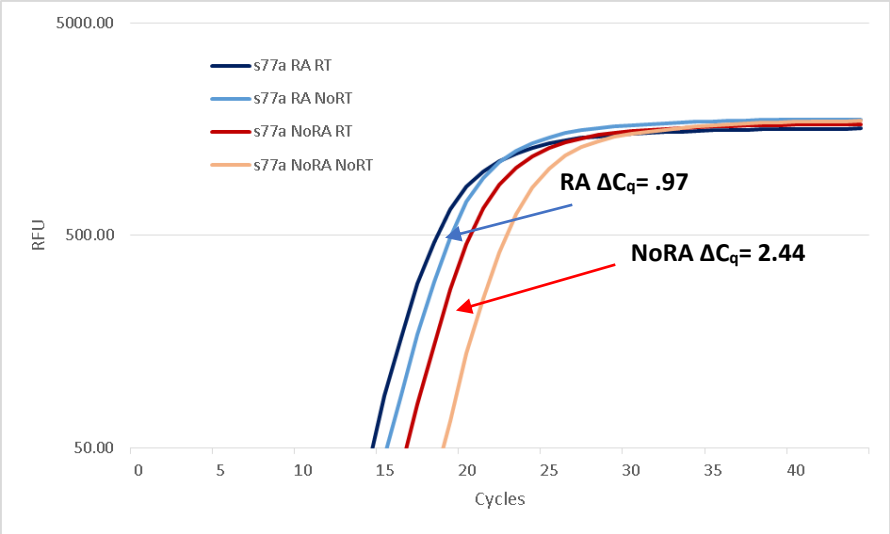

Figure 22: Transcriptional suppression in S77A RARα.

activation and suggested that further experiments would require a better experimental setup and should focus specifically on proline 78. Towards this end, a luciferase assay was explored as an alternative to RT-qPCR.

1.3.5 Evaluation of P78 Using a Luciferase Assay

In a final attempt to explore the effect of proline 78 on RARα regulation, a luciferase assay was designed to circumvent the issues associated with RT-qPCR. Cells were transfected as they were for the RT-qPCR experiments, but a *renilla* luciferase control plasmid was added so that the luminescence intensities could be normalized. After a 24 hour incubation, cells were lysed using a buffer compatible with luminescence evaluation. Cell lysates were then mixed with a luciferase assay buffer, plated into a 96 well plate, and evaluated for luminescence using a Flexstation 3. The luminescence of the control luciferase was also recorded. Using this method, it was observed that the RARE-Luc construct had little signal independently, but significant signal when used in the presence of ATRA and RARα (Figure 23). Given this significant improvement in signal relative to the RT-qPCR assay, a P78TAG mutant of RARα was generated to assess the role of P78 in RARα transcriptional regulation. As expected, this mutant led to complete ablation of luciferase activity in the absence of complementary tRNA. Unfortunately, attempts at recovering WT activity with a proline-modified tRNA were inconclusive. Some initial positive results using chemically acylated tRNA were quickly brought into doubt when significant recovery was

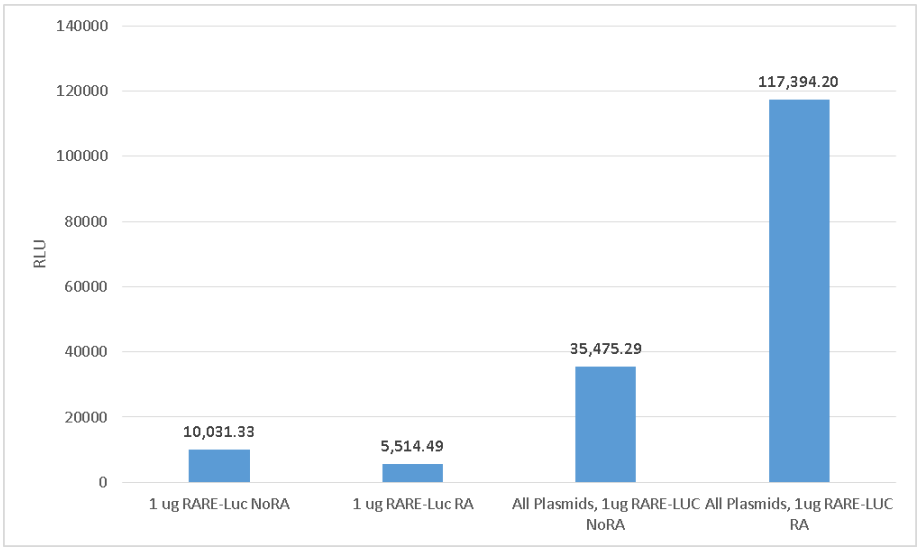

Figure 23: Luciferase expression in the presence of ATRA and RARα.

observed using unacylated tRNA (76mer). This suggested than any signal increase that was observed could be due to the acylation of tRNA inside the cell. Furthermore, the signal obtained with unacylated tRNA was significantly greater than that of acylated tRNA charged with either a proline (WT recovery) or a proline derivative (Figure 24), suggesting that enzymatic reacylation was the most significant factor in any observed signal. In an attempt to address this issue, a screen was run using a number of full length tRNAs from different origins. Unfortunately, none of these gave better results than THG73 76mer, suggesting that the issue could not be resolved by using an alternative tRNA.

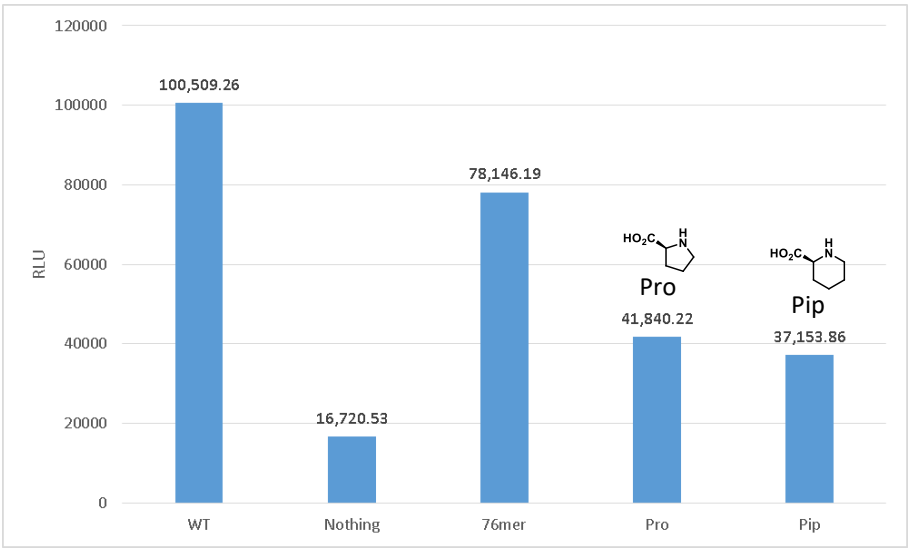

Figure 24: 76mer, THG73-Pro, and THG73-Pip incorporation into P78TAG RARα. The structures of the Pip and Pro amino acids are shown.

The reason that chemically acylated tRNA failed to give significantly higher signal than unacylated tRNA remains unresolved. It could be a transfection failure or a translation failure, but ultimately this prompted a different question: can chemically acylated tRNA be efficiently introduced into mammalian cells? This question took precedence over investigation of the role of P78 in the RARα transcriptional pathway, and ultimately led to a halt in the project

1.4 Conclusion

The regulation of transcription factors remains an incredibly important issue. They play a significant role in many diseases, and a large portion of them are considered undruggable. Unfortunately, despite significant efforts to develop and optimize an RT-qPCR assay for studying nuclear receptors in the context of noncanonical amino acids, a reliable assay could not be developed. The reproducibility issues encountered in oocytes and the inability to efficiently introduce chemically-acylated tRNA into mammalian cells mean that the promise of this project cannot be capitalized on at this point. This project, however, remains a worthwhile intellectual endeavor, and as better transfection reagents are developed attempts to study nuclear receptors using noncanonical amino acids in mammalian cells should be reconsidered.

1.5 Materials and Methods

1.5.1 Materials

pSV Sport RXRα (ID: 8882), pcDNA6 FLAG-RARα (ID: 35555), and pGL3 RARE Luciferase (ID: 13458) constructs were obtained from Addgene. All-trans retinoic acid (ATRA) was purchased as a powder from Sigma, suspended as a 10 mM stock in DMSO and stored at -80 °C. HEK-293T cells were obtained from frozen stocks, previously purchased from ATCC. MDA-MB-231 cells were obtained as a gift from the Dervan group.

1.5.2 Preparation of Oocytes

Harvested stage V–VI *Xenopus* oocytes were washed in four changes of Ca^{2+}-free OR2 buffer (82.5 mM NaCl, 2 mM KCl, 1 mM $MgCl_2$, 5 mM HEPES, pH = 7.5), defolliculated in 1 mg/mL collagenase for approximately 1 h, washed again in four changes of Ca^{2+}-free OR2 and transferred to

ND96 (96 mM NaCl, 2 mM KCl, 1.8 mM $CaCl_2$, 1 mM $MgCl_2$, 5 mM HEPES, pH = 7.5) supplemented with 0.28 mg/mL pyruvate, 0.05 mg/mL Gentamicin, and 0.12 mg/mL theophylline. Oocytes were injected with either cDNA plasmids or mRNA produced by *in vitro* transcription using the mMESSAGE mMACHINE kit (Ambion, Austin, Texas, USA) from cDNA subcloned into pGEMHE.

Oocyte nuclei were injected by allowing the nucleus to rise against the animal pole. Oocytes were injected deeply and directly into the center of discolored regions the animal pole that appeared after such incubation with 2 ng of reporter plasmid per oocytes (varying amounts were used for injection screens). Oocyte cytoplasms were injected shallowly at the edge of the animal pole with 10 ng of mRNA for each transcription factor (varying amounts were used for injection screens). 24 hours after the second injection, oocytes were incubated with ATRA or vehicle overnight in a blacked out container.

1.5.3 Cell Culture and Harvesting Techniques

MDA-MB-231 (gift of the Dervan lab) cells were cultured in high glucose DMEM (Sigma) with 10% FBS (Sigma) and 1% Pen/Strep (Sigma) in a 5% CO_2 atmosphere at 37 °C. HEK-293T cells (ATCC) were cultured in DMEM:F12 (1:1) with GlutaMax-1 (Gibco) with 10% FBS (Sigma) and 1% Pen/Strep (Sigma) in a 5% CO_2 atmosphere at 37 °C. Cells were cultured using 100 mm cultures dishes (Corning), and split to 35 mM dishes (Corning) for experimental purposes. Cells were passaged at approximately 80% confluency. For each cell line, passaging procedures were similar, differing only in the media used. Passaging was performed by removing the media from the cells, washing with PBS (10 mM Na_3PO_4, 150 mM NaCl, pH 7.8), and adding TrypLE. Cells were incubated for 5 minutes, at which point detachment was verified by microscopy. 9 mL of fresh media was then added to quench the TrypLE. Cells were resuspended until homogenous. New plates were seeded at a 1:10 dilution factor for the HEK-293T cells and a 1:5 dilution factor for the MDA-MB-231 cells.

For experiments, cells were transfected using either PEI (Sigma) or Xfect (Clontech, now Takara Bio). For PEI, 1.5 μL of DNA and 9 μL of a 1 mg/ml solution of PEI were added to 300 μL of media lacking FBS and pen/strep. After 10 minutes, this was diluted to 3 mL of media total, and added to cells overnight. After washing with PBS, fresh media was added in the morning to stimulate growth. For Xfect,

0.3 µL of Xfect polymer was added per 1 µg DNA to 100 µL of Xfect buffer. This solution was incubated for 10 minutes, then added directly to cells. After 4 hours, cells were washed and the media replaced. Transfected cells were given 24-36 hours to produce protein, at which point they were incubated with ATRA or vehicle. For harvesting, cells were washed with PBS, detached using TrypLE, and then resuspended using media. The resulting solution was spun down, the media was removed, cells washed once more with PBS, and then the appropriate lysis buffer was added depending on the assay.

1.5.4 RNA Isolation and Reverse Transcription

RNA isolation was performed using RNeasy kit (Qiagen). Deviations from standard protocol are detailed below. For oocytes, four oocytes were lysed in 350 µL buffer RLT and vortexed to homogenize until no macroscopic oocyte structure remained intact. For mammalian cells, harvested cells were lysed in 350 µL buffer RLT and sheared by needle and syringe to ensure lysis. Ethanol precipitation proceeded directly on either lysed sample without centrifugation. 8 µL DNAse I in an 80 µL buffered solution (Roche or Qiagen) was applied to the column and incubated at room temperature for 15 minutes. RNA was eluted in 20 µL of RNAse-free water. This eluent was then passed through the column a second time for complete recovery. Samples were stored at -80 °C until ready for reverse transcription.

Reverse transcription was performed using the Transcriptor First-Strand cDNA Synthesis kit (Roche). Deviations from standard protocol are detailed below. 1 µg (initially 2 µL) of total RNA extract was added to a 20 µL reaction containing polythymine $[dT]_{18}$ primer. RNA, primer, and water were denatured at 65 ºC for 10 minutes and cooled on ice before the addition of buffer, dNTPs, RNase inhibitor and reverse transcriptase in a master mix. This reaction was incubated for 30 min at 50 °C before transcriptase denaturation by incubation at 85 °C for 5 min.

1.5.5 Quantitative Polymerase Chain Reaction

20 µL qPCR reactions employed the 2X SYBR Green Master Mix (Roche). 1.25 µL each from 10 µM forward and reverse primer stocks was added along with 2 µL from the reverse transcription reaction. DNA obtained from the RT reaction was used to seed luciferase and reference gene reactions. Each condition was run in triplicate.

18 μL of each sample was transferred to a 96-well plate taking care to avoid bubbles, covered, and run on a Bio-Rad CFX96 Real-Time system qPCR with a 2-step cycle. An initial denaturation of 95 °C for 10 minutes preceded 40 cycles of 10 seconds at 95 ºC and 30 seconds at the annealing temperature (63.5 °C for the luciferase reactions, 48 °C for all reference genes). A fluorescence measurement was taken at the end of each cycle. Following the final cycle, a temperature gradient ramping from 58 – 88 °C, raising two degrees per minute, was run.

1.5.6 Western Blot

Both oocytes and mammalian cells were lysed in radioimmunoprecipitation assay buffer (50 mM Tris pH 8, 150 mM NaCl, .1% SDS, .5% sodium deoxycholate, 1% Triton X, protease inhibitor tablet (Roche)) with 50 μL being used per oocyte and 200 μL for a harvested 35 mm plate of cells. Oocytes were lysed by vortexing, mammalian cells by needle and syringe. Cell lysates were spun down for 20 minutes at 4°C, and the supernatant isolated. Prior to loading onto a polyacrylamide "Any-kD" gel (Bio-Rad), lysate was mixed with 4X SDS-loading buffer (100 mM Tris pH 6.8, 4% SDS, .2% bromophenol blue, 20 % glycerol, 200 mM DTT). Unused lysate was flash frozen using liquid nitrogen. Gels were run for ~50 minutes using SDS-running buffer (25 mM Tris, 192 mM glycine, 0.1% SDS) before being transferred to Immun-blot® LF PVDF (Bio-Rad) using a wet transfer technique.[42] The PVDF was blocked for 1 hour using 5% evaporated milk (Carnation) in TPBS (10 mM Na_3PO_4, 150 mM NaCl, pH 7.8, .1% Tween), then incubated for 1 hour in 5% evaporated milk in TPBS with a 1:1000 dilution of anti-His6 antibody (Pierce) or a 1:5000 dilution of anti-FLAG antibody (gift of the Hsieh-Wilson group). The membrane was washed 4 times with TPBS, incubated for another hour with 5% evaporated milk in TPBS with a 1:3000 dilution of goat anti-mouse 680 antibody (Life Technologies), then washed 3 more times. Blots were visualized using the Odyssey imaging apparatus (Licor).

1.5.7 Luciferase Assay

Luciferase assays were performed using the luciferase assay system (Promega). Following transfection and treatment with the either ATRA or vehicle, cells were lysed using the cell culture lysis reagent (Promega). Briefly, 300 μL of Cell Culture Lysis Reagent (Promega) was generated from a 5X stock for

each plate of cells to be lysed. This solution was then pipetted vigorously with the cells. Once all cellular material was suspended, the solution was transferred to an Eppendorf tube and allowed to rock for 15 minutes at 4° C. This solution was then spun down at 10,000 g, and the supernatant used to seed a luminescence assay. Specifically, 60 µl of the lysis solution was added to 300 µl of luciferase assay reagent (Promega). From this solution, three 100 µL aliquouts were removed for analysis by a 96-well plate luminescence assay using a Flexstation 3 (Molecular Devices). After assessing the firefly luciferase signal, Stop and Glo buffer (Promega) was added to quench the firefly luciferase signal and initiate the renilla luciferase signal. The renilla luciferase luminescence was then recorded using a Flexstation 3 (Molecular Devices). The triplicates were averaged and standardized against the renilla luciferase signal for a final luminescence value.

1.6 References

1 T. C. Stadtman, *Science*, 1974, **183**, 915–922.
2 C. J. Noren, S. J. Anthony-Cahill, M. C. Griffith and P. G. Schultz, *Science*, 1989, **244**, 182–188.
3 M. W. Nowak, P. C. Kearney, J. R. Sampson, M. E. Saks, C. G. Labarca, S. K. Silverman, W. Zhong, J. Thorson, J. N. Abelson and N. Davidson, *Science*, 1995, **268**, 439–442.
4 J. T. Ngo and D. A. Tirrell, *Acc. Chem. Res.*, 2011, **44**, 677-685.
5 N. Ayyadurai, K. Deepankumar, N. S. Prabhu, S. Lee and H. Yun, *Chem. Commun.*, 2011, **47**, 3430–3432.
6 J. A. Johnson, Y. Y. Lu, J. A. Van Deventer and D. A. Tirrell, *Curr Opin Chem Biol*, 2010, **14**, 774–780.
7 L. Johansson, G. Gafvelin and E. S. J. Arnér, *Biochim. Biophys. Acta*, 2005, **1726**, 1–13.
8 J. W. Chin, *Annu. Rev. Biochem.*, 2014, **83**, 379–408.
9 T. S. Young and P. G. Schultz, *J. Biol. Chem.*, 2010, **285**, 11039–11044.
10 D. A. Dougherty and E. B. Van Arnam, *Chembiochem*, 2014, **15**, 1710–1720.
11 M. Arya, I. S. Shergill, M. Williamson, L. Gommersall, N. Arya and H. R. Patel, *Expert Review of Molecular Diagnostics*, 2005, **5**, 209–219.
12 Universal SYBR Green Quantitative PCR Protocol, https://www.sigmaaldrich.com/technical-documents/protocols/biology/sybr-green-qpcr.html, (accessed January 2, 2019).
13 C. Helsen and F. Claessens, *Molecular and Cellular Endocrinology*, 2014, **382**, 97–106.
14 R. M. Evans and D. J. Mangelsdorf, *Cell*, 2014, **157**, 255–266.
15 V. J. Hilser and E. B. Thompson, *J. Biol. Chem.*, 2011, **286**, 39675–39682.
16 J. Liu, N. B. Perumal, C. J. Oldfield, E. W. Su, V. N. Uversky and A. K. Dunker, *Biochemistry*, 2006, **45**, 6873–6888.
17 V. Chandra, P. Huang, Y. Hamuro, S. Raghuram, Y. Wang, T. P. Burris and F. Rastinejad, *Nature*, 2008, **456**, 350–356.
18 V. Chandra, P. Huang, N. Potluri, D. Wu, Y. Kim and F. Rastinejad, *Nature*, 2013, **495**, 394–398.
19 X.-H. Tang and L. J. Gudas, *Annual Review of Pathology: Mechanisms of Disease*, 2011, **6**, 345–364.
20 W. Bourguet, V. Vivat, J.-M. Wurtz, P. Chambon, H. Gronemeyer and D. Moras, *Molecular Cell*, 2000, **5**, 289–298.
21 J.-P. Renaud, N. Rochel, M. Ruff, V. Vivat, P. Chambon, H. Gronemeyer and D. Moras, *Nature*, 1995, **378**, 681–689.

22 N. Bruck, D. Vitoux, C. Ferry, V. Duong, A. Bauer, H. de Thé and C. Rochette-Egly, *The EMBO Journal*, 2009, **28**, 34–47.
23 E. Gaillard, N. Bruck, Y. Brelivet, G. Bour, S. Lalevée, A. Bauer, O. Poch, D. Moras and C. Rochette-Egly, *PNAS*, 2006, **103**, 9548–9553.
24 K. Sun, V. Montana, K. Chellappa, Y. Brelivet, D. Moras, Y. Maeda, V. Parpura, B. M. Paschal and F. M. Sladek, *Mol Endocrinol*, 2007, **21**, 1297–1311.
25 K. P. Lu and X. Z. Zhou, *Nature Reviews Molecular Cell Biology*, 2007, **8**, 904–916.
26 V. Brondani, Q. Schefer, F. Hamy and T. Klimkait, *Biochemical and Biophysical Research Communications*, 2005, **328**, 6–13.
27 K. P. Lu, G. Finn, T. H. Lee and L. K. Nicholson, *Nature Chemical Biology*, 2007, **3**, 619–629.
28 E. B. Van Arnam, H. A. Lester and D. A. Dougherty, *ACS Chem. Biol.*, 2011, **6**, 1063–1068.
29 A. Jabs, M. S. Weiss and R. Hilgenfeld, *Journal of Molecular Biology*, 1999, **286**, 291–304.
30 S. C. R. Lummis, D. L. Beene, L. W. Lee, H. A. Lester, R. W. Broadhurst and D. A. Dougherty, *Nature*, 2005, **438**, 248–252.
31 M. Lu, R. Mira-y-Lopez, S. Nakajo, K. Nakaya and Y. Jing, *Oncogene*, 2005, **24**, 4362–4369.
32 R. Šindelka, Z. Ferjentsik and J. Jonák, *Developmental Dynamics*, 2006, **235**, 754–758.
33 A. Tomita, D. R. Buchholz, K. Obata and Y.-B. Shi, *J. Biol. Chem.*, 2003, **278**, 30788–30795.
34 T. F. Miles, phd, California Institute of Technology, 2015.
35
36 M. L. Wong and J. F. Medrano, *BioTechniques*, 2005, **39**, 75–85.
37 L. Feng, S. Lintula, T. H. Ho, M. Anastasina, A. Paju, C. Haglund, U.-H. Stenman, K. Hotakainen, A. Orpana, D. Kainov and J. Stenman, *BioTechniques*, 2012, **52**, 263–270.
38 L. M. Hoffman, K. Garcha, K. Karamboulas, M. F. Cowan, L. M. Drysdale, W. A. Horton and T. M. Underhill, *J. Cell Biol.*, 2006, **174**, 101–113.
39 P. Thomas and T. G. Smart, *Journal of Pharmacological and Toxicological Methods*, 2005, **51**, 187–200.
40 C. C. Liu and P. G. Schultz, *Annual Review of Biochemistry*, 2010, **79**, 413–444.
41 S. L. Monahan, H. A. Lester and D. A. Dougherty, *Chemistry & Biology*, 2003, **10**, 573–580.
42 S. L. Chua, W. C. See Too, B. Y. Khoo and L. L. Few, *Cytotechnology*, 2011, **63**, 645–654.
43 H. de The, M. del Mar Vivanco-Ruiz, P. Tiollais, H. Stunnenberg and A. Dejean, *Nature*, 1990, **343**, 177–180.
44 J. Zhu, M. Gianni, E. Kopf, N. Honoré, M. Chelbi-Alix, M. Koken, F. Quignon, C. Rochette-Egly and H. de Thé, *PNAS*, 1999, **96**, 14807–14812.

Chapter 2: Further Work on the Use of Chemical Acylation for Noncanonical Amino Acid Mutagenesis in Mammalian Cells

2.1 Abstract

Chemically acylated tRNA is a powerful tool for introducing novel functionality into proteins. Unfortunately, expanding its use beyond the study of ion channels in *Xenopus laevis* oocytes has proven particularly challenging. Described herein are attempts at expanding the methodology into mammalian cells, first in nuclear receptors and then in luciferase proteins. Nuclear receptors were initially chosen due to the signal amplification they provide upon transcription and their relevance in cell biology. Estrogen receptor alpha was chosen specifically as its activity is well characterized in the literature. Following unsuccessful attempts at recovery of transcriptional activation, a simpler system was devised based on a TAG mutant of *Renilla* luciferase. In this system, incorporation of a noncanonical amino acid was directly correlated with an observable luminescence. Unfortunately, luminescence recovery was also unsuccessful, suggesting a more fundamental issue with the system. Attempts were next made to control the pathways responsible for tRNA stability, both by upregulation of the stabilizing protein elongation factor 1a and the (suspected) destabilizing protein BPNT1. Despite efficient upregulation and suppression of these two proteins, respectively, no luminescence recovery was obtained following transfection with chemically acylated tRNA.

2.2 Introduction

2.2.1 The Chemical Acylation Methodology and Mammalian Cells

As mentioned in chapter 1, noncanonical amino acid incorporation is an extremely powerful tool for studying and manipulating proteins. This can be performed in one of two ways: site-specific incorporation or residue-specific incorporation. Each method offers unique advantages, and together they provide a robust toolset for studying proteins.[1] Of the two, site-specific incorporation via nonsense suppression has been of particular interest in our lab, as we are interested in studying chemical scale interactions in proteins such as ion channels.[2] There are two methods to acylate the tRNA used for nonsense suppression. The first, enzymatic acylation, has found widespread use. It is robust, offers high yields, and requires only a catalytic amount of tRNA.[3] Despite the many strengths of this method, it is limited by the

need for a unique synthetase for each amino acid to be used. The second method, chemical acylation, is a complete foil to enzymatic acylation. It is much less robust and requires a stoichiometric amount of tRNA, however, it can be used to easily install any amino acid that is accepted by the ribosome.[2]

Our lab has used the flexibility of chemical acylation methods to explore a range of phenomena in ion channels in the *Xenopus laevis* oocyte. Electrostatic interactions via fluorinated aromatic amino acids, *cis-trans* preferences via proline analogs, and backbone interactions via α-hydroxy acids have all been probed.[2,4] The choice of protein class and model system abrogates the weaknesses of the chemical acylation method, ultimately producing a robust assay. Unfortunately, it has been difficult to expand the methodology. Some success was found studying GPCRs in *Xenopus* oocytes using an ion channel linked assay. However, beyond this no other class of proteins has been explored outside a test tube.[5,6] Chapter 1 dealt with attempts to expand the methodology to another set of proteins, nuclear receptors. This chapter discusses attempts to expand the system to a model system besides *Xenopus* oocytes, as different model systems could confer unique advantages. Specifically, studying ion channels in their native environment, mammalian cells, could yield new insights into function.

Introduction of acylated tRNA into mammalian cells is significantly more complicated than it is in *Xenopus* oocytes. Due to the large size of the *Xenopus* oocyte, tRNA can be physically injected, ensuring delivery of tRNA. For mammalian cells, tRNA must be introduced the same way as any other RNA – through transfection or electroporation. These methods are less reliable than physical injection, and each provides a host of technical challenges. Previous work in our lab has tested both methods. Work by Sarah Monahan demonstrated the successful incorporation of a fluorinated derivative of tryptophan using electroporation.[7] Despite this initial success, the method was found to be unreliable and resource intensive, requiring a significant amount of acylated tRNA for each electroporation. This work was followed by exploration of transfection based methods by Kristina Daeffler and Nyssa Puskar.[8]

Daeffler and Puskar screened a number of conditions using different transfection reagents, but they were ultimately unable to incorporate a noncanonical amino acid by transfecting acylated tRNA. They were, however, able to make some progress in optimizing transfection conditions using the tRNA known

as the human serine amber suppressor (HSAS). This tRNA is enzymatically acylated in human cells by the serine synthetase, however, it recognizes an amber stop codon rather than a traditional serine codon and therefore can be used for nonsense suppression. [9] This allowed the duo to evaluate conditions where tRNA transfection was occurring at levels too low to give a stoichiometric readout and optimize conditions for the transfection of chemically acylated tRNA. Although Daeffler and Puskar were unable to transfect acylated tRNA, the conditions they devised using HSAS tRNA provide important groundwork for continued experiments.

Ion channels provide sufficient signal amplification for studies in oocytes, however, it is possible that they are an inappropriate readout for mammalian cells, particularly for the experiments carried out by Daeffler and Puskar. In these experiments, transfected cells were plated into 96 well plates and incubated with a voltage-sensitive fluorescent dye.[8] Drug was then applied, and an increase in fluorescence was observed depending on the efficiency of ion channel opening.[8] Although this assay worked reasonably well for wild type ion channels, insufficient signal was obtained when it was used with chemically acylated tRNA. The fluorescent turn-on failed to provide a comparable amount of signal amplification as electrophysiology, and thus was an insufficient readout for the low protein yields associated with the nonsense suppression methodology.

Going forward, a different readout is required, one that offers significant signal amplification. Transcription and translation both amplify a chemical signal, making transcription factors a good target for a new assay. Furthermore, by selecting an appropriate gene, synthesized protein can provide additional signal amplification. For this reason, an assay linking a transcription factor to expression of a catalytic reporter protein was designed. As the basis for this new assay, estrogen receptor alpha (ERα) was chosen as the transcription factor and luciferase as the reporter protein.

2.2.2 Estrogen Receptor Alpha

ERα is a member of the nuclear receptor superfamily, and it is one of two nuclear receptors that binds estrogen, with the other being estrogen receptor beta (ERβ).[10] It is an extremely well-studied protein due to its association with a number of biological events, making it a good target for assay development. The

receptor binds an endogenous set of hormones known as estrogens, however, it is fairly promiscuous, also binding a myriad of other compounds, some of them bearing little resemblance to estrogen.[10] Classically, binding of estrogen to ERα was thought to induce dimerization of the receptor (either with ERα or ERβ), translocation of the dimer to the nucleus, DNA binding, and transcriptional activation. Although through the years it has been shown that this is somewhat of an oversimplification, what remains fundamentally true is that ERα ligand binding induces recruitment to transcriptional activator elements known as estrogen response elements (EREs).[10] These response elements vary significantly in composition, however, the core consensus sequence usually consists of a thirteen base pair palindromic repeat.[11]A number of plasmids have been developed containing estrogen response elements, with a variety of different genes linked to the response element. Luciferase is a particularly attractive gene, as it offers additional signal amplification in the form of its chemilumescence readout.

To use a combined ERα/luciferase assay to test tRNA transfection techniques, an ERα TAG mutant was required; judicious selection of the site required an analysis of the protein's entire structure. ERα is a multi-domain protein consisting of an N-terminal domain, a DNA binding domain, a hinge region, a ligand binding domain, and a C-terminal domain, all of which play important roles in the regulation and activity of the protein.[10] The DNA binding domain and ligand binding domain have been well characterized structurally, however, the N-terminal domain, C-terminal domain, and hinge region have been difficult to characterize due to their intrinsic disorder. This makes them ideal targets for the chemical scale analyses performed in the Dougherty lab, therefore these regions were initially targeted for the development of TAG mutants. Ultimately, a C-terminal mutant at tyrosine 526 was generated for initial experiments. This location was selected for two reasons. For one, replacement of a tyrosine with fluorinated phenylalanine derivatives is routinely done in our lab, making tyrosine a good amino acid for

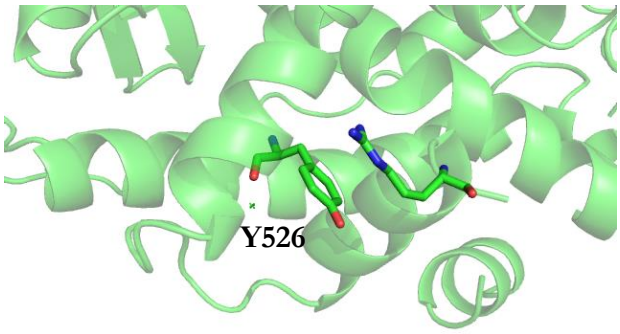

Figure 1: Potential cation-pi interaction in ERα. Positioning of Y526 and a nearby arginine in the agonist bound form of ERα.

initial replacement experiments. In addition, in the agonist bound form Y526 appears to be interacting with a nearby arginine (Figure 1), making a cation-pi interaction worth 5.1 kcal/mol according to the Cation-π Trends Using Realistic Electrostatics (CaPTURE) computational method.[12] In the event that incorporation is successful, this interaction could be probed as a true proof of concept.

2.3 Results and Discussion

2.3.1 TAG Suppression Attempts in Estrogen Receptor Alpha

To begin developing a more efficient assay for tRNA incorporation in mammalian cells, two plasmids were ordered from Addgene, one containing an eGFP-ERα construct and the other containing a 3X Estrogen Response Element coupled to a luciferase reporter. Initial experiments with these two constructs and β-estradiol (an estrogen) in HEK-293T cells demonstrated low background signal in the absence of estradiol and a nearly 4-fold transcriptional activation when a sufficient amount of eGFP-ERα DNA was transfected (Figure 2). Inherent transcriptional activation in the absence of estradiol suggests that either estrogens within the cell are regulating the ERα or that activation of ERα is occurring through

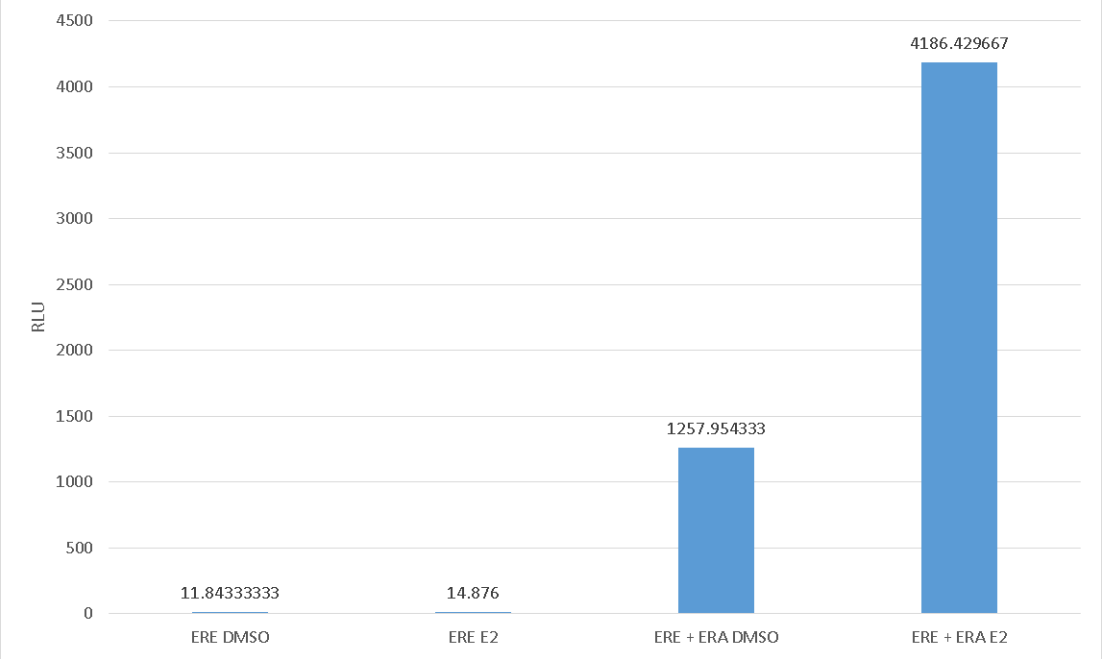

Figure 2: ERα transcriptional activation in the presence of E2. Evaluated by luminescence response.

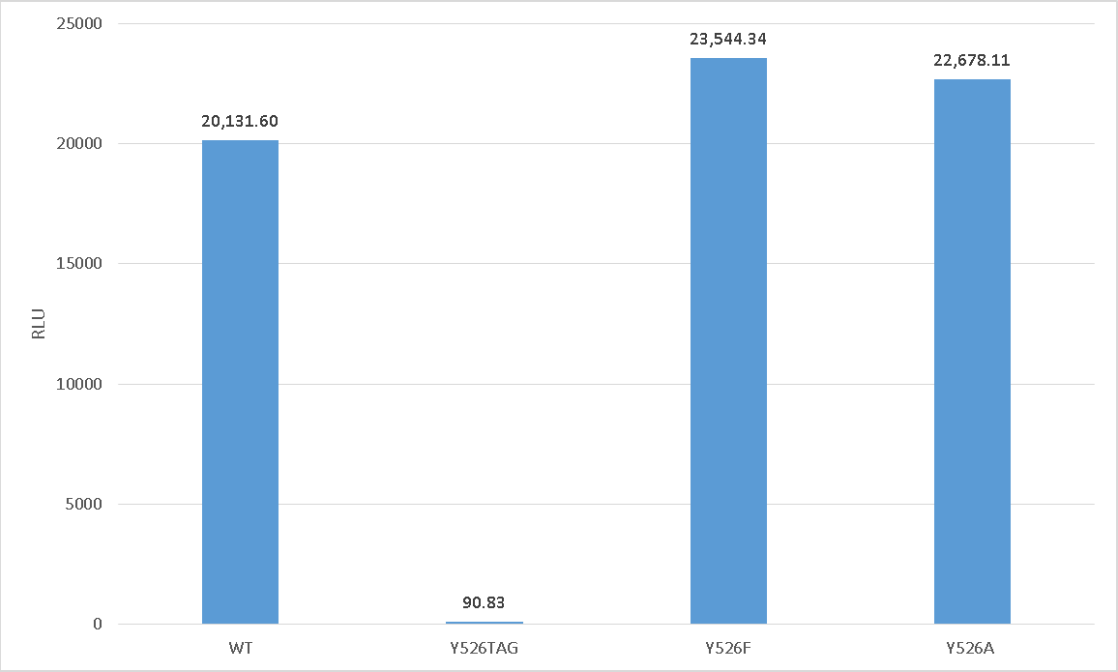

Figure 3: Evaluation of Y526 as a sight for further experiments.

other pathways, a phenomenon that has previously been described.[13] Despite some inherent background, this activation was considered sufficient enough to warrant studies with mutant estrogen receptors.

As mentioned in the introduction, the initial site selected for mutation was Y526. Three mutants were made. Y526F and Y526A were generated to probe the sensitivity of the site to mutation, and Y526TAG was made for noncanonical amino acid mutagenesis experiments. Evaluation of Y526F and Y526A demonstrated that Y526 did not play a significant role in estrogen receptor activation, invalidating the proposed cation-pi theory. The results did not totally discourage exploration of the site, however, as Y526TAG demonstrated complete ablation of activation (Figure 3.) Based on these results, incorporation of chemically acylated tRNA was attempted, using THG73 76mer as a control. These results were significantly less encouraging, as only a small amount of recovery was observed using chemically acylated tRNA (either the F_4-Phe unnatural or Tyr wild type recovery), with much greater signal being observed with the 76mer control (Figure 4). To determine whether or not this recovery was specific to the control used, a number of other control tRNAs were evaluated (TQAS 76mer, TQOPS' 76mer, THG73 7474mer). Although none gave as large a response as THG73, they all gave a larger result than the chemically acylated tRNAs tested, suggesting reacylation at the site was a significant issue. Interestingly,

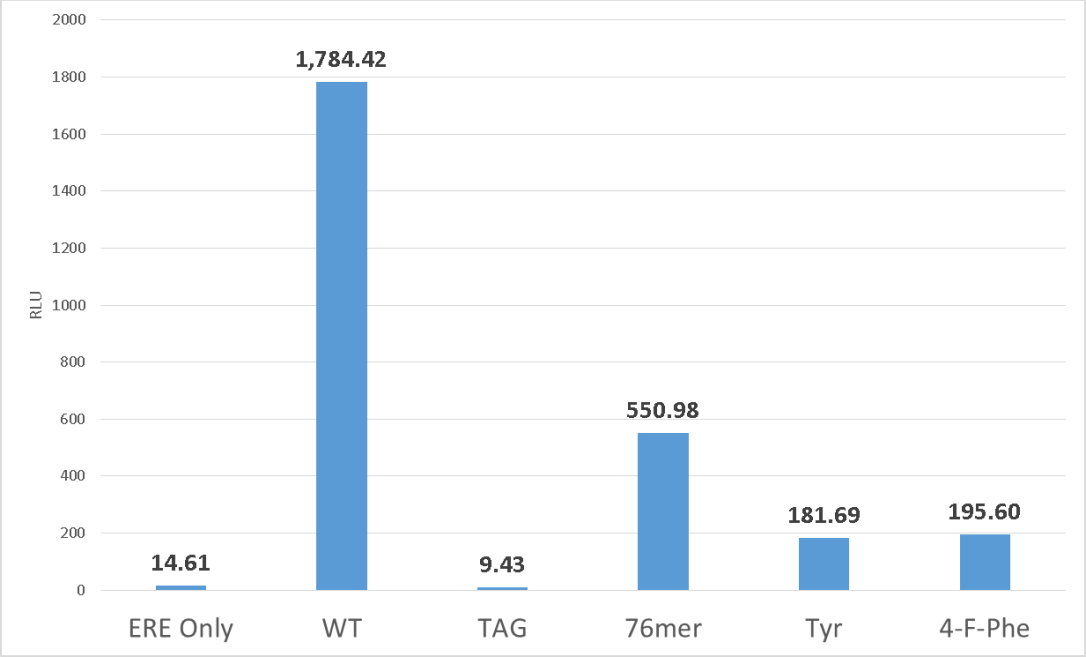

Figure 4: Chemical acylation incorporation attempts. Notably, the 76mer control gives greater luminescence signal than either of the two chemically acylated tRNA.

when a protein gel was run to look for full length protein from the Y526TAG mutant transfected with THG73 76mer, only truncated product was observed, suggesting that observed signal increase was not due to the presence of full length protein, but perhaps an artifact of transfection.

To account for the possibility that the results obtained for Y526TAG ERα were a consequence of the site used, a number of other mutants were explored. One mutant, Y43TAG, gave significant activation in the presence of E2 and was avoided. The other two, Y191TAG and Y248TAG, had higher mutant background signal than Y526, but no notable activation in the presence of THG73 76mer. These two mutants were transfected with chemically acylated tRNA, but no activation was observed above background (Figure 5). Although additional sites could be explored, the results suggested that combined transcriptional-luciferase readout was too complicated, and that optimization of chemically acylated tRNA incorporation should be performed in a simpler system. To reduce the number of transfected plasmids as well as the number of steps between amino acid incorporation and readout, a *Renilla* luciferase containing a TAG mutation was explored.

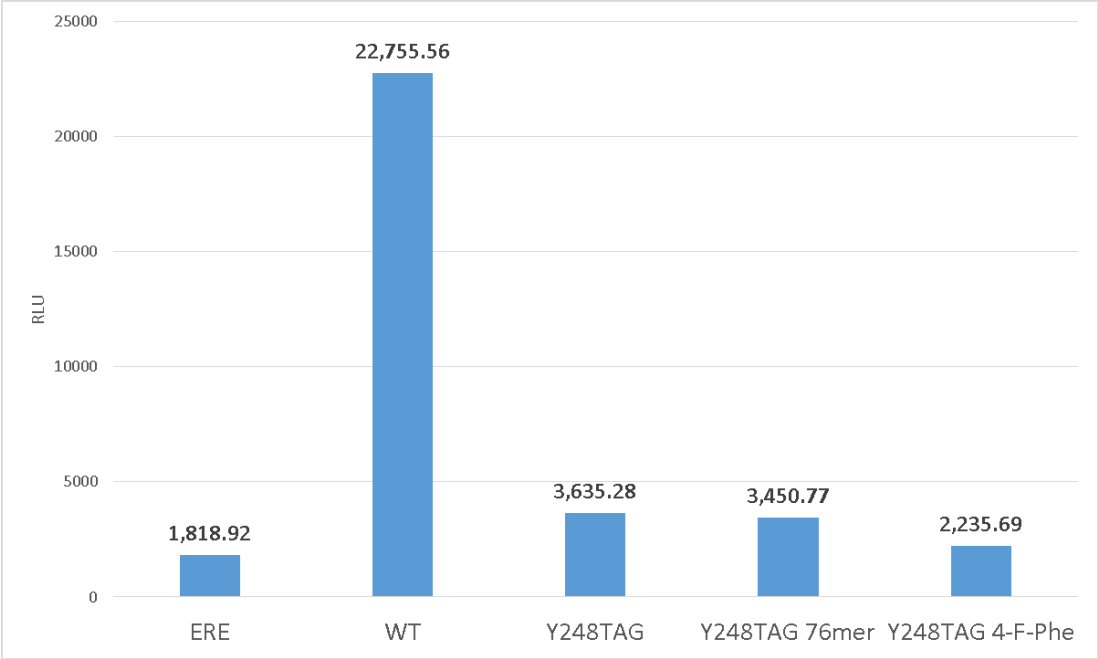

Figure 5: Transfection attempts using Y248TAG mutant of ERα.

2.3.2 TAG Suppression Attempts in Renilla Luciferase

Starting with a plasmid from Addgene containing a constitutively expressed wild type *Renilla* luciferase (pRL-SV40P), an F49TAG mutant of *Renilla* luciferase was generated. As expected, this mutant was completely inactive. Recovery was subsequently attempted with THG73 alpha hydroxy phenylalanine, as it has been demonstrated that alpha hydroxy acids typically give higher incorporation efficiency than corresponding amino acids using the chemical acylation method.[14] Unfortunately, the mutant could not be rescued by either THG73 76mer or THG73 acylated with alpha hydroxy phenylalanine (Figure 6). Rescue with a pyrrolysine derived tRNA was next attempted[15,16], followed by rescue using a different transfection reagent (Effectene). Neither attempts were successful. As a last resort, another mutant (Y6TAG) was generated, but this mutant was also not responsive to transfection of chemically acylated tRNA. These results suggested that a more fundamental issue existed regarding tRNA transfection, and that a different approach was required. Towards this end, the literature regarding tRNA transfection was reevaluated.

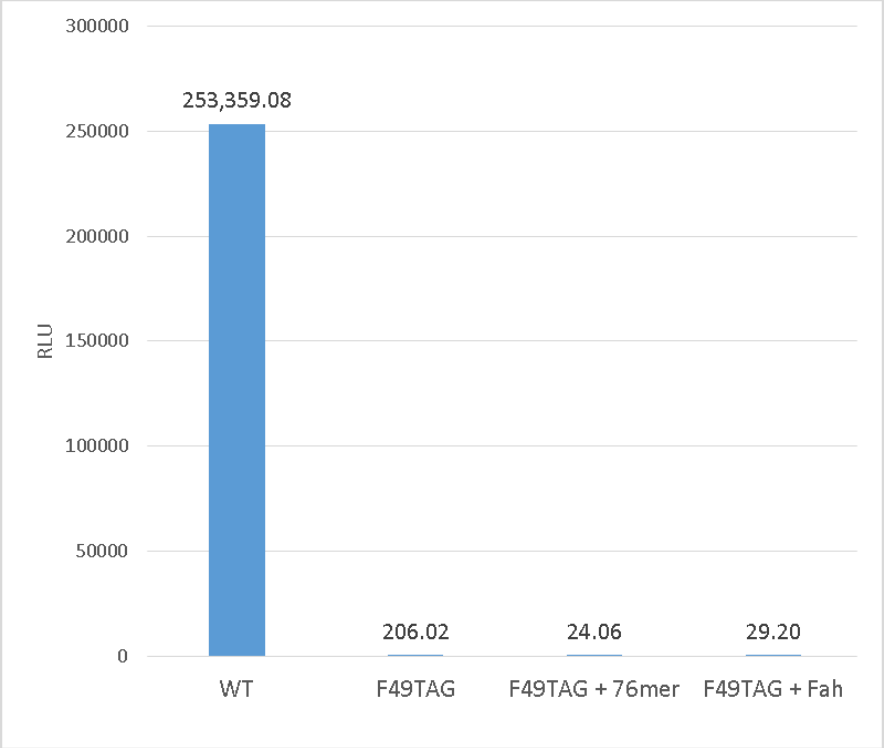

Figure 6: F49TAG *Renilla* luciferase recovery attempts.

The literature is fairly divided on the fate of transfected tRNA in a cell. Although some groups have observed successful incorporation of endogenously introduced tRNA into a cell's tRNA pool (our group included), others have observed significant degradation of introduced tRNA. It is likely that these two outcomes are both possible, but the pathway that predominates is circumstantial.[7,17,18] There are two ways that one could consider biasing this pathway. The first would be to overexpress proteins involved in tRNA stabilization. Elongation factor 1a (EF1a) is one of the predominant proteins known to do this, rescuing tRNA from degradative pathways.[19,20] The second would be to knock down pathways associated with tRNA degradation. Although there are multiple pathways for degradation, one of the most significant in yeast is known as the tRNA Rapid Decay Pathway, which reduces the half-life of tRNA to about 15 minutes under conditions of stress, such as transfection.[19,21] Although this pathway has not been characterized in mammalian cells, a set of homologous proteins exists, predominant among which is BPNT1.

Both EF1a overexpression and BPNT1 knockdown were explored as ways to regulate tRNA stability in transfected cells. For EF1a overexpression, a plasmid containing eEGFP-eEF1a was obtained from

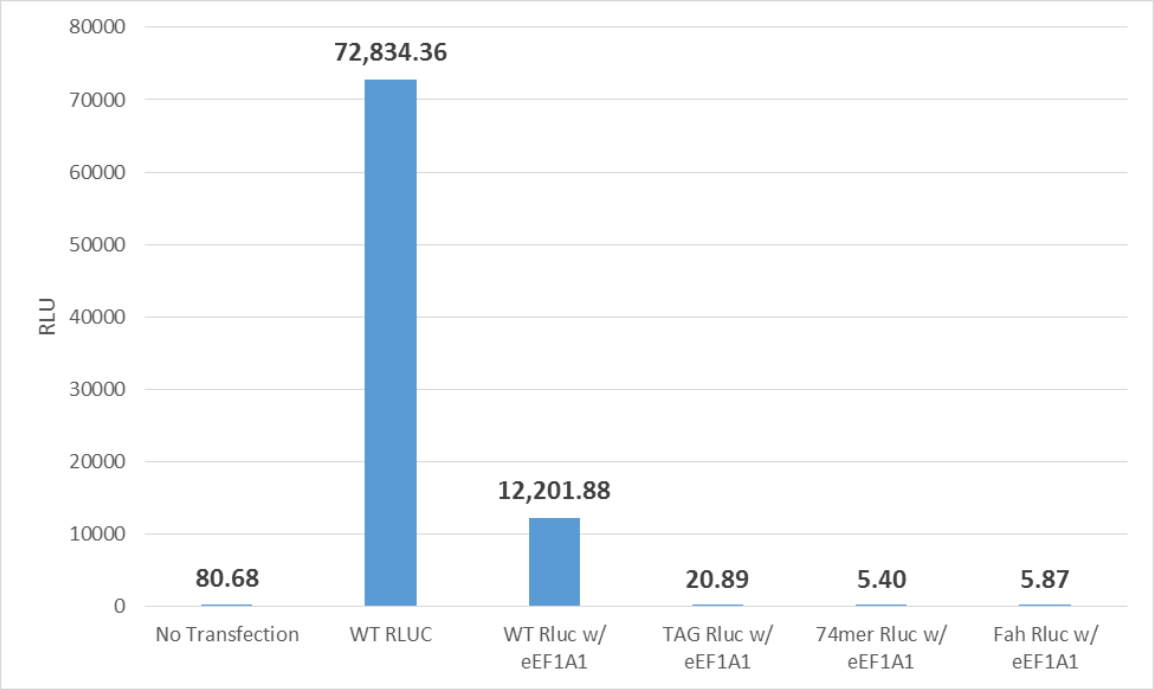

Figure 7: Effects of EF1a overexpression on F49TAG *Renilla* luciferase recovery.

the Nudler lab at NYU. Overexpression was monitored by eGFP fluorescence using either the Flexstation or gel electrophoresis in combination with a Typhoon fluorescence imager. Once overexpression was validated, transfection conditions were optimized and F49TAG *Renilla* luciferase recovery experiments were attempted. Unfortunately, overexpression of EF1a had no notable effect on luciferase recovery (Figure 7). For BPNT1 knockdown, BPNT1 siRNA and a BPNT1 antibody were ordered from Santa Cruz Biotech. Expression of BPNT1 was then evaluated under knockdown conditions, using tubulin to control for protein expression and blotting efficiency (Figure 8). The results of the knockdown experiment suggested that suppression of BPNT1 expression was

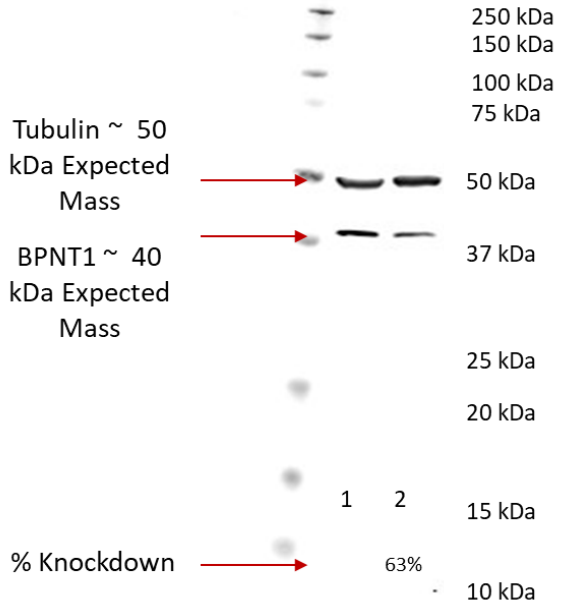

Figure 8: BPNT1 knockdown with BPNT1 siRNA. Lane 1 contains WT HEK-293T lysate and lane 2 contains BPNT1 knockdown (6 pm BPNT1 siRNA) HEK-293T lysate.

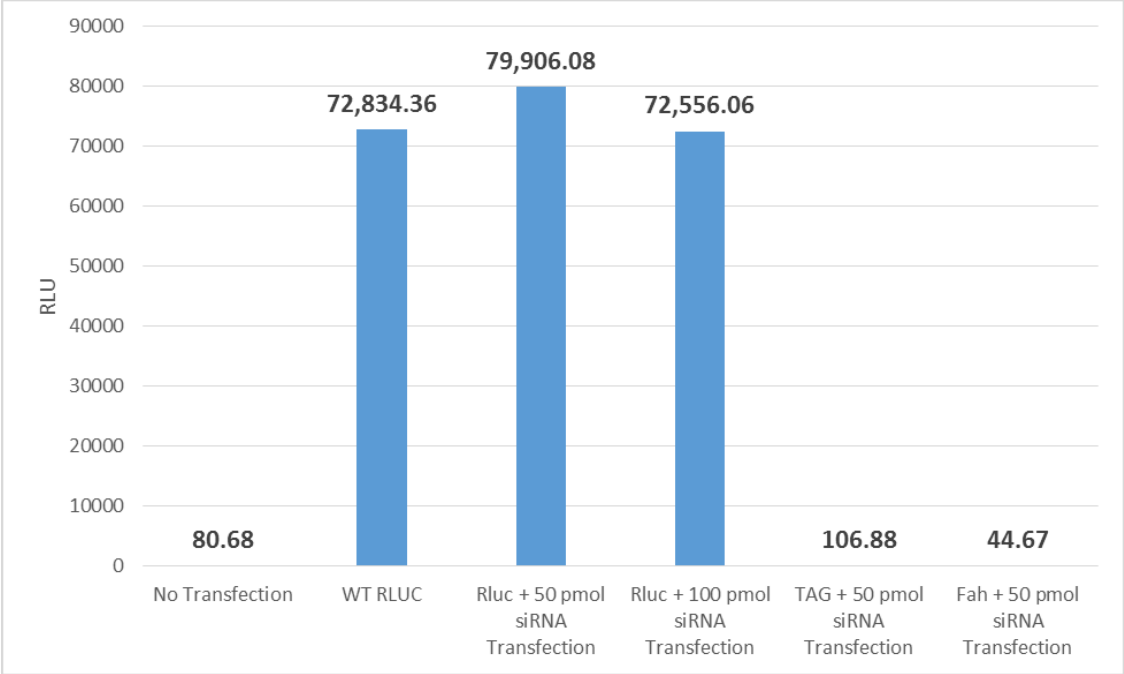

Figure 9: Effects of BPNT1 knockdown on F49TAG *Renilla* luciferase recovery.

indeed possible, although higher concentrations (>10 picomoles) would be required to obtain significant knockdown. Knockdown was subsequently attempted in the context of F49TAG *Renilla* luciferase recovery, but no significant change was observed (Figure 9), even with greater than 70% BPNT1 knockdown. One last attempt was made incorporating both EF1a overexpression and BPNT1 knockdown, but once again no recovery was observed.

At this point, noncanonical amino acid incorporation via enzymatic methods was attempted to ensure that recovery at the mutant was possible. The use of a synthetase and media containing p-azidophenylalanine led to recovery of activity, albeit at about 15% of the wild type levels. Still, this demonstrated that rescue was possible and that F49TAG could not be entirely blamed for the failure of the method.

Having explored most other conditions, it seems that transfection conditions are likely responsible for the poor incorporation/uptake of the tRNA. A number of conditions had been evaluated by Daeffler and Puskar, but none stood out as exceedingly better. This suggests that the current generation of transfection reagents is insufficient for the efficient transfection of tRNA and that further progress is dependent on the development of novel transfection reagents. Monahan's results were predicated on

electroporation, which may be the only method that is currently capable of incorporating chemically acylated tRNA into mammalian cells. Unfortunately, this method is too impractical to use beyond proof of concept experiments.

2.4 Conclusion

Significant effort was made to expand the use of chemically acylated tRNA into mammalian cells. Initial attempts were made in the context of nuclear receptors, which have the potential to provide significant signal amplification and are integral to a number of complex cellular pathways. After recovery could not be achieved in nuclear receptors, the system was simplified to reduce the number of steps between amino acid incorporation and readout. Although this led to cleaner controls and lower background, recovery was still not observed. Finally, cell biology was manipulated in an attempt to stabilize the transfected tRNA. This was done through upregulation of a stabilizing pathway and down regulation of a suspected destabilizing pathway. Neither of these led to recovery, suggesting that a more fundamental issue exists, likely with regards to the transfection reagent. Although progress in this project has been halted for the time being, novel transfection reagents – like those produced in the Waymouth and Wender groups at Stanford – are likely to reinvigorate exploration of this challenging topic.

2.5 Materials and Methods

2.5.1 Materials

HA-ERα, estrogen response element, and Renilla luciferase constructs were obtained from Addgene (pcDNA-HA-ER WT, 3X ERE TATA.luc, and pRL-SV40P respectively). An eGFP-eEF1a1 construct was obtained from the Nudler lab at NYU. Estradiol was purchased as a powder from Sigma-Aldrich. BPNT1 siRNA and mouse anti-BPNT1 antibody were obtained from Santa Cruz Biotech. Mouse anti-tubulin antibody was obtained from Sigma Aldrich.

2.5.2 Mammalian Cell Culture

HEK-293T cells (ATCC) were cultured in DMEM:F12 (1:1) with GlutaMax-1 (Gibco) with 10% FBS (Sigma) and 1% Pen/Strep (Sigma) in a 5% CO_2 atmosphere at 37°C. Cells were cultured using 100 mm culture dishes (Corning), and split to 35 mM dishes (Corning) for experimental purposes. Cells were

passaged at approximately 80% confluency. Passaging was performed by removing the media from the cells, washing with PBS (10 mM Na_3PO_4, 150 mM NaCl, pH 7.8), and adding TrypLE. Cells were incubated for 5 minutes, at which point detachment was verified by microscopy. 9 mL of fresh media was then added to quench the TrypLE. Cells were resuspended until homogenous. New plates were seeded at a 1:10 dilution factor for the HEK-293T cells.

For experiments, cells were transfected using Xfect, RNA Xfect, or a combination of the two depending on the transfection being performed (Clontech, now Takara Bio). For DNA Xfect transfections, 0.3 μL of Xfect polymer was added per 1 μg DNA to 100 μl of Xfect buffer. This solution was incubated for 10 minutes, then added directly to cells. After 4 hours, cells were washed and the media replaced. For RNA Xfect transfections, 2 μg of RNA was diluted to a volume of 100 μl with Xfect reaction buffer. This was combined with a solution containing 10 μl of RNA transfection polymer and 100 μl of Xfect reaction buffer. This solution was incubated for 10 minutes, then added directly to cells. After 4 hours, cells were washed and the media replaced. If greater amounts of RNA were transfected, the amount of polymer was increased proportionally. For combined Xfect transfections, 2 μg of RNA and up to 8 μg of DNA were diluted to a volume of 120 μl with Xfect reaction buffer. This was combined with a solution containing 0.3 μg of transfection polymer per μg of DNA diluted to 120 μl in Xfect reaction buffer and 10 μl of RNA transfection polymer. This solution was incubated for 10 minutes, then added directly to cells. After 4 hours, cells were washed and the media replaced. If DNA and RNA were transfected separately in the same dish, a 16-hour recovery buffer was given before the second transfection. After the final transfection, a 4-hour recovery period was given, at which point media was exchanged, either for media containing estradiol or DMSO vehicle. After 12-16 hours, cells were harvested for analysis. For protein expression analysis, cells were lysed using 0.1% SDS (Bio-Rad) with a protease inhibitor tablet (Roche) and vigorous pipetting, at which point they were run on a poly-acrylamide gel (Bio-Rad, Any Kd gel). For luminescence analysis, cells were lysed using Cell Culture Lysis Reagent (Promega), which has been shown to be compatible with luminescence experiments.

2.5.3 Protein Visualization

Cells were lysed in 0.1% SDS (Bio-Rad) containing a protease inhibitor pellet (Roche), with 200 μl used to harvest cells from a 35 mm plate. Lysate was mixed 3:1 with 4X SDS-loading buffer (100mM Tris, pH 6.8, 4% SDS, 0.2% bromophenol blue, 20 % glycerol, 200 mM DTT), then loaded onto polyacrylamide "Any Kd" gels (Bio-Rad). Unused lysate was flash frozen using liquid nitrogen and kept for additional experiments. Gels were run for ~50 minutes using SDS-running buffer (25 mM Tris, 192 mM glycine, 0.1% SDS). At this point, proteins containing a fluorescent marker, such as eGFP-eEF1a, were visualized directly using the Typhoon (GE Healthcare). Although this method does not allow for quantitative analysis – since some percentage of the GFP chromophore will have bleached on the denaturing gels – it does provide an approximate comparison for conditions run on the same gel. To analyze proteins that did not contain fluorescent proteins, western blots were run. Completed gels were transferred to Immun-blot® LF PVDF (Bio-Rad) using a wet transfer technique. The PVDF was blocked for 1 hour using 5% evaporated milk (Carnation) in TPBS (10 mM Na_3PO_4, 150 mM NaCl, pH 7.8, .1% Tween), then incubated for 1 hour in 5% evaporated milk in TPBS with the appropriate antibody (all mouse derived, for use with goat anti-mouse secondary). Concentrations were adjusted to obtain reasonable signal relative to an anti-tubulin antibody. The membrane was washed 4 times with TPBS, incubated for another hour with 5% evaporated milk in TPBS with a 1:3000 dilution of goat anti-mouse 680 antibody (Life Technologies), then washed 3 more times. Blots were visualized using the Odyssey imaging apparatus (Licor).

2.5.4 Luminescence Assay Protocol

Luciferase assays were performed using the dual luciferase assay system or *Renilla* luciferase assay system depending on the experiment (Promega). Following transfection and treatment with either estradiol or vehicle, cells were lysed using the Cell Culture Lysis Reagent (Promega), which is compatible with all luciferase assays. Briefly, 300 μL of Cell Culture Lysis Reagent (Promega) was generated from a 5X stock for each plate of cells to be lysed. This solution was then pipetted vigorously with cells. Once all cellular material was suspended, the solution was transferred to an Eppendorf tube and allowed to rock for 15 minutes at 4° C. This solution was then spun down at 10,000 g, and the supernatant used to

seed a luminescence assay. Specifically, 60 μl of the lysis solution was added to 300 μl of a luciferase assay reagent, either LAR II for the dual luciferase assay or *Renilla* Luciferase Assay Reagent for the *Renilla* luciferase assay (Promega). From this solution, three 100 μL aliquots were removed for analysis by a 96-well plate luminescence assay using a Flexstation 3 (Molecular Devices). For the *Renilla* luciferase assay this was the end, but for the dual assay system, after assessing the firefly luciferase signal, Stop and Glo buffer (Promega) was added to quench the firefly luciferase signal and initiate the *Renilla* luciferase signal. The *Renilla* luciferase luminescence was then also recorded using a Flexstation 3 (Molecular Devices). For the dual assay system, the triplicates were averaged and standardized against the *Renilla* luciferase signal for a final luminescence value.

2.5.5 Estrogen Receptor Recovery Experiments

HEK-293T cells were transfected as previously described with three plasmids: one containing an estrogen response element, one containing a *Renilla* luciferase, and one containing estrogen receptor, either the wild type or a mutant. tRNA was all transfected, usually at the same time, although temporally separated transfections were also evaluated. Estradiol was added between 8-12 hours after the start of transfection (to allow time for transfection and recovery) via a media exchange. Many concentrations of estradiol were initially tested, but ultimately all data was collected with 10 μM estradiol, a value that fell within the middle of the literature range. After 12-16 hours of incubation in estradiol, transcriptional activation was evaluated by luciferase assay, with *Renilla* luciferase activity serving as a control for transfection efficiency, protein concentration, and machine variability. Although 12-16 hours is a somewhat quick turnaround time for protein expression, a number of different time points were tested, and significant differences in wild type signal were not observed in incubations ranging from 12-36 hours. Since chemically acylated tRNA is not expected to persist unused in the cellular environment, an earlier time point was ultimately selected to increase the concentration of noncanonical amino acid containing protein. Further time points were still tested with acylated tRNA, but a rigorous time course was not performed due to the value of acylated tRNA.

2.5.6 Renilla Luciferase Recovery Experiments

The *Renilla* luciferase recovery experiments were designed to simplify the overall recovery assay by reducing the number of required plasmids to one and eliminating steps in between noncanonical amino acid incorporation and observable chemiluminescence. Towards this end, a plasmid containing *Renilla* luciferase or a mutant *Renilla* luciferase was transfected along with tRNA. Although this tRNA was usually transfected along with the plasmid, temporally separated transfections were also evaluated. 12-16 hours after the transfection was completed, cells were harvested and a *Renilla* luciferase assay was run. In these experiments, there was no control luciferase, but the decreased complexity of the transfection suggested this was less of an issue. For EF1a upregulation experiments or BPNT1 downregulation experiments, two sequential transfections were run. In the first, the *Renilla* luciferase plasmid was transfected with either the EF1a plasmid or BPNT1 siRNA. After screening for concentration effects, 4μg of ER1a and 50 pm of BPNT1 siRNA were determined to be the optimal amounts. Following this first transfection and an 8-12 hour recovery period, a second transfection was run to introduce tRNA. After another 12-16 hours, protein was isolated for analysis by gel electrophoresis or for luminescence experiments.

2.5.7 Synthetase Control Experiment

To ensure that the selected TAG sites could indeed withstand mutant incorporation, a plasmid containing the F6TAG mutant of *Renilla* luciferase was transfected along with PU6 plasmids from the Krogsgaard lab containing a tRNA/synthetase pair for para-azidophenylalanine. These two plasmids were transfected at a ratio of 6 μg to 2 μg (respectively) following the previously outlined transfection protocols. Cells were subsequently incubated in media containing 0.5 mM N_3Phe for 24 hours prior to lysis, and the luminescence determined.

2.5.8 Molecular Biology

Mutations were made using the QuickChange method (Stratagene) and DNA isolated using Qiagen mini prep or maxi prep kits. Chemically acylated tRNA was generated as previously described.[14,22] 74mer and 76mer tRNA were generated using the Ambion T7MEGAshortscript kit by transcription from a DNA oligonucleotide template modified to enhance RNA transcript homogeneity, as described in the literature.[23] Crude tRNA-amino acid or tRNA-hydroxy acid product was used without desalting, and the

product was confirmed by matrix-assisted laser desorption ionization time-of-flight mass spectrometry on a 3-hydroxypicolinic acid matrix. Deprotection of the NVOC group on the tRNA-amino acids was carried out by photolysis for 5 minutes on a 300-watt high-pressure mercury arc lamp with WG-335 and UG-11 filters. This was done immediately prior to transfection.

2.6 References

1 J. A. Johnson, Y. Y. Lu, J. A. Van Deventer and D. A. Tirrell, *Curr Opin Chem Biol*, 2010, **14**, 774–780.
2 E. B. Van Arnam and D. A. Dougherty, *J. Med. Chem.*, 2014, **57**, 6289–6300.
3 T. S. Young and P. G. Schultz, *J. Biol. Chem.*, 2010, **285**, 11039–11044.
4 M. Rienzo, S. C. R. Lummis and D. A. Dougherty, *Chemistry & Biology*, 2014, **21**, 1700–1706.
5 K. N.-M. Daeffler, H. A. Lester and D. A. Dougherty, *J. Am. Chem. Soc.*, 2012, **134**, 14890–14896.
6 E. B. V. Arnam, H. A. Lester and D. A. Dougherty, *ACS Chem. Biol.*, 2011, **6**, 1063-1068.
7 S. L. Monahan, H. A. Lester and D. A. Dougherty, *Chemistry & Biology*, 2003, **10**, 573–580.
8 K. N.-M. Daeffler, phd, California Institute of Technology, 2014.
9 J. P. Capone, P. A. Sharp and U. L. RajBhandary, *EMBO J.*, 1985, **4**, 213–221.
10 N. Heldring, A. Pike, S. Andersson, J. Matthews, G. Cheng, J. Hartman, M. Tujague, A. Ström, E. Treuter, M. Warner and J.-Å. Gustafsson, *Physiological Reviews*, 2007, **87**, 905–931.
11 M. D. Driscoll, G. Sathya, M. Muyan, C. M. Klinge, R. Hilf and R. A. Bambara, *J. Biol. Chem.*, 1998, **273**, 29321–29330.
12 J. P. Gallivan and D. A. Dougherty, *PNAS*, 1999, **96**, 9459–9464.
13 A. Maggi, *Biochim Biophys Acta*, 2011, **1812**, 1054–1060.
14 P. M. England, H. A. Lester and D. A. Dougherty, *Tetrahedron Letters*, 1999, **40**, 6189–6192.
15 D. T. Infield, J. D. Lueck, J. D. Galpin, G. D. Galles and C. A. Ahern, *Scientific Reports*, 2018, **8**, 5166.
16 K. Nozawa, P. O'Donoghue, S. Gundllapalli, Y. Araiso, R. Ishitani, T. Umehara, D. Söll and O. Nureki, *Nature*, 2009, **457**, 1163–1167.
17 B. S. Negrutskii and M. P. Deutscher, *Proc. Natl. Acad. Sci. U.S.A.*, 1991, **88**, 4991–4995.
18 C. Köhrer, L. Xie, S. Kellerer, U. Varshney and U. L. RajBhandary, *PNAS*, 2001, **98**, 14310–14315.
19 J. M. Dewe, J. M. Whipple, I. Chernyakov, L. N. Jaramillo and E. M. Phizicky, *RNA*, 2012, **18**, 1886–1896.
20 A. N. Sasikumar, W. B. Perez and T. G. Kinzy, *Wiley Interdiscip Rev RNA*, 2012, **3**, 543–555.
21 J. M. Whipple, E. A. Lane, I. Chernyakov, S. D'Silva and E. M. Phizicky, *Genes Dev.*, 2011, **25**, 1173–1184.
22 M. W. Nowak, J. P. Gallivan, S. K. Silverman, C. G. Labarca, D. A. Dougherty and H. A. Lester, *Meth. Enzymol.*, 1998, **293**, 504–529.
23 C. Kao, M. Zheng and S. Rüdisser, *RNA*, 1999, **5**, 1268–1272.

Chapter 3: Exploration of Singlet Oxygen-Mediated Upconversion as an Upconversion Phenomenon with Potential Applications in Biological Systems

3.1 Abstract

In recent years, significant interest has arisen in understanding complex photophysical phenomena and exploiting them for a variety of biological and chemical purposes. Singlet fission, triplet-triplet annihilation, and delayed fluorescence are all actively being adapted into practical applications. One photophysical phenomenon that has yet to be fully explored is singlet oxygen-mediated upconversion (SOMUC). A complex interplay of energy transfer events that ultimately produces an excited state singlet, SOMUC occurs when a ground state dye interacts with singlet oxygen and is subsequently excited to the triplet state. This triplet state dye subsequently interacts with a second molecule of singlet oxygen and undergoes a second energy transfer event to reach the singlet excited state. From this point, the molecule behaves as a directly excited molecule would. If a dye is capable of generating singlet oxygen itself, this process can occur long after an initial excitation event, giving delayed fluorescence. Unfortunately, due to the small number of dyes that undergo SOMUC and the lack of a defined application, research in the area has been slow. Still, recent interest in novel imaging techniques involving singlet oxygen, such as singlet oxygen triplet energy transfer, suggest that biological applications may exist for SOMUC. A better understanding of the photophysics involved in the process would help determine whether this was true. Described herein are attempts to better described the process of SOMUC in water using a robust singlet oxygen generator, Rose Bengal, and a SOMUC acceptor, $AlPcS_4$.

3.2 Introduction

3.2.1 Photophysics of Singlet Oxygen-Mediated Upconversion

Complex photophysical phenomena in dyes are being investigated with increasing intensity as their utility is becoming more apparent. Although a number of processes have been described, singlet fission, triplet-triplet annihilation, and delayed fluorescence are the most prominent among them, particularly in terms of practical applications. Singlet fission is being used to develop novel solar materials, triplet-triplet annihilation is being used as the basis for dye-sensitized solar cells, and delayed fluorescence is being used for organic light emitting diodes. [1–4] All three processes have been integral in redefining the use of light

in day-to-day chemistry. Although they seem complex, these processes are ultimately relatively straightforward events in the context of a Jablonski diagram. In singlet fission, one excited state singlet chromophore interacts with a neighboring ground state chromophore to generate two excited state triplet chromophores, providing a greater number of excited state species at lower energies (Figure 1A). Due to the short lifetime of the singlet state, this is usually an intramolecular event. In triplet-triplet annihilation, two excited state triplet chromophores interact to produce one excited state singlet chromophore and one ground state chromophore (Figure 1B). This can be intramolecular or intermolecular, as the triplet state is much longer lived than the singlet state. In delayed fluorescence, a molecule that has relaxed into a lower energy excited state is returned to an emissive excited state allowing it to fluoresce (Figure 1C). This can occur via a number of ways, but one of the most common is through thermal excitation.

A photophysical process that has received significantly less attention than the three denoted is singlet oxygen-mediated upconversion (SOMUC). In this process a chromophore is excited from the ground state to the triplet state by interacting with an excited state oxygen molecule known as singlet oxygen (Figure 2).[5] Following this initial energy transfer, the now triplet state chromophore interacts with a second molecule of singlet oxygen, initiating a second energy transfer and producing an excited state singlet chromophore. A variation on this process exists where two chromophores are first excited to the triplet state via singlet oxygen, then interact with each other via

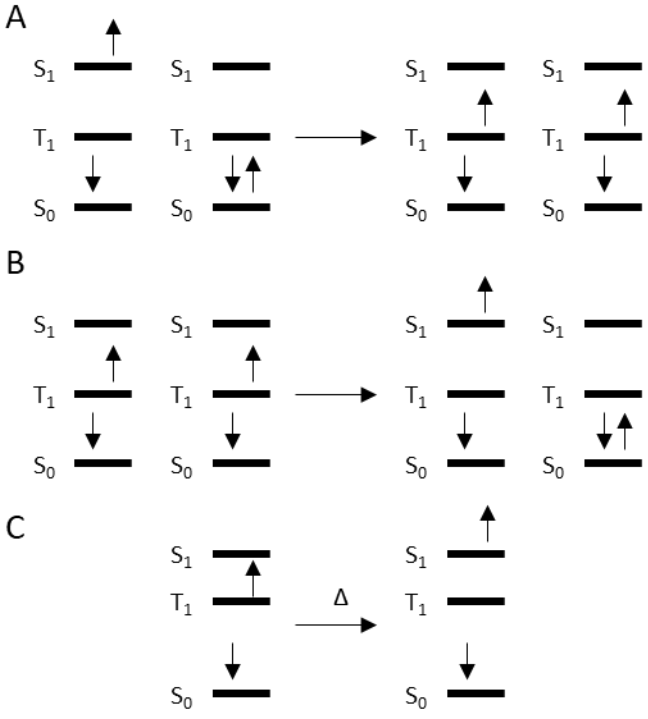

Figure 1: Energy level diagrams for common photophysical processes. A.) Singlet fission. B.) Triplet-triplet annihilation. C.) Delayed fluorescence (thermally activated in this case).

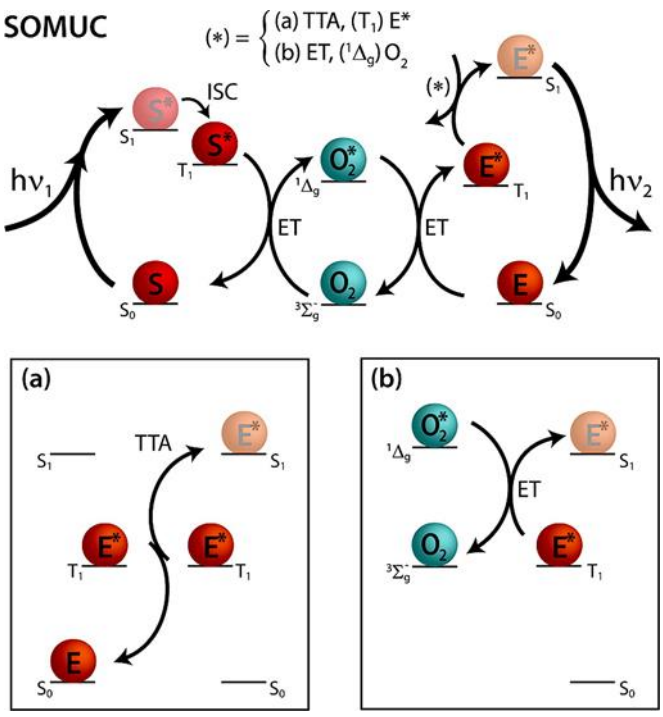

Figure 2: Singlet Oxygen-Mediated Upconversion. The S stands for sensitizer and the E for emitter. Adapted from Fückel et al.[5]

triplet-triplet annihilation to generate a singlet excited state chromophore and a ground state chromophore. As described so far, SOMUC requires both a sensitizer capable of generating singlet oxygen and a chromophore capable of using the energy; however, in a number of systems explored, the same dye serves both roles.

There are three reasons why SOMUC has not yet been explored in depth. The first is that the process is fairly complex. Singlet fission, triplet-triplet annihilation, and delayed fluorescence all required a single step after excitation to obtain the final excited state, whereas SOMUC is a multistep process. The second is that few dyes are capable of accepting energy from singlet oxygen, which has hampered attempts to develop SOMUC systems. The third is that few practical applications for SOMUC have been shown to date. Although NIR upconversion has been demonstrated using the method, the low quantum yields obtained were far from compelling.[5] Despite these limitations, SOMUC is still being studied, albeit at a much slower pace than previously mentioned biophysical processes.

A version of SOMUC that leads to fluorescence, known as singlet oxygen-sensitized delayed fluorescence (SOSDF), was first demonstrated in 1968 using the chromophore violanthrone.[6] When exposed to chemically generated singlet oxygen, the chromophore was shown to glow red, suggesting excitation of the dye was occurring via an energy transfer process. Over the years, similar processes were observed in the context of chemically generated singlet oxygen, thermally generated singlet oxygen, and photochemically generated singlet oxygen, supporting the notion that singlet oxygen was capable of

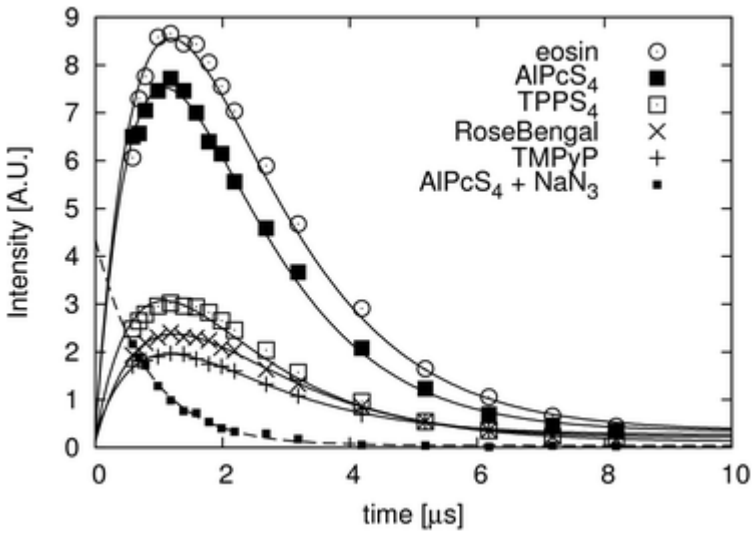

Figure 3: Singlet oxygen-sensitized delayed fluorescence with common water soluble photosensitizers. A trace including NaN_3 (as singlet oxygen quencher) is included as a control. Adapted from Scholz et al.[10]

exciting certain chromophores from the ground state to the excited state via energy transfer processes.[7–10] Most recent among these studies was an investigation into different chromophores and their SOSDF in the context of an aqueous environment.[10] This study analyzed the ability of six common water soluble photosensitizers ($AlPcS_4$, $TPPS_4$, TMPyP, Methylene Blue, Rose Bengal, and Eosin Y) to mediate singlet oxygen-sensitized delayed fluorescence.[10] All of the dyes except methylene blue were capable of producing a delayed fluorescence response, although Eosin Y and $AlPcS_4$ did so the most robustly (Figure 3).[10] To ensure that this fluorescence was a consequence of singlet oxygen generation, a number of controls were run. First, the excitations and observation were carried out in the presence of NaN_3, a known singlet oxygen quencher. The presence of azide significantly inhibited delayed fluorescence, suggesting that the effect was oxygen mediated.[10] To provide further proof, SOSDF experiments were next run in deuterated solvent. Since solvent deuteration increases the lifetime of singlet oxygen, it was expected that the lifetime of the delayed fluorescence would also increase if the delayed fluorescence was singlet oxygen dependent. An increased fluorescence lifetime was observed in D_2O, corroborating the azide results.[10] Finally, the intensity of SOSDF was evaluated as a function of the concentration of oxygen in solution. Interestingly, a parabolic curve was observed, suggesting that SOSDF was indeed dependent on the concentration of oxygen, but that the mechanism was fairly complex.[10] In total, these results demonstrated that a number of common photosensitizers were capable of SOSDF.

3.2.2 Singlet Oxygen in Biology

In addition to verifying the oxygen dependent nature of SOSDF in select water soluble photosensitizers, the authors examined SOSDF in the context of mammalian cells, specifically 3T3 mouse fibroblasts.[10] They determined that SOSDF was possible in cells using a suspension of fibroblasts[10], a result that was later corroborated in adherent cells.[11] Although this observation itself is of little practical use, it is interesting in the context of other singlet oxygen based phenomena. Specifically, singlet oxygen has previously been used to characterize protein-protein interactions through a method known as singlet oxygen triplet energy transfer (STET). Although this method is incredibly robust for evaluating long range protein-protein interactions, it cannot provide temporal information. The ability to evaluate protein-protein interactions in real time through a singlet oxygen mediated event would provide a significant breakthrough in understanding long range protein-protein interactions, and the fact that SOSDF occurs in cells suggests that SOSDF may be able provide the temporal component absent in STET.

STET is a process by which the spatial relationship of a singlet oxygen generator and a singlet oxygen sensor are determined based on quenching of the singlet oxygen sensor by the singlet oxygen generator (Figure 4).[12] This method can conceptually be compared to FRET, where an energy transfer event produces either quenching or excitation, however, it is an irreversible process, as the quenching is chemical in nature and can occur only once. The value of STET is that it can evaluate long range protein-protein interactions due the distance singlet oxygen can travel in its lifetime.[12] Its limitation is that is has no temporal resolution; once the singlet oxygen sensor is quenched, no additional observations can be made.[12] A process in which an event mediated by singlet oxygen was reversible would overcome the limitations inherent to STET. Although chemical quenching events are either too destructive or too slow to be considered reversible in the context of a cell, it is

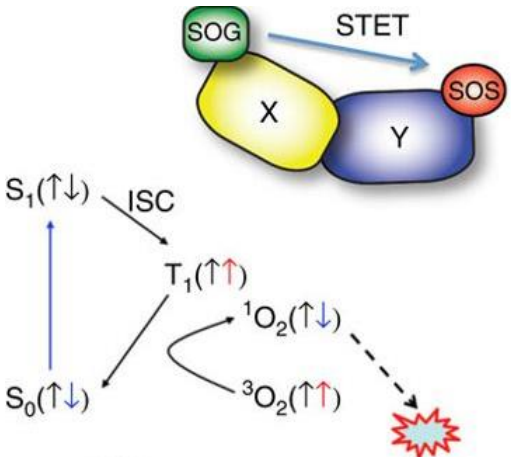

Figure 4: Schematic of STET. Both the biological and photophysical principles are shown. Adapted from To et al.[11]

possible that a photophysical event, such as SOSDF, would provide a reversible, observable readout. Before exploring the potential biological applications of SOSDF, however, a greater photophysical description of the process is required.

3.3 Results and Discussion

3.3.1 Development of an SOSDF Assay

To determine whether or not SOSDF could be of practical use in a biological system, a better understanding of the underlying photophysical processes was pursued. Because a novel data collection setup had to be developed, the first attempts at using singlet oxygen-mediated upconversion were focused on recapitulating data previously obtained with a robust SOSDF system.[9] Specifically, an upconversion-capable phthalocyanine known as tBPc and the singlet oxygen sensitizer C60 were irradiated in C_6D_6.[9] tBPc was selected for its high SOMUC efficiency and solubility in nonpolar solvents, C60 was chosen for its high singlet oxygen yields and low fluorescence background, and C_6D_6 was chosen for the extremely long lifetime of singlet oxygen in the solvent. In combination, the system produced delayed fluorescence that lasted hundreds of microseconds.[9] Working with Oliver Shafaat on developing a data collection setup, we were capable of reproducing previously observed data (Figure 5). Importantly, upon freeze-pump-thawing samples (a process that removes most oxygen), no delayed fluorescence was observed, demonstrating that the observed process was indeed a singlet oxygen mediated event.

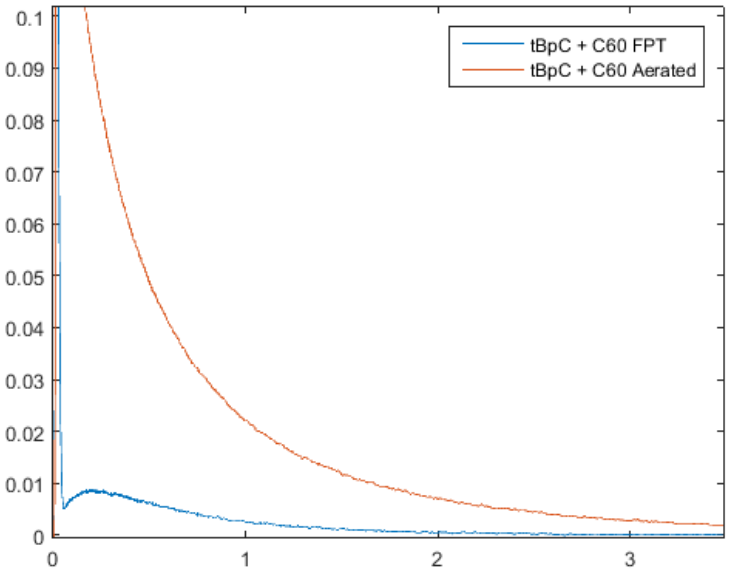

Figure 5: SOMUC of tBPc in C_6D_6 via excitation of C60. C60 was excited at 532 nm. Extreme signal decrease is seen upon FPT, demonstrating that the process is singlet oxygen dependent. The X-axis is time in seconds and Y-axis is relative intensity.

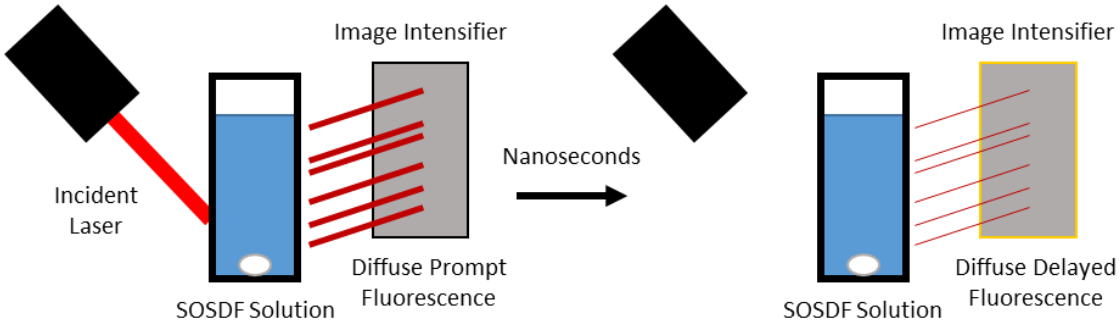

Figure 6: Simplified setup for the collection of SOSDF data. Laser excitation of an SOSDF solution produces prompt fluorescence, which is not collected by the image intensifier, as it is not on. After hundreds of nanoseconds, the image intensifier turns on and begins collecting emission data, however, at this point all light collected is either phosphorescence or delayed fluorescence. Due to the low intensity of delayed fluorescence, significant surface area on the image intensifier is required to get enough signal.

Following the success of this initial event, the setup was refined to allow analysis of systems with much shorter lifetimes in D_2O (Figure 6). To simplify initial attempts with this setup, SOSDF was attempted with a single chromophore, $AlPcS_4$, rather than with a two component system. Capturing these data proved significantly more difficult, as the shortened fluorescence life time in D_2O led to significant overlap between prompt fluorescence and delayed fluorescence. This prompt fluorescence would overload the image intensifier, making it impossible to capture the subtleties associated with delayed fluorescence. To overcome this issue, we instituted a trigger that offset photon collection by 100s of nanoseconds from the initial irradiation event. This allowed a majority of the prompt fluorescence to cease prior to collection, which resulted in much cleaner delayed fluorescence spectra. Using a 625 nm excitation laser, a delayed fluorescence lifetime was obtained that was comparable to that previously reported.[10] As in the initial experiments, a freeze-pump-thawed (FPT) sample was compared to an atmospheric sample to determine the effect of oxygen on the $AlPcS_4$ delayed fluorescence spectra. Interestingly, signal was observed for both the FPT and the atmospheric sample, but the traces were very different. The FPT sample gave a long, slow decline, suggestive of phosphorescence, whereas the atmospheric sample gave a sharp curve comparable to previous SOSDF data (Figure 7). Either way, these data demonstrated that delayed emissions for $AlPcS_4$ could be visualized using our setup, and that more complicated experiments could be run.

3.3.2 Exploration of Factors Affecting SOSDF Signal Intensity and Duration

Having determined a suitable setup for measuring delayed fluorescence, the SOSDF intensity was evaluated at varying concentrations of $AlPcS_4$ (Figure 8). As expected, an approximately linear trend was observed for intensity as a function of concentration. Interestingly, the fluorescence lifetime also shifted a small amount as a function of $AlPcS_4$ concentration, but never significantly enough to suggest that it would be a variable worth monitoring in the context of a biological application. The consistent results obtained with $AlPcS_4$ prompted exploration of two component SOSDF systems.

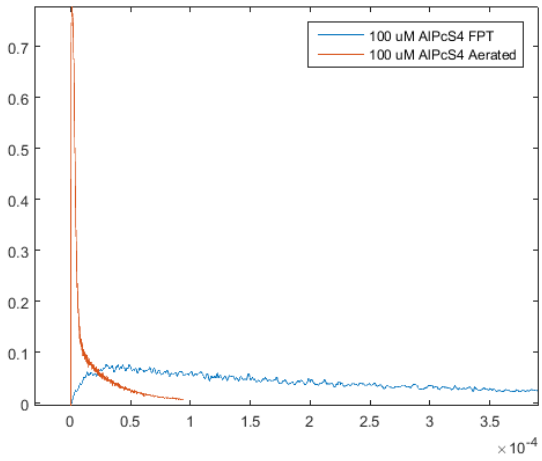

Figure 7: Delayed emission spectra of $AlPcS_4$. Shown are atmospheric and FPT samples. The X-axis is time in seconds and Y-axis is relative intensity.

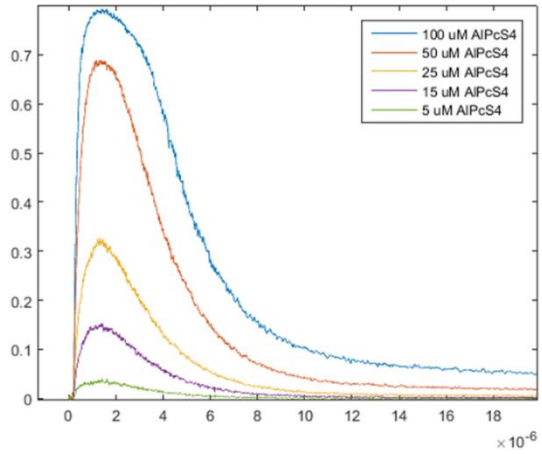

Figure 8: $AlPcS_4$ SOSDF as function of concentration. The X-axis is time in seconds and Y-axis is relative intensity.

Three dyes were initially considered to complement $AlPcS_4$: Eosin Y, TMPyP, and Rose Bengal. Eosin Y was explored first due to its synthetic utility, however, it produced too low of a signal to be used. TMPyP was explored next due to its desirable photophysical properties. Unfortunately, it formed a ground-state complex with $AlPcS_4$ (as seen by UV-Vis), making it impossible to generate singlet oxygen. Rose Bengal was explored last. Even though it has favorable photophysical properties and water solubility, its emission profile overlaps with the absorption profile of $AlPcS_4$, and therefore was avoided on the off chance that it participated in other photophysical processes such as FRET. Despite this initial concern, Rose Bengal produced the best two component SOSDF signal with $AlPcS_4$ and was selected for use in all future studies (Figure 9). This initial excitation and all subsequent excitations utilizing Rose Bengal were carried out at a 532 nm excitation wavelength.

Before proceeding with further SOSDF experiments, three concerns were addressed. The first was the fact that in all previous setups, a small amount of background signal existed regardless of the conditions used. To explore lower concentration SOSDF solutions, this background needed to be eliminated completely, so the optical setup was optimized with blackout curtains to ensure no extraneous light entered. This ultimately had a large effect, reducing the background noise to negligible levels for subsequent experiments. The second was that Rose Bengal and $AlPcS_4$ could possibly FRET and obscure the SOSDF results in the process. To determine whether or not this was an issue, picosecond absorption spectroscopy was done to evaluate the lifetime of the Rose Bengal excited state as a function of the $AlPcS_4$ concentration (Figure 10). A lifetime of approximately 100 picoseconds was observed for all concentrations of $AlPcS_4$, demonstrating that FRET was not a significant phenomenon, even at high levels of $AlPcS_4$ and suggesting that the duo was worth using for continued SOSDF experiments. The final concern addressed was whether or not $AlPcS_4$ would undergo SOSDF upon excitation at 532 nm. Although $AlPcS_4$ does not have significant absorbance in this area, any autonomous SOSDF would have

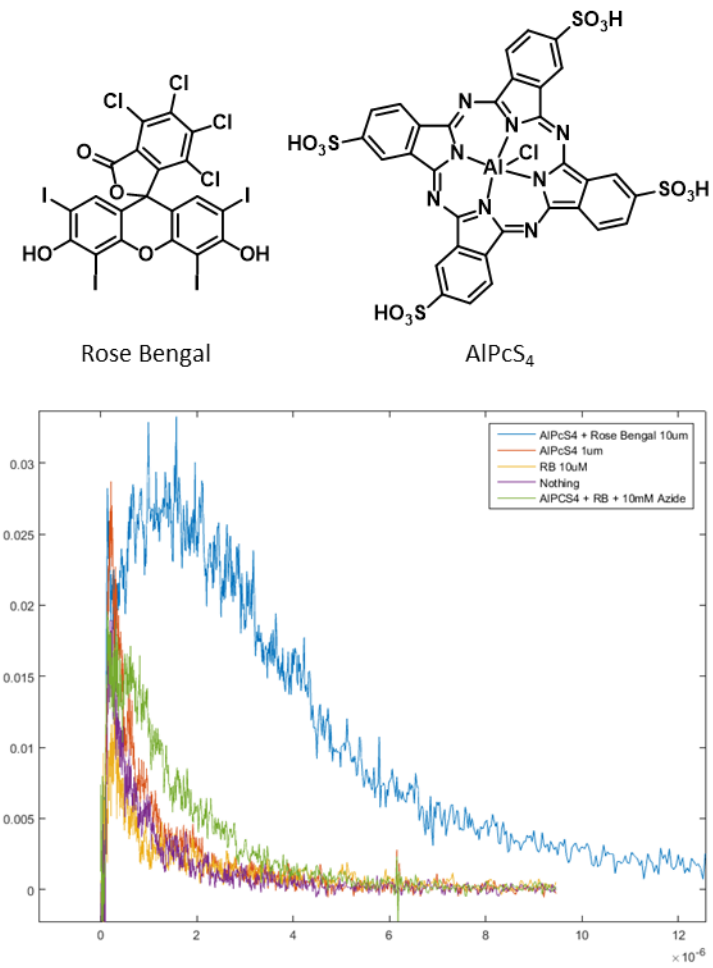

Figure 9: RB-$AlPcS_4$ SOSDF. Rose Bengal and $AlPcS_4$ are shown above the spectra. The complete excitation system is shown in blue, whereas all other colors represent controls. Notably, a small amount of background signal exists regardless of the solution, suggesting some inherent noise in the imaging conditions. The X-axis is time in seconds and Y-axis is relative intensity.

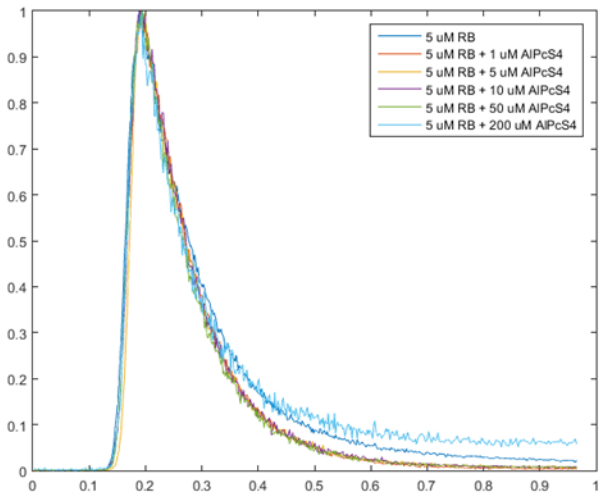

Figure 10: Rose Bengal lifetime as a function of $AlPcS_4$ concentration. The X-axis is time in nanoseconds and Y-axis is relative intensity.

an effect on the final results and should be considered. Surprisingly, a small amount of delayed fluorescence was observed when irradiating $AlPcS_4$ at 532 nm (Figure 11). The results were inconsistent (even when irradiating at similar concentrations), but in all cases the observed lifetimes were significantly less than those associated with the Rose Bengal-$AlPcS_4$ combination. Although this result was slightly disheartening, the small magnitude of the emission suggested that it would not significantly affect interpretation of the combination SOSDF data.

Having addressed the three concerns associated with the SOSDF setup and chromophore combination, a series of experiments was run to understand the effects of concentration on the two component system. Starting by keeping the Rose Bengal concentration constant at 10 μM, the concentration of $AlPcS_4$ was varied (Figure 12). Unfortunately, the precautions taken to limit the amount of background signal significantly reduced overall signal, resulting in noisier spectra. That being said, the spectra were still interpretable. Interestingly, the concentration of $AlPcS_4$ seemed to have little effect on either the lifetime or intensity produced by the SOSDF. An increase in the $AlPcS_4$ concentration should mean that more singlet oxygen is being funneled into ground state $AlPcS_4$ rather than the $AlPcS_4$ excited state

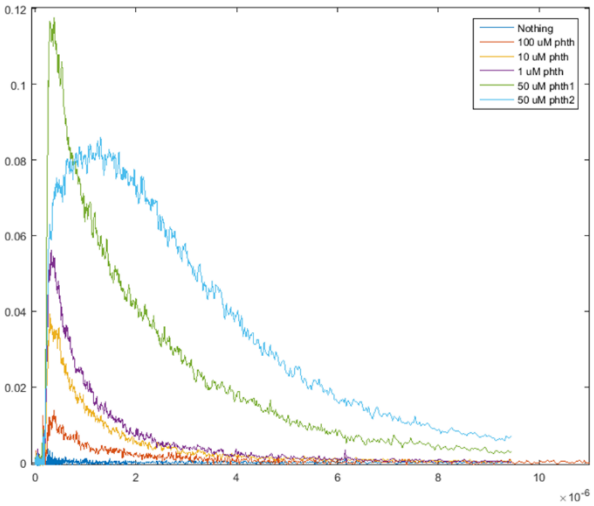

Figure 11: $AlPCs_4$ SOSDF at 532 nm. The X-axis is time in nanoseconds and Y-axis is relative intensity.

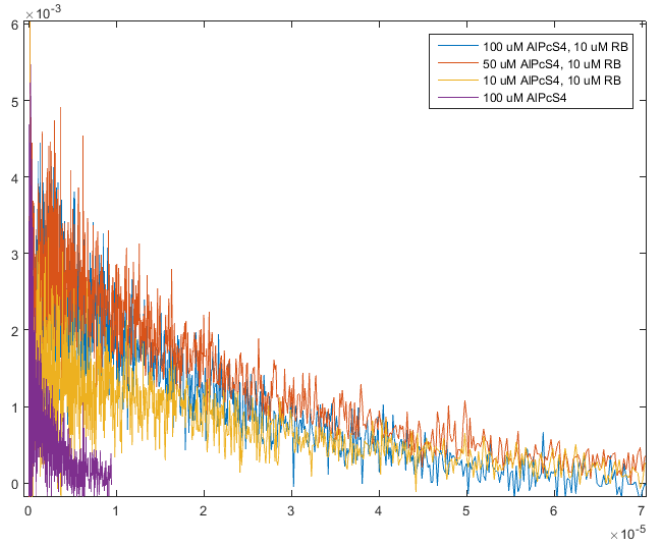

Figure 12: RB-AlPcS$_4$ SOSDF as a function of AlPcS$_4$ concentration. The X-axis is time in seconds and Y-axis is relative intensity.

triplet, failing to produce delayed fluorescence. However, these data demonstrate that the end result of excitation is similar regardless. This suggests that the generated AlPcS$_4$ triplet state is still productive in the context of SOSDF, either undergoing triplet-triplet annihilation to generate singlet excited states or relaxing via sensitization of oxygen and reinitiating the process. Next, the concentration of Rose Bengal – and consequently singlet oxygen – was varied while the concentration of AlPcS$_4$ was kept constant at 10 μM (Figure 13). This had a significantly larger effect on the signal intensity, as well as on the lifetime. Although the signal intensity increased approximately linearly as a function of Rose Bengal concentration, the lifetime decreased slightly as the Rose Bengal concentration increased. This is a somewhat surprising result, but the effect was not large enough to warrant a more in depth evaluation. As mentioned previously, some inherent SOSDF is observed when AlPcS$_4$ is irradiated at 532 nm. Although a factor of ten difference in lifetime exists between AlPcS$_4$ SOSDF and dual chromophore SOSDF at this wavelength, to understand this result more qualitatively, traces from both systems were normalized and compared. Reassuringly, the two decay patterns differ significantly (Figure 14). Although autonomous SOSDF

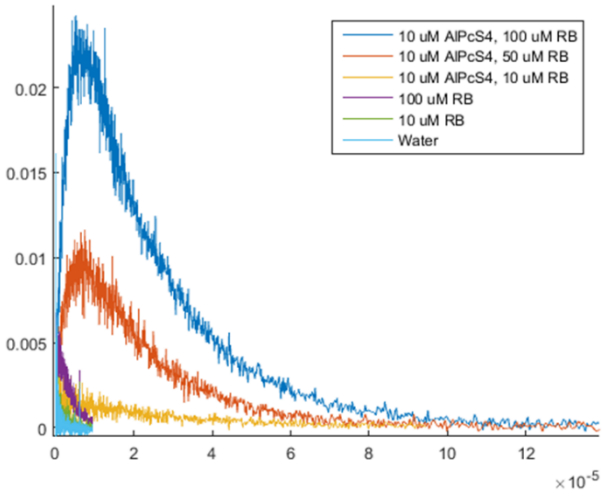

Figure 13: AlPcS$_4$-RB SOSDF as a function of RB concentration. The X-axis is time in seconds and Y-axis is relative intensity.

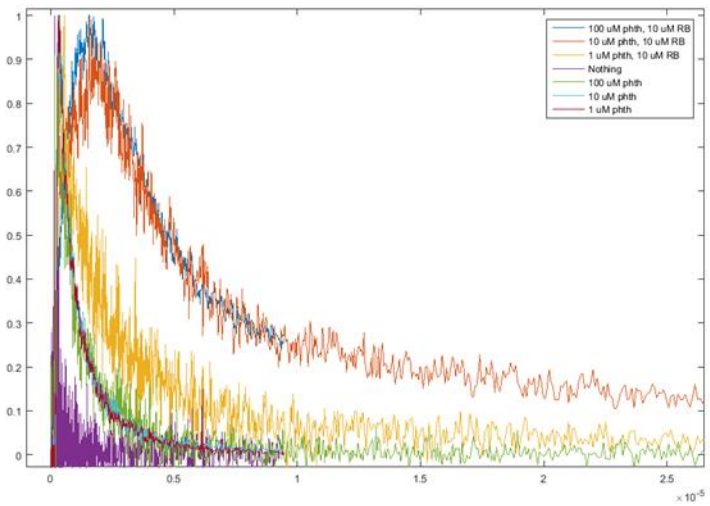

Figure 14: Comparison of $AlPcS_4$ SOSDF (denoted phth) and $AlPcS_4$-RB SOSDF. The X-axis is time in seconds and Y-axis is relative intensity.

is unavoidable in this system, it seems as though it does not obscure the dual chromophore SOSDF results.

Having determined the concentration effects of the two partners, the sensitivity of the process to singlet oxygen was next evaluated. First, a FPT irradiation containing 100 μM of both chromophores was run and compared to an atmospheric sample. As expected, no significant delayed fluorescence was observed (Figure 15). Since quenching with azide had already been demonstrated in earlier SOSDF combo experiments, solvent effects were next evaluated.

As expected, irradiation in H_2O gave significantly different lifetimes than irradiation in D_2O (Figure 16). Interestingly, the lifetime difference – a factor of 10 – tracks well with the difference in singlet oxygen lifetimes in the two solvents. Having extensively demonstrated the dependence of the delayed fluorescence on oxygen, the next step was to evaluate the phenomenon in a more biological setting.

To approximate a more biological setting, SOSDF experiments were next run in cell lysate. Starting with a low concentration of cell lysate (10 %) mixed with either H_2O and D_2O, lifetimes were observed that were similar to samples containing no cell lysate (Figure 17). Interestingly, although the lifetime did not change significantly, a decrease in SOSDF

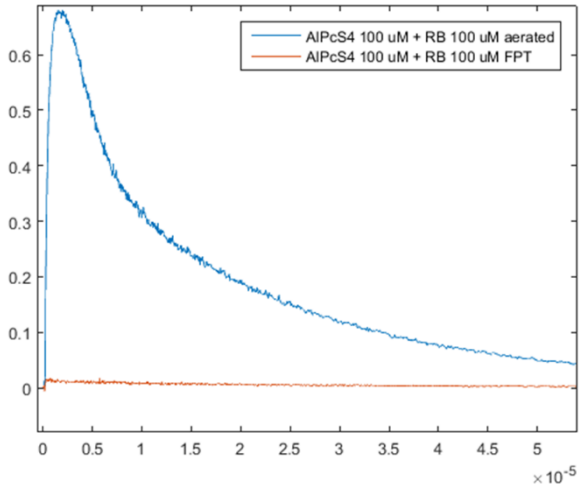

Figure 15: $AlPcS_4$ SOSDF under atmospheric and FPT conditions. The X-axis is time in seconds and Y-axis is relative intensity.

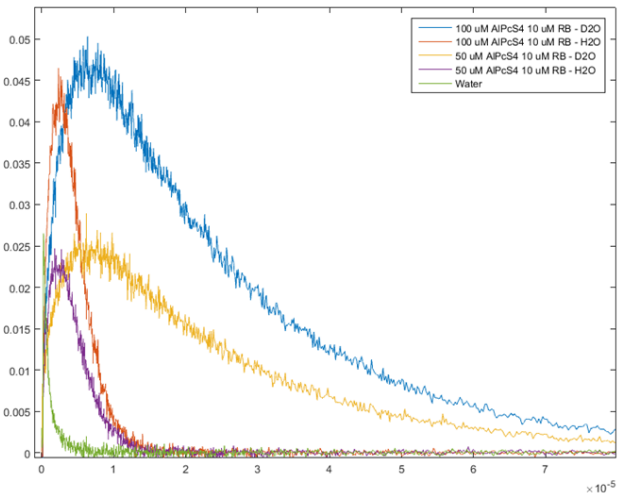

Figure 16: Effects of solvent deuteration on SOSDF. The X-axis is time in seconds and Y-axis is relative intensity.

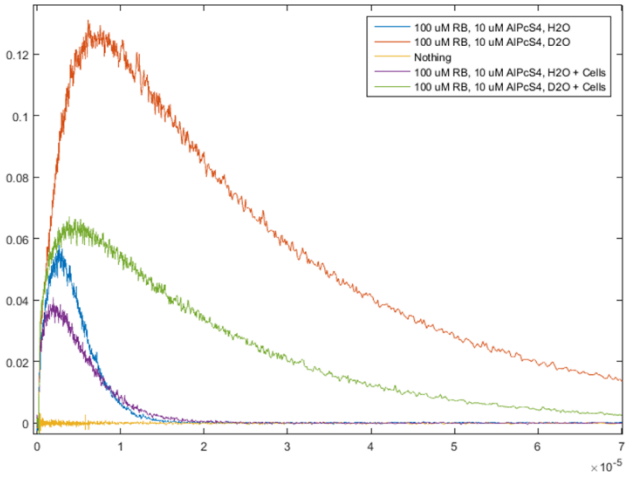

Figure 17: SOSDF in the presence of 10% cell lysate. The X-axis is time in seconds and Y-axis is relative intensity.

intensity was noticeable, suggesting that fluorescence is either being absorbed or scattered by the lysate. Upon increasing the concentration of lysate to 55%, a shift in lifetime was observed in the case of the D_2O sample. Given that the lysate is in H_2O, it is somewhat difficult to determine whether or not the effect is a consequence of the biological environment or the H_2O. Regardless, the H_2O sample did not shift significantly, suggesting that at the very least the described dual chromophore SOSDF could work in a biological system.

At this point, the Rose Bengal-$AlPcS_4$ combination had been thoroughly vetted, however, before moving into a more complicated system, I wanted to find a set of dyes capable of singlet oxygen-mediated upconversion. By using singlet oxygen to upconvert a long wavelength excitation to a shorter wavelength emission, ambiguities associated with $AlPcS_4$ self-excitation would be cleaned up and ultimately a more robust SOSDF system would be developed. Furthermore, upconversion is itself of practical importance. No dye like this existed, so I set out to synthesize one. Unfortunately, my Ph.D. completed before I was capable of revisiting this topic with a novel set of dyes.

3.4 Conclusion

Singlet oxygen sensitized delayed fluorescence is an unexplored photophysical phenomenon. Described herein were efforts to better describe SOSDF in the context of an aqueous, dual chromophore system. Results demonstrated the importance of individual components, and suggested that the obtained signal was sensitive to both the environment and the concentration of singlet oxygen, facts that could potentially be exploited for biological imaging. Further exploration of SOSDF is warranted, both in the context of the described Rose Bengal-$AlPcS_4$ system and in the context of upconversion.

3.5 Materials and Methods

3.5.1 Materials

$AlPcS_4$ was obtained from Frontier Scientific. Rose Bengal, Eosin Y, and TMPyP were obtained from Sigma-Aldrich. Deuterated solvents were obtained from Cambridge Isotope Laboratories. Quartz cuvettes were obtained from Starna Cells, and FPT capable quartz cuvettes were generated in the glass shop at Caltech.

3.5.2 Irradiation Experiments

Irradiation experiments were carried out on laser tables in Caltech's Beckman Institute Laser Resource Center with the help of Oliver Shafaat and Jay Winkler. Two different lasers were used depending on the application. A nanosecond laser was used for all SOSDF experiments, and a picosecond laser was used for all FRET experiments with Rose Bengal. The nanosecond laser used was a Spectrophysics Quanta Ray Nd:YAG OPO system capable of producing a range of visible wavelengths for irradiation. Data from Nd:YAG irradiations were collected via an Oriel Image Intensifier, which was set to activate after the end of the irradiation pulse. All setup was monitored using a Teledyne Lecroy Wavejet Touch 364 oscilloscope. The picosecond laser setup was devised by Jay Winkler, and also utilizes an Nd:YAG laser source. Data collection for the FRET experiments was performed using a Hamamatsu spectrophotometer. All irradiations were performed using quartz cuvettes with a 1 cm path length and stirring solutions.

3.5.3 Freeze-Pump-Thaw Protocol

Using a specially designed quartz cuvette, solvent was frozen under atmospheric conditions in an attached glass bulb. A vacuum was then applied to remove all gas, and the solvent allowed to thaw under the degassed conditions. This allowed dissolved gas to escape into the headspace. The process was repeated twice more without exposing the system to the atmosphere. After the final cycle of thawing, the sample was placed under argon and transferred from the glass bulb to the quartz cuvette for irradiation.

3.6 References

1 B. D. Ravetz, A. B. Pun, E. M. Churchill, D. N. Congreve, T. Rovis and L. M. Campos, *Nature*, 2019, **565**, 343.
2 Y. Liu, C. Li, Z. Ren, S. Yan and M. R. Bryce, *Nature Reviews Materials*, 2018, **3**, 18020.
3 J. Zhao, S. Ji and H. Guo, *RSC Adv.*, 2011, **1**, 937–950.
4 M. B. Smith and J. Michl, *Chem. Rev.*, 2010, **110**, 6891–6936.
5 B. Fückel, D. A. Roberts, Y. Y. Cheng, R. G. C. R. Clady, R. B. Piper, N. J. Ekins-Daukes, M. J. Crossley and T. W. Schmidt, *J. Phys. Chem. Lett.*, 2011, **2**, 966–971.
6 E. A. Ogryzlo and A. E. Pearson, *J. Phys. Chem.*, 1968, **72**, 2913–2916.
7 Y. Fu, A. A. Krasnovsky and C. S. Foote, *J. Am. Chem. Soc.*, 1993, **115**, 10282–10285.
8 A. A. K. Jr and V. S. Stremedlovskaya, *Journal of Porphyrins and Phthalocyanines*, 2008, **12**, 1194-1200.
9 S. T. Murphy, K. Kondo and C. S. Foote, *J. Am. Chem. Soc.*, 1999, **121**, 3751–3755.
10 M. Scholz, R. Dědic, T. Breitenbach and J. Hála, *Photochemical & Photobiological Sciences*, 2013, **12**, 1873–1884.
11 M. Scholz, A.-L. Biehl, R. Dědic and J. Hála, *Photochem. Photobiol. Sci.*, 2015, **14**, 700–713.
12 T.-L. To, M. J. Fadul and X. Shu, *Nature Communications*, 2014, **5**, 4072.

Chapter 4: Exploration of Phenothiazine Derivatives as Singlet Oxygen-Mediated Photoremovable Protecting Groups

4.1 Abstract

Recent work by Schnermann and coworkers has demonstrated the potential of singlet oxygen-mediated photodeprotection. Their work was inspired by the oxidative instability of cyanine dyes, which collapse upon interaction with singlet oxygen. By joining a cyanine dye to an appropriate leaving group, the method was used to liberate both alcohols and amines. Despite the success of these cyanine dye protecting groups, this design principle has yet to be expanded to other systems. This is surprising, as the potential of this breakthrough is significant; the photochemical generation of singlet oxygen has been demonstrated at much longer wavelengths than has direct photochemical deprotection, providing an opportunity for long wavelength photodeprotection. Further expansion of the methodology could be pursued via a number of avenues, however, of particular interest are scaffolds based on a phenothiazine backbone. The phenothiazine backbone is particularly promising due to the high singlet oxygen quantum yields and synthetic modularity that are associated with it. Described herein are initial attempts to generate scaffolds capable of singlet oxygen-mediated photorelease based on a phenothiazine backbone. Different phenothiazine derivatives are explored, as are different cages that collapse in the presence of singlet oxygen. Here I describe progress in the realm of singlet oxygen mediated photorelease.

4.2 Introduction

4.2.1 Photoremovable Protecting Groups and Singlet Oxygen-Mediated Deprotection

Protecting groups are integral in both chemistry and biology. In chemistry, they help define reactivity and selectivity, affording new approaches for complex syntheses. In biology, they allow for the regulation of complex networks. Although the protecting groups used in the two disciplines vary drastically, they tend to overlap in the context of photochemistry. Photoremovable protecting groups have been shown to be immensely impactful in chemical biology since the first reports of photochemically caged cAMP and ATP were published approximately 50 years ago.[1,2]

Over the past 50 years, photochemists have primarily focused on trying to push the speed, selectivity, and applicability of photochemical processes, irrespective of the wavelength they utilize.[3] Recently,

however, an interest in *in vivo* biological applications for photoremovable protecting groups has brought to light the need for photochemical reactions that occur at longer wavelengths, where greater tissue penetration is obtained and less biological damage is incurred.[3] Significant progress has been made in this area – as a number of new reactions have been developed that utilize visible light – however, there is still much room for improvement.[4–9]

In the context of visible light mediated photodeprotection, three strategies have primarily been used. The first is direct deprotection via the excited state. Although this is challenging, exciting work is being done in this field, particularly with BODIPY dyes.[5,6,10] The second is deprotection mediated through secondary thermal events. Recently, our group has had success in this area, developing a quinone trimethyl lock photocage.[7] The third – a novel strategy that has been employed relatively recently – is the use of singlet oxygen to mediate oxidative events that lead to deprotection. This method has been met with significant excitement over the past few years[9,11], however, the breadth of this strategy has yet to be explored. Of these three strategies, the third is most applicable to long wavelength photochemistry; dyes (such as indocyanine green) are known that absorb above 800 nm and generate singlet oxygen.[12]

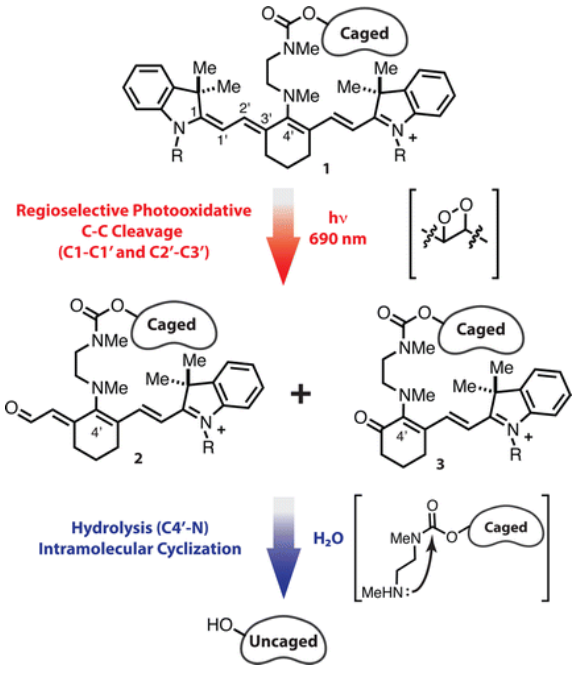

Figure 1: Proposed mechanism for cyanine photodeprotection mediated by singlet oxygen.

Schnermann and coworkers demonstrated that irradiation of cyanine dyes leads to the formation of singlet oxygen which adds to the conjugated backbone (Figure 1).[9] Following addition of singlet oxygen, subsequent collapse of the backbone occurs, which leaves behind an unstable intermediate. Further collapse of this intermediate can be coupled to ejection of a protecting group that will cyclize and release a free product. This process can be initiated across a range of cyanine dyes[9,11,13,14], and can be modified to release amines. Despite the promise

of this system, it suffers from a number of flaws. The first is the speed. The process is inherently slow, due to both low singlet oxygen quantum yields inherent to cyanine dyes and subsequent dark steps that occur slowly. This inhibits its utility in dynamic systems – initial experiments required a 30-minute irradiation followed by a four-hour incubation at 37°C to achieve 60% photorelease.[13] The second is the toxicity of the byproducts. Many of the cyanine dye decomposition byproducts are suspected to be toxic, limiting the use of the cage in biological systems. The final flaw is the substrate scope. Although recent papers have attempted to address this issue, the scope is still somewhat limited.[9,11,14]

4.2.2 *New Approaches for Singlet Oxygen-Mediated Deprotection*

To improve upon the concept of singlet oxygen mediated photorelease, a potent singlet oxygen generator must be combined with a singlet oxygen sensitive cage that is rapid and robust. For biological purposes the entire construct should be water soluble, suggesting an ideal starting point would be water soluble dyes. Although a number of water soluble dyes are known that generate singlet oxygen, phenothiazine dyes are particularly attractive, as they are synthetically accessible and can be modified for subsequent use. The most well-known phenothiazine dye is methylene blue (Figure 2A), which has found a number of uses in chemistry and biology. It is perhaps best known for its place on the World Health Organization's List of Essential Medicines – as it is used to treat methemoglobinemia – however, from a photochemist's perspective it is a robust singlet oxygen generator, with a quantum yield of 39%.[15] Notably, methylene blue derivatives have been described in which the amino methyl groups are replaced with more complex alkyl groups (Figure 2B), providing a starting point for subsequent modification with singlet oxygen sensitive cages.[16] Beyond methylene blue, some longer wavelength phenothiazine derivatives capable of generating singlet oxygen have been described, suggesting that singlet oxygen-mediated photodeprotection could be performed at wavelengths above 900 nm (Figure 2C).[17,18]

Although different singlet oxygen sensitive moieties have been described, two in particular standout. The first is an alkene dithioether comprised of two thioethers bridged by an alkene (Figure 3A). Collapse of this group is initiated by the addition of singlet oxygen across the double bond, leading to formation

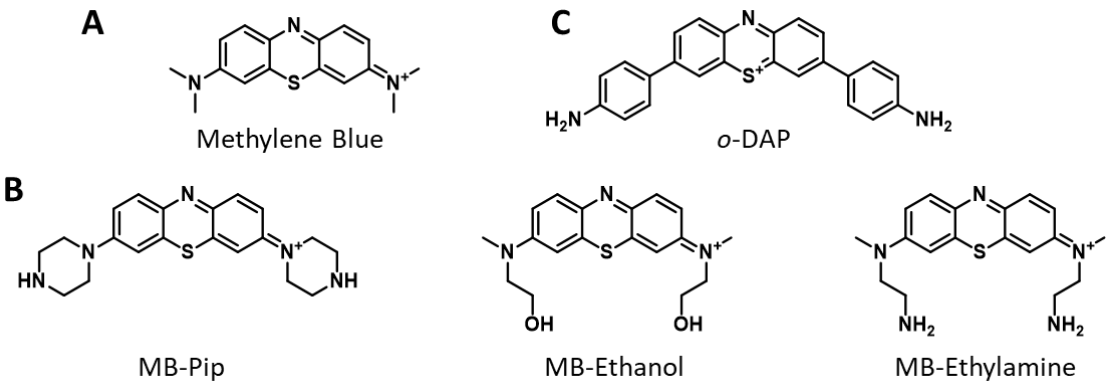

Figure 2: Methylene Blue and associated phenothiazine derivatives. A.) Structure of methylene blue. B.) Structure of select methylene blue derivatives characterized by Gollmer et al.[16] C.) Structure of NIR-phenothiazine derivative characterized by Hsieh et al.[18]

of a dioxetane. This dioxetane subsequently collapses to release thioesters, separating the previously linked components. This process is well characterized, and has been utilized in a number of applications where physical release is more important than the chemical context.[19,20] This cage is not without its flaws – mainly lower yields due to thioether oxidation and a thioester scar that is appended to the leaving group – however, it is fairly robust and is a good starting point for initial explorations into singlet oxygen mediated photorelease. The second singlet oxygen sensitive moiety to consider is anthracene. Singlet oxygen is known to readily add across anthracene, which is actually the basis for a number of singlet oxygen detectors, such as singlet oxygen sensor green.[21] Although this addition leads to no additional chemistry in the parent anthracene, in 9,10-dialkoxyanthracene derivatives (Figure 3B), the bridged oxygen will collapse following addition, leading to the formation of anthraquinone and the release of the alkoxy groups.[22] This process has only been demonstrated using alcohols, however, it stands to reason

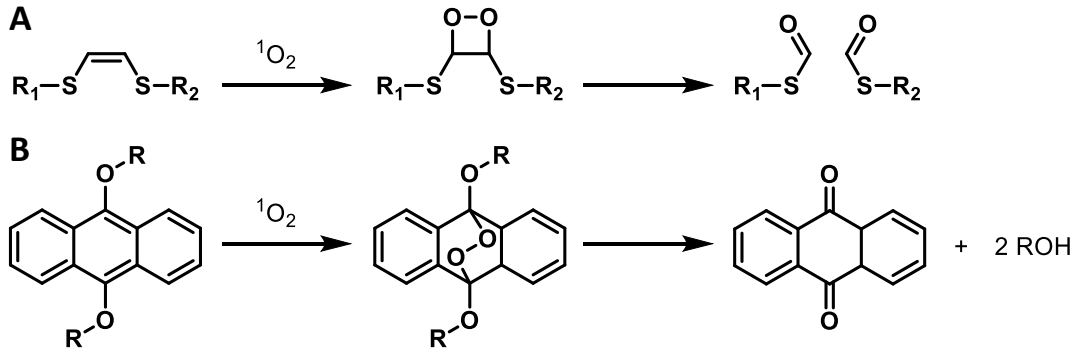

Figure 3: Singlet oxygen-mediated photorelease. A.) Alkene dithioether singlet oxygen-mediated photorelease. B.) Dialkoxyanthracene singlet oxygen mediated photorelease.

that similar reactivity would be obtained from anthracenes derivatized with amines and thiols, both of which are synthetically acessible.[23,24]

4.3 Results and Discussion

4.3.1 Exploration of Phenothiazine Derivatives as Singlet Oxygen Generators

To explore the possibility of singlet oxygen mediated-deprotection in the context of phenothiazines, derivatives were synthesized and evaluated for their ability to generate singlet oxygen. The first phenothiazine derivatives explored were based on a previously described long-wavelength phenothiazine derivative, *o*-DAP (Figure 2C). This dye has a λ_{max} of 957 nm, and was shown to decrease the signal associated with a singlet oxygen sensor – 1,3-diphenylisobenzofuran (DPBF) – upon irradiation with a broad spectrum NIR light (700-1000nm), which suggests that the dye can form singlet oxygen.[18] Despite the lack of a few notable controls, these results suggested that *o*-DAP was worth exploring further. Although the literature provided a synthetic route that purported reasonable yields, it was found that the described synthesis was difficult to recapitulate, particularly due to side product formation via cross-coupling to the amine of dibromophenothiazine. An alternative path to the product was designed (Figure 4), one that also afforded modification of the terminal anilines prior to the final deprotection and oxidation steps. Briefly, phenothiazine was brominated in the presence of bromine and acetic acid to produce dibromophenothiazine. This compound was subsequently subjected to protection via Boc anhydride, which gave protected product in good yield. Other protection strategies were explored, but were less robust. Next, a Suzuki coupling was used to couple the chromophore-extending aniline groups.

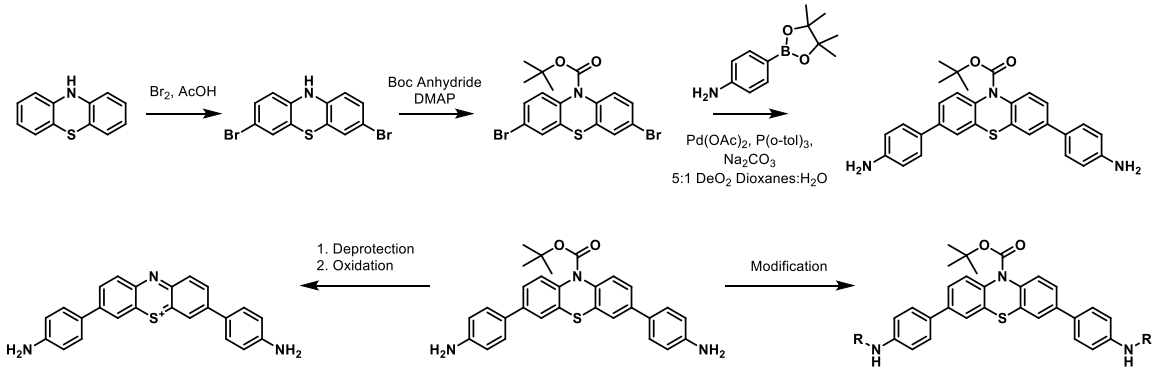

Figure 4: Redesigned *o*-DAP synthesis. A new synthesis was designed to obtain a protected *o*-DAP precursor that could either be deprotected and oxidized to give *o*-DAP or modified prior to deprotection and oxidation give an *o*-DAP derivative. This synthesis was designed due to an inability to recapitulate a reported synthesis.

Due to the protection of the phenothiazine amine, this reaction proceeded efficiently, yielding a product that was ready for subsequent modification or deprotection/oxidation. Overall, the pathway to the protected product proved robust. More difficult, however, was determining conditions for subsequent deprotection and oxidation reactions.

Different deprotection conditions was explored, and ultimately 10% TFA in DCM was selected as the best deprotection condition. This left the product as a TFA salt, which could be quenched with saturated sodium bicarbonate and extracted into DCM. The obtained *o*-DAP precursor failed to exactly match the NMR spectra of the previously characterized *o*-DAP precursor despite having similar physical properties and the correct mass, suggesting that the deprotection left the dye in a slightly different state than the direct coupling. Subsequent oxidation of this dye with iodine led to a product with the UV-Vis (Figure 5) and mass spectra associated with *o*-DAP. However, an interpretable NMR could not be obtained, likely due to solubility issues. Different oxidation conditions were evaluated, however, iodine oxidation gave the best results.

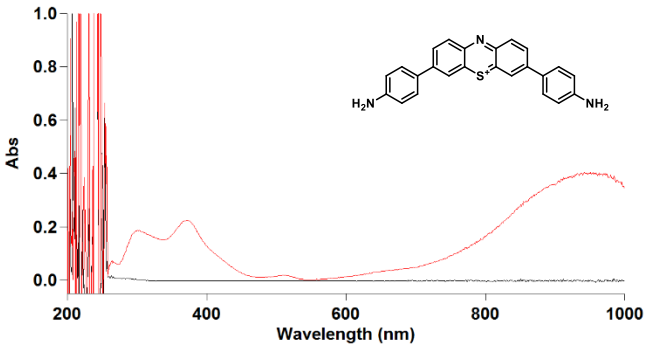

Figure 5: o-DAP UV-Vis Spectrum. Taken in DMSO.

Multiple attempts were made at producing singlet oxygen using a 940 nm LED and subsequently a 980 nm laser, but, in comparison to a dark control no singlet oxygen generation was detected by DPBF degradation (Figure 6). In fact, the dark control suggested that the published DPBF signal decrease was a consequence of some process that was occurring in the dark. Additional singlet oxygen sensors, such as 9,10-anthracenediyl-bis(methylene)dimalonic acid (ABDA), were tested to no avail. Taken together, this suggested that reported singlet oxygen generation by *o*-DAP was not going to be recapitulated. However, before abandoning the dye completely, functionalization was explored to ensure that aggregation or solubility issues were not responsible for the observed results. Functionalization was initially attempted using the protected *o*-DAP precursor shown in Figure 6. Sulfonation was first evaluated

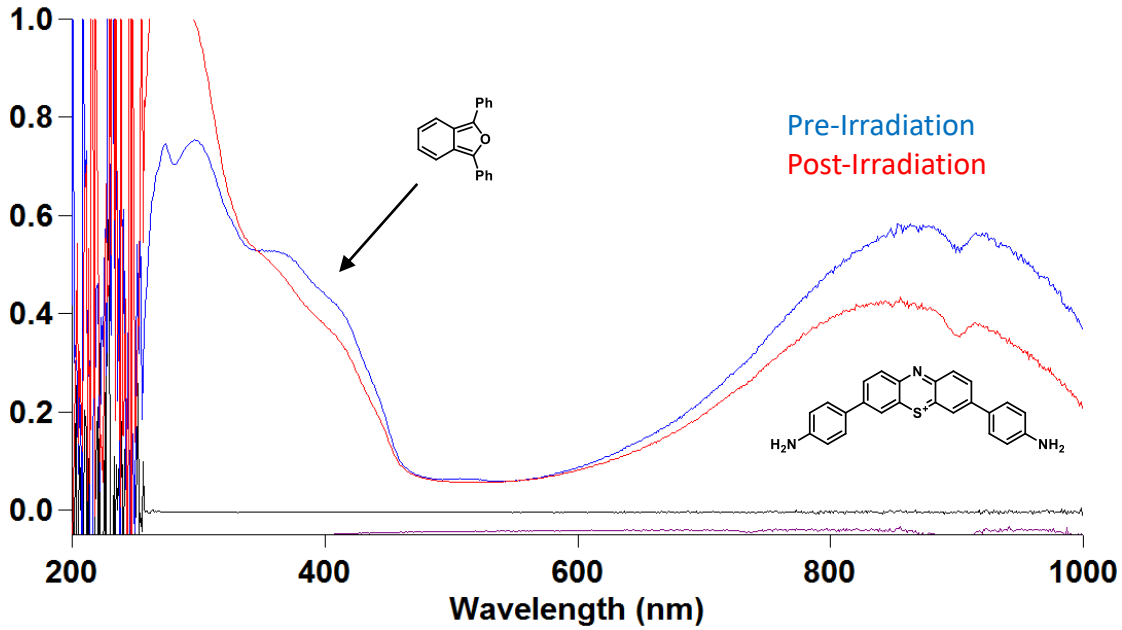

Figure 6: Evaluation of *o*-DAP mediated singlet oxygen generation. Following irradiation with a 940 nm LED over the course of an hour, no significant change in DPBF signal was observed despite a notable decrease in *o*-DAP absorbance.

using 1,3-propanesultone. Although product formation could be observed by LC-MS, the reaction mixture was a complicated milieu involving multiple sulfonation products, making it nearly impossible to cleanly isolate a single one. To further complicate matters, Boc deprotection was observed as the reaction proceeded. To avoid the complicated product mixture produced by 1,3-propanesultone, alkylation with other groups was next explored. Although the ultimate goal was alkylation with masked solubilizing groups – such as esters that could be deprotected to form carboxylic acids – methylation was explored as a proof of principle. Attempts to methylate the *o*-DAP precursor directly proved unsuccessful, however, a methylated precursor could be used for the coupling reaction, giving clean product. Upon deprotection and oxidation, this precursor gave tetramethyl *o*-DAP, which could be characterized by mass spectrometry and NMR (Figure 7). Although tetramethyl *o*-DAP was not soluble in water, it was soluble

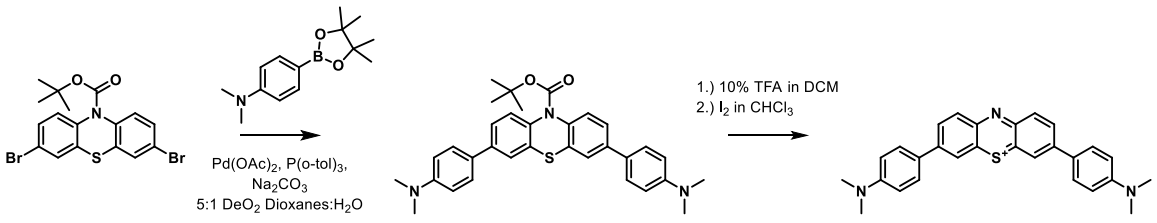

Figure 7: Tetramethyl *o*-DAP synthesis.

in chloroform, and therefore was irradiated in $CDCl_3$ in the presence of DPBF in an attempt to generate singlet oxygen. Unfortunately, no significant change in DPBF signal was observed when compared to a dark control. This once again suggested that *o*-DAP was incapable of generating singlet oxygen. However, this successful methylation opened the door to the possibility of alkylation with other groups and prompted attempts to generate a water soluble *o*-DAP.

Alkylation of the protected *o*-DAP precursor with masked acetate groups was next evaluated using ethyl iodoacetate. Although this alkylation was cleaner and more robust than the previous *o*-DAP methylation attempts, it was still difficult to obtain complete alkylation. The use of long reaction times helped. Other alkylating reagents were also explored, such as methyl bromoacetate, however, only ethyl iodoacetate gave complete alkylation. Isolation of the alkylated *o*-DAP proved challenging, but clean product was obtained and verified by NMR (Figure 8). Subsequent Boc deprotection and oxidation reactions gave a chloroform soluble product with a reasonably clean NMR. This product still failed to convincingly produce singlet oxygen, demonstrating a decrease in DPBF signal in $CDCl_3$ in both an irradiated sample and a dark control. Despite this failure, one final attempt was made to generate water soluble *o*-DAP in hopes that some solvent effect was preventing singlet oxygen generation. Unfortunately, attempts to form carboxylic acids from the ester precursors were unsuccessful, generating a complicated mixture of products that could not be separated. In all, this suggested that *o*-DAP and its derivatives were not useful for generating singlet oxygen at near-infrared wavelengths. Before completely abandoning *o*-DAP as a singlet oxygen generator, a counterion exchange was attempted to ensure that the iodine counterion was not affecting the photochemistry. Exchange for tetrafluoroborate led to no change in the observed photochemistry.

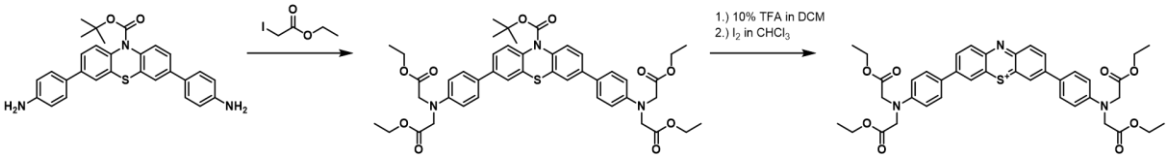

Figure 8: Alkylated *o*-DAP synthesis.

Although the failure of *o*-DAP and its derivatives to produce singlet oxygen meant that long-wavelength photorelease was unlikely using phenothiazine derivatives, the accessibility of methylene blue derivatives suggested that singlet oxygen-mediated photorelease should still be explored in the context of visible light. Although a number of phenothiazine derivatives were prepared according to a literature procedure[16], a piperazine derivative was of particular interest as it contained an additional amine for further functionalization (Figure 9). Singlet oxygen sensitive cages were next explored.

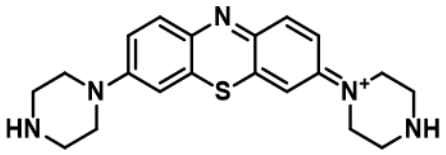

Figure 9: Piperazine methylene blue derivative for derivatization.

4.3.2 Exploration of Singlet Oxygen Sensitive Cages

As mentioned previously, two singlet oxygen sensitive cages were considered. Initial efforts were focused on the alkene dithioether cage, specifically on functionalization of 1,2-dichloroethylene with alkane thiols, such as 2-mercaptoethanol (Figure 10). Ultimately these syntheses proved challenging, as complete separation of the alkane thiol precursor from the product was difficult to achieve. Although isolated cages could be cleaved in the presence of photochemically generated singlet oxygen, the process was far from robust, and focus was subsequently shifted to the development of anthracene photocages.

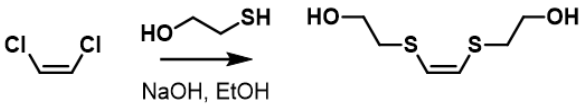

Figure 10: 1,2-dichloroethylene functionalization with 2-mercaptoethanol.

To explore anthracene photocages, an alcohol-terminal 9,10-dialkoxyanthracene was first synthesized (Figure 11). Although this dialkoxyanthracene was not water soluble – and therefore not ideal for biological applications – it provided an opportunity to explore a previously described 9,10-dialkoxyanthracene synthesis. The synthesis proceeded as expected according to literature procedure, and the anthracene decomposed in the presence of photochemically generated singlet oxygen (as determined by HPLC). Anthraquinone was recovered following decomposition, demonstrating that

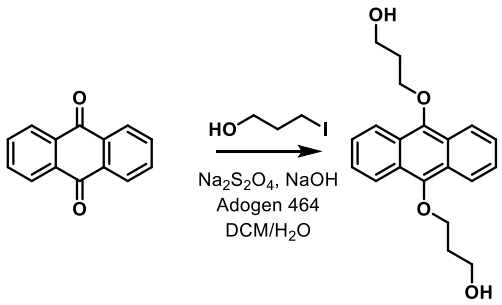

Figure 11: 9,10-dialkoxyanthracene synthesis.

the photocage was working as previously described. These results suggested that heteroatom linked anthracenes were worth pursuing as singlet oxygen sensitive cages.

To explore the scope of anthracene photocages, the singlet oxygen-mediated release of heteroatoms other than oxygen was next evaluated. The incorporation of both amines and thiols at the 9 and 10 positions of anthracene has previously been described[23,24], and initial synthetic attempts were based on literature precedent. Both dipropylamine and ethane thiol were successfully incorporated (Figure 12), generating a 9,10-diaminoanthracene and a 9,10-dithioanthracene respectively. To determine their sensitivity to singlet oxygen, each was combined with methylene blue and irradiated in methanol. Both anthracenes collapsed under these conditions and formed an identical product, ultimately identified to be anthraquinone (Figures 13 and 14). To ensure that this process was mediated by singlet oxygen, each sample was also irradiated after a freeze-pump-thaw procedure, which deoxygenated the solvent completely. The 9,10-dithioanthracene derivative was shown to be completely stable to irradiation of methylene blue under these conditions, suggesting that its decomposition was mediated solely by a path that required singlet oxygen formation. Interestingly, after freeze-pump-thawing, the 9,10-diaminoanthracene was still susceptible to decomposition upon irradiation in the presence of methylene blue, albeit at a significantly slower rate. This suggested that degradation of the 9,10-diaminoanthracene occurred via multiple pathways, of which not all required singlet oxygen formation. This could be due to electron transfer events mediated by methylene blue, a process that has previously been observed in

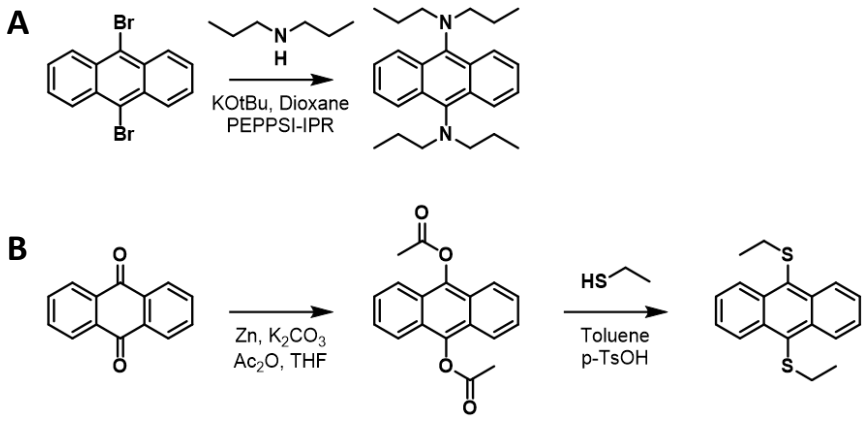

Figure 12: Synthesis of (A) diaminoanthracene and (B) dithioanthracene derivatives.

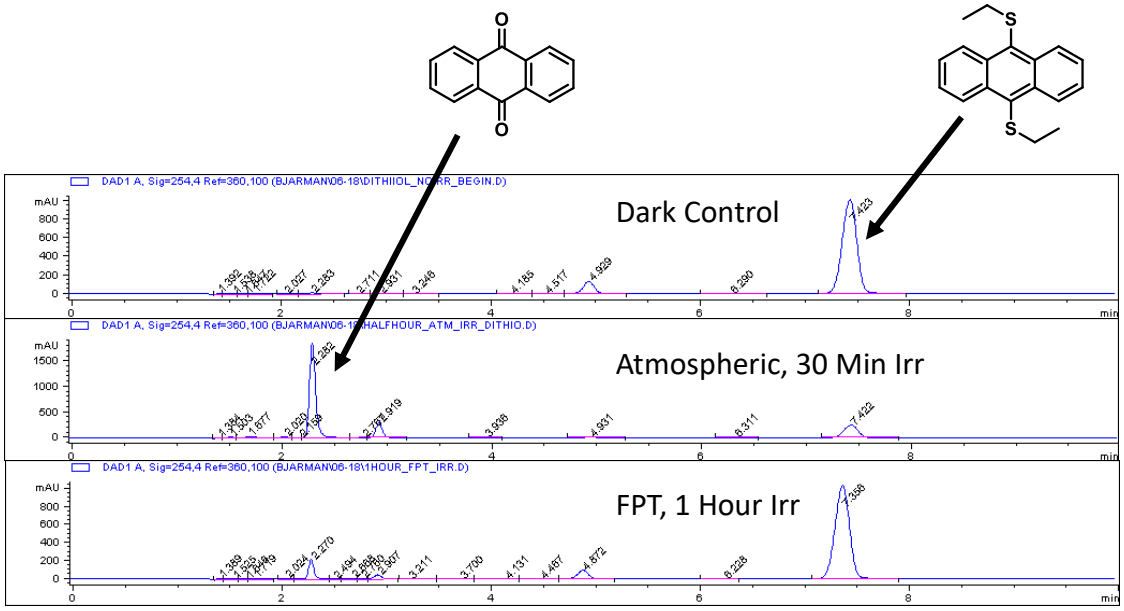

Figure 13: 9,10-dithioanthracene singlet oxygen sensitivity. Notably, degradation of the 9,10-dithioanthracene occurs only in the absence of oxygen.

anilines.[25] Regardless, the singlet oxygen mediated-pathway was still dominant in the 9,10-diaminoanthracene, as evidenced by the observed rate difference following freeze-pump-thawing. Taken together, these results demonstrated that 9,10-anthracene heteroatom derivatives were susceptible to degradation in the presence of singlet oxygen, which suggested that a large breadth of molecules could be released by singlet oxygen using anthracene cages.

Concurrent to explorations of heteroatom specificity, methods to increase the water solubility of 9,10-dialkoxyanthracenes were being explored. Initial attempts focused on increasing the solubility of the

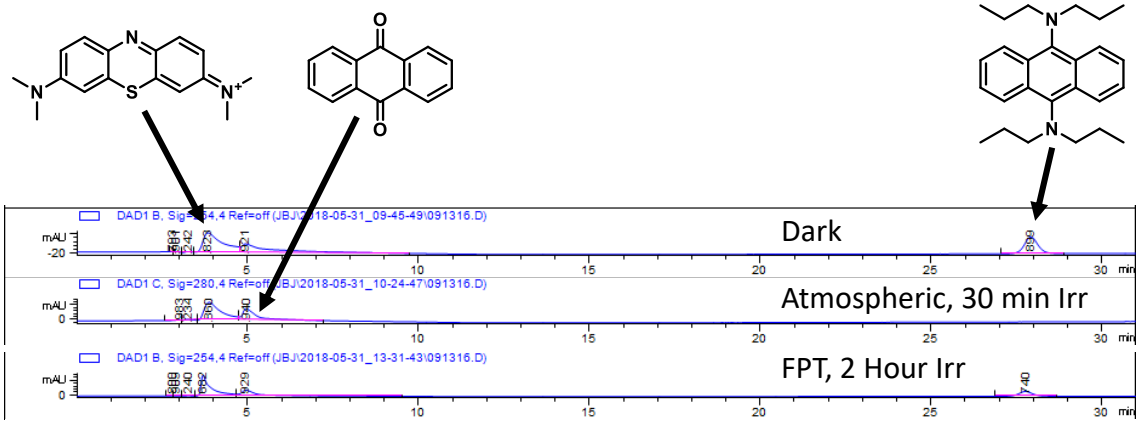

Figure 14: 9,10-diaminoanthracene singlet oxygen sensitivity. Notably, degradation of the 9,10-diaminoanthracene occurs in the absence of oxygen (the FPT sample) suggesting that an oxygen-free photochemistry is occurring, albeit at a slower rate.

caged group. The first route evaluated was selective oxidation of the terminal alcohols in 9,10-dialkoxyanthracenebispropanol. Although this oxidation did produce some terminally oxidized product, it was part of a complex product mixture that was too difficult to separate. The next route explored was generation of 9,10-dialkoxyanthracenes with esters that could be cleaved to give carboxylic acids. Unfortunately, poor alkylation was observed, limiting progress along this synthetic route. Given the limited success of these attempts and the fact that the caged group itself is application dependent, subsequent attempts to increase solubility focused on modification of the anthracene cage.

2-chloroanthraquinone was chosen as a starting point for the development of more complex anthracene cages. Initial functionalization was attempted via condensation with piperazine, which gave 2-piperazinylanthraquinone upon heating in ethanol. This new cage had significantly increased water solubility, and attempts were made to generate a new 9,10-dialkoxyanthracene from this scaffold. Unfortunately, subsequent attempts at reduction and alkylation were unsuccessful, likely due alkylation of the free amine. To avoid this side reaction, two avenues were explored. The first was to invert the order of modification, generating a 2-chloro-9,10-dialkoxyanthracene first and modifying it via condensation with piperazine second. Although a 2-chloro-9,10-dialkoxyanthracene was readily generated, it could not be subsequently modified to a 2-piperazinyl-9,10-dialkoxyanthracene. The second avenue explored was use of a protecting group to prevent the side reactivity associated with the piperazinyl amine. 1-Boc-piperazine was condensed onto 2-chloroanthraquinone, mimicking the piperazine condensation, however, this time the addition of a base (triethylamine) was required to give good yields. Subsequent alkylation to form a 9,10-dialkoxyanthracene was difficult to evaluate due to the insolubility of the product, but isolation of crude product and immediate Boc deprotection yielded a product that could be isolated. Although a combination of DCM/TFA gave better solubility for the crude

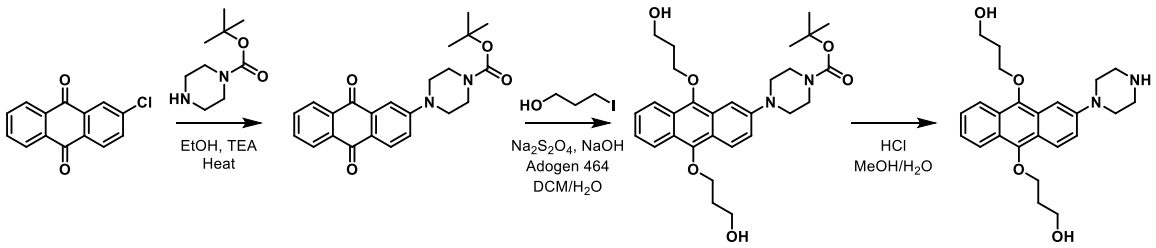

Figure 15: 2-piperazinyl-9,10-dialkoxyanthracene synthesis.

deprotection, an aqueous solution containing methanol and HCl was ultimately used as it gave cleaner conversion to product (Figure 15). The isolated 2-piperazine-9,10-dialkoxyanthracene was soluble in water and sensitive to photochemical singlet oxygen generation (Figure 16). Notably, when running an irradiation experiment using a freeze-pump-thawed sample, starting material disappearance was still observed, suggesting that piperazinyl modification of the anthracene cage enabled an oxygen free degradation mechanism not seen in the parent 9,10-dialkoxyanthracene. Given that this compound contains a pendant amine, it is likely that this molecule and 9,10-diaminoanthracene collapse by the same mechanism in the absence of oxygen.

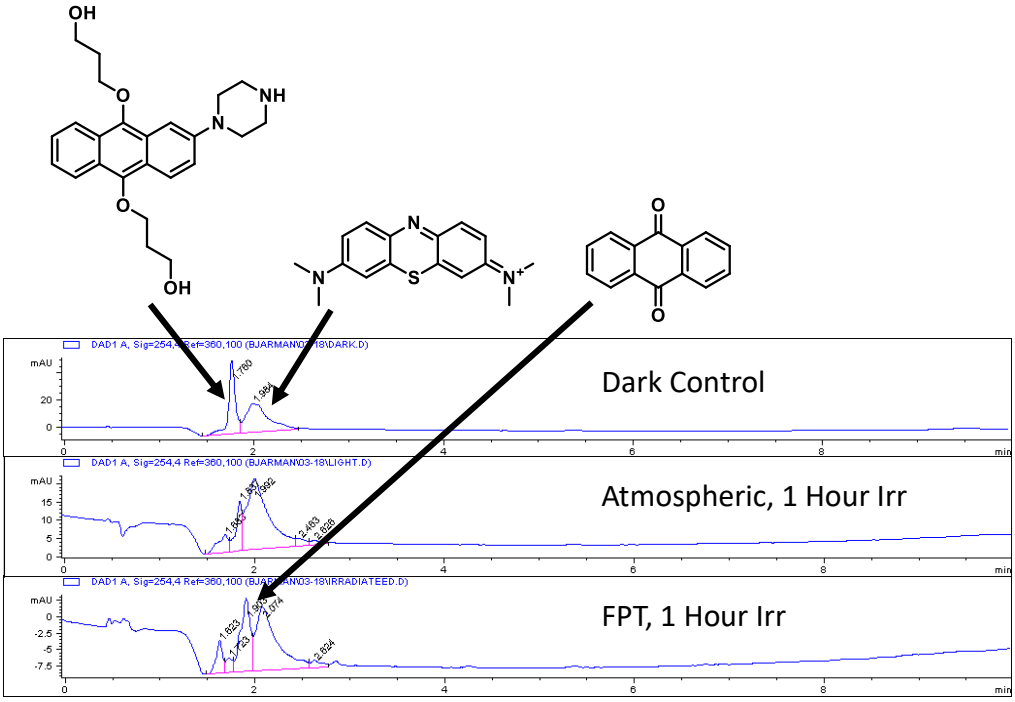

Figure 16: 2-piperazinyl-9,10-dialkoxyanthracene singlet oxygen sensitivity. Notably, degradation of the 2-piperazinyl-9,10-dialkoxyanthracene occurs in the absence of oxygen, suggesting that oxygen-free photochemistry is occurring, albeit at a slower rate.

4.3.3 Construction of a Scaffold for Singlet Oxygen Mediated Photorelease

Having demonstrated successful synthesis of a piperazinyl methylene blue derivative and 2-piperazinyl-9,10-dialkoxy anthracene (Figure 17), the final step was to combine the two components to generate a complete scaffold for singlet oxygen-mediated photorelease. To start with the simplest system possible, the addition of 2-piperazinyl-anthraquinone to oxidized phenothiazine was attempted, similar to the reaction used to generate piperazinyl methylene blue. The addition of an array of secondary amines

to oxidized phenothiazine has been described in the literature[16], although never in the context of an amine as complicated as 2-piperazinyl-anthraquinone. Unfortunately, this reaction was difficult to follow due to solubility issues, and never generated a significant amount of product. A comparable condensation with 2-piperazinyl-9,10-dialkoxyanthracene was also unsuccessful. Coupling chemistry was explored next.

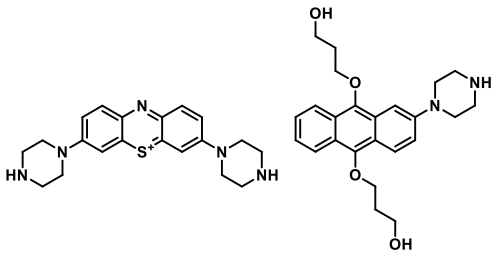

Figure 17: Piperazinyl methylene blue (left) and 2-piperazinyl-9,10-dialkoxyanthracene (right). Combination of these two components through the two amines of piperazine would result in a complete scaffold for singlet oxygen-mediated photorelease.

Initial attempts to couple 2-piperazinyl-anthraquinone to Boc-dibromophenothiazine through Buchwald-Hartwig chemistry gave no product. To explore whether or not 2-piperazinyl-anthraquinone reactivity was in some way hampered due to steric constraints on the piperazine, 2-N,N'-dimethylethylenediamine-anthraquinone was synthesized as a flexible analog. Although this molecule also exhibited limited reactivity, coupling conditions were ultimately determined that produced an anthraqunione-phenothiazine conjugate (Figure 18). Unfortunately, subsequent attempts at formation of a dialkoxyanthracene product in the context of this larger scaffold proved unsuccessful. Although the exact reason was unclear, mass spectrometry data suggested that some sort of cyclization was occurring, perhaps due to the flexibility associated with the N,N'-dimethylethylenediamine linker. To determine whether or not this was the case, coupling with 2-piperazinyl-anthraquinone was revisited in the context of the determined coupling conditions. These conditions were used to generate a piperazine linked scaffold – albeit very long reaction times were required. The piperazine linked anthraquinone-

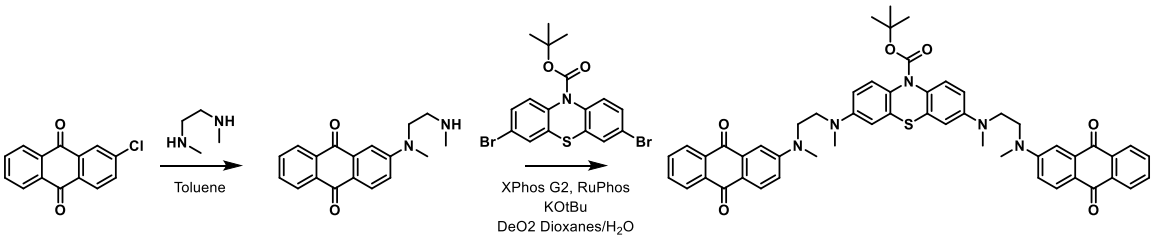

Figure 18: N,N'-dimethylethylenediamine anthraquinone-phenothiazine conjugate synthesis.

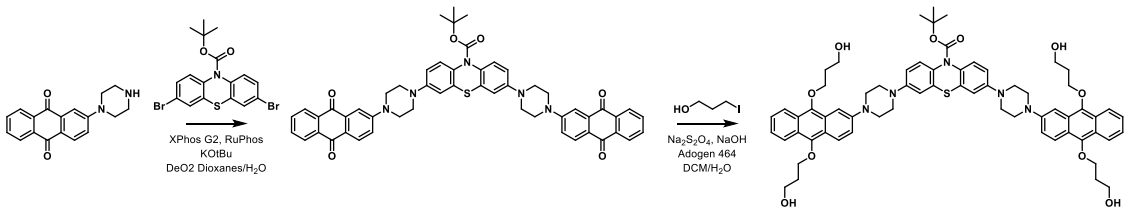

Figure 19: Synthesis of a piperazine linked dialkoxyanthracene-phenothiazine conjugate.

phenothiazine conjugate was then used to synthesize a dialkoxyanthracene scaffold, albeit in low yields (Figure 19). At this point, a molecule had been developed that was a single Boc deprotection and oxidation away from the envisioned scaffold for singlet oxygen-mediated photorelease. Unfortunately, Boc deprotection of this product proved too harsh, giving a range of products, from which the final photocage could not be isolated.

In an attempt to circumvent the Boc deprotection issue, a number of alternative protecting groups were explored. NVOC-dibromophenothiazine and benzyl-dibromophenothiazine could both be obtained with reasonable purity as a starting point for scaffold development, however, only deprotection of the benzyl-dibromophenothiazine proceeded cleanly. Subsequent coupling to 2-piperazinyl-anthraquinone and dialkoxyanthracene formation were both successful starting with benzyl-dibromophenothiazine, however, deprotection of the final scaffold once again proved problematic. These results suggested that the final scaffold was either too unstable or too difficult to isolate.

In a final attempt to work around this issue, thiol substitution was explored, as the 9,10-dithioanthracenes had been shown to be more stable. Unfortunately, the thiol compounds proved equally difficult to work with. At this point, despite being close to a complete scaffold, it became apparent that a major synthetic rework would be required. Although development of such a scaffold still has significant merit, a new synthetic strategy will be required to fully explore singlet oxygen-mediated photochemical release in the context of a phenothiazine scaffold.

4.4 Conclusion

The principle of singlet oxygen-mediated photorelease is still relatively unexplored. Despite the initial findings of Schnermann and coworkers, there has not yet been any significant follow-up by the photochemical community. This is likely because the development of scaffolds capable of both

generating singlet oxygen and mediating photorelease is a significant challenge. To address this deficiency in the field, attempts were made to generate such a scaffold by combining the singlet oxygen sensitization capabilities of phenothiazine derivatives, such as methylene blue, with the singlet oxygen sensitivity of moieties such as 9,10-dialkoxyanthracene. In specific, a long wavelength phenothiazine derivative known as *o*-DAP was initially explored as a promising singlet oxygen generator. When it was shown that previous reports of singlet oxygen generation could not be recapitulated, functionalizable methylene blue derivatives were evaluated instead. To complement these chromophores, heteroatom modified anthracenes were investigated as singlet oxygen sensitive cages. It was demonstrated that 9,10-dialkoxyanthracene, 9,10-diaminoanthracene, and 9,10-dithioanthracene all collapsed in the presence of singlet oxygen, liberating protected groups. Attempts were then made at combining anthracene derivatives and a phenothiazine derivative into a single molecule capable of undergoing singlet oxygen-mediated photorelease. Unfortunately, despite significant progress on this front, a complete scaffold was not obtained. Despite this setback, the field of singlet oxygen-mediated photorelease is still filled with opportunity, and the described system is worth revisiting in the context of a different synthetic route.

4.5 Materials and Methods

4.5.1 Materials

Commercial reagents and solvents were purchased from Sigma-Aldrich, VWR, and Thermo-Fisher Scientific and used as received. Deuterated solvents were purchased from Cambridge Isotope Laboratories and used without further purification. Reactions involving air or moisture sensitive reagents were run under argon, with samples purged of air prior to use. Flash chromatography was performed using neutral silica gel from Merck (230-400 mesh). TLC analysis was performed with plates from Merck (60 A pore size, F_{254}, 0.25 mm).

4.5.2 Instrumentation

^{1}H NMR spectra were obtained using Varian NMR instruments. Chemical shifts are reported in parts per million (ppm, δ) referenced to the residual ^{1}H resonance of the solvent. Splitting patterns are designated as follows: s, singlet; br, boad; d, doublet; dd, doublet of doublets; t, triplet; q, quartet; m,

multiplet. Mass spectrometry data were obtained using an Agilent 1100 LC/MSD equipped with an ESI-APCI source. LC-MS runs were performed using a binary solvent system consisting of Omnisolv acetonitrile and ultrapure water with .1% acetic acid. An Agilent C-18 column was used for separations. For crude product mixtures an LCT Premier XE ESI-TOF-MS was used to validate product formation through injection of crude material. Irradiations were performed using LED-driver combinations obtained from Thor labs. A 660 nm LED was used to irradiate methylene blue and its derivatives, and a 980nm LED was used to irradiate *o*-DAP and its derivatives. UV-VIS spectra were obtained using a Cary UV-VIS spectrometer.

4.5.3 Anthracene Derivative Irradiation and HPLC Analysis

All anthracene derivatives were evaluated in the context of methylene blue irradiation. Specifically, solutions in methanol were generated that contained both heteroatom functionalized anthracenes (at various concentrations depending on solubility) and methylene blue. A concentration of methylene blue was used that produced an absorbance of 1.0 at 660 nm. These solutions were irradiated with a 660 nm LED while stirring in Starna quartz cuvettes, and kept in the dark besides. Following irradiation, solutions were loaded onto the LC/MS. Freeze-pump-thaw samples were generated using glassware designed at the Caltech glass shop. Analysis of the 2-piperazine-9,10-dialkoxyanthracene and the 9,10-dithioanthracene irradiation experiments was carried out using a 70%-95% solvent gradient (where the percent represents the percent acetonitrile) over the course of 10 minutes. These conditions failed to elute the 9,10-diaminoanthracene molecule, therefore a 30 min 70%-95% run was used. Comparisons were made between control, freeze-pump-thawed, and irradiated samples at the same initial concentration.

4.5.4 Syntheses

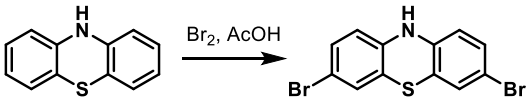

3,7-dibromo-phenothiazine

In a 500 ml round bottom flask, 5 grams of phenothiazine were added to 250 ml of acetic acid. 3.2 mL of bromine (2.5 equivalents) were subsequently added to this solution. The solution turned purple, becoming heterogenous and difficult to stir. Reaction was stirred for two hours. After two hours, 5 ml of water and 3.16 grams (2 equivalents) of sodium sulfite were added. The reaction was allowed to stir for an additional 15 minutes, at which point 4 equivalents of 1 M sodium hydroxide were added. The reaction was stirred until the purple color had faded to gray and a precipitate had formed. This product was filtered, washed briefly with acetone, then constantly washed with hexanes. Obtained a light blue/green powder upon drying via vacuum filtration. ^{1}H-NMR (300 MHz, $CDCl_3$) δ: 8.83 (s, 1H), 7.13 (m, 4H), 6.56 (d, 2H). ESI-MS (MH^+) calculated: 355.8, found 355.9.

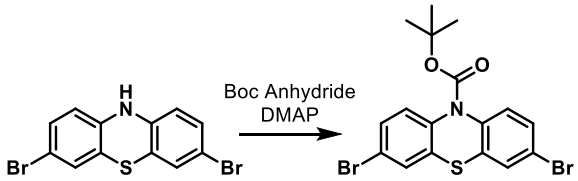

N-Boc-3,7-dibromophenothiazine

To 2 grams of 3,7-dibromophenothiazine in 100 ml of acetonitrile in a 250 ml round bottom flask was added 1.5 grams (1.2 equivalents) of di-tert-butyl dicarbonate (Boc Anhydride). A catalytic amount of DMAP (100 mg, .1 equivalent) was also added, and the reaction was allowed to stir overnight. A peach liquid with a white precipitate was obtained after overnight stirring. The precipitate was isolated and washed with additional acetonitrile and hexanes. It was then taken up in DCM, and run on a 100% DCM silica gel column. The product was isolated as a white, UV active spot. ^{1}H-NMR (300 MHz, $CDCl_3$) δ: 7.48 (d, 2H), 7.40 (m, 4H), 1.57 (s, 9H). ESI-MS (MH^+) calculated: 457.2, found 457.6

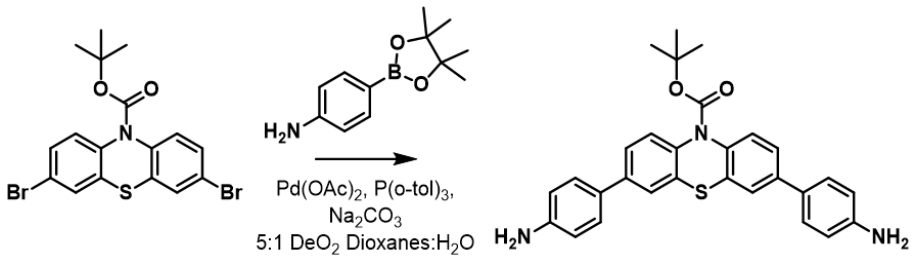

N-Boc-3,7-bis(4-aminophenyl)-phenothiazine

A 25 ml, flame-dried round bottom flask was charged with 100 mg of N-Boc-3,7-dibromophenothiazine. To this was added 105 mg (2.2 equivalents) of 4-aminophenylboronic acid pinacol ester, an excess of sodium carbonate (100 mgs, roughly 4 equivalents) and a catalytic amount of palladium acetate (1 mg) and tri(o-tolyl)phosphine (10mg). The solids were dissolved in a mixture of 5:1 dioxanes:water, with both solvents having been previously deoxygenated. The reaction was run at heat (80° C) for 4 hours and monitored by TLC as well as LC/MS. Upon disappearance of the starting material, the reaction was quenched via extraction into DCM. After pumping down, the product was purified using a 2:1 hexanes:acetone silica column. The product was isolated as a slightly off-white powder. ^{1}H-NMR (300 MHz, $CDCl_3$) δ: 7.56 (m, 6H), 7.45 (m, 4H), 6.75 (m, 4H), 1.57 (s, 9H). ESI-MS (MH^+) calculated: 482.2, found 482.4.

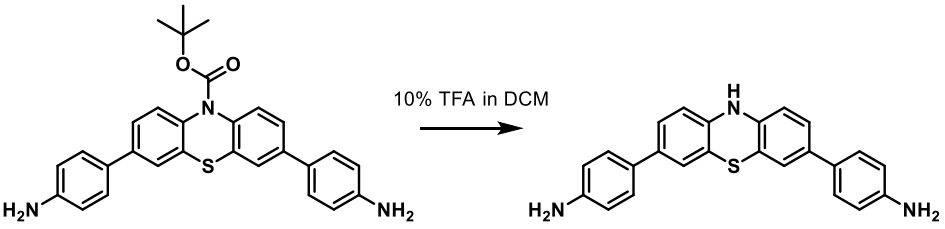

3,7-bis(4-aminophenyl)-phenothiazine

A 25 ml round bottom flask was charged with 20 mg of N-Boc-3,7-bis(4-aminophenyl)-phenothiazine, which was subsequently charged with DCM containing 10% TFA. The reaction was monitored by LC/MS. After 4 hours, the starting material had disappeared and was replaced with a combination of 3,7-bis(4-aminophenyl)-phenothiazine and what appeared to be an oxidized version. The 10% TFA in DCM solution was pumped off, then brought back up in DCM. This was done three times. After the third time, the DCM was washed with saturated sodium bicarbonate, yielding a yellow brown

product. An NMR spectrum of this product could not be obtained. ESI-MS (MH^+) calculated: 382.1, found 382.4.

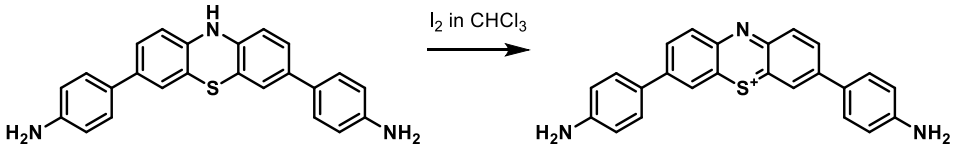

3,7-bis(4-aminophenyl)-phenothiazinium

A 10 ml round bottom flask was charged with 10 mg of 3,7-bis(4-aminophenyl)-phenothiazine, to which an excess of I_2 (10 equivalents) in $CHCl_3$ was added. The oxidation proceeded instantaneously by UV-VIS, but was allowed to proceed for an hour to ensure complete conversion. Product was isolated as a black solid via vacuum filtration and washed with DCM to remove excess iodine. An NMR spectrum of this product could not be obtained. ESI-MS (M^+) calculated: 380.1, found 380.2.

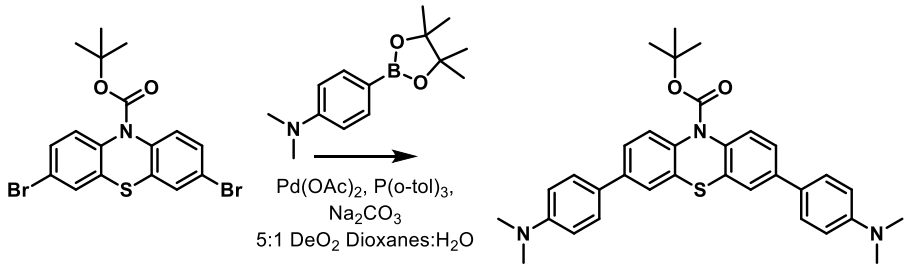

N-Boc-3,7-bis(4-dimethylaminophenyl)-phenothiazine

A 25 ml, flame-dried round bottom flask was charged with 100 mg of N-Boc-3,7-dibromophenothiazine. To this was added 120 mg (2.2 equivalents) of 4-aminophenylboronic acid pinacol ester, an excess of sodium carbonate (100 mgs, roughly 4 equivalents) and a catalytic amount of palladium acetate (1 mg) and tri(o-tolyl)phosphine (10mg). The solids were dissolved in a mixture of 5:1 dioxanes:water, with both solvents having been previously deoxygenated. The reaction was run at heat (80° C) for 4 hours and monitored by TLC as well as LC/MS. Upon disappearance of the starting material, the reaction was quenched via extraction into chloroform. After pumping down, the product was purified using a chloroform column. The product was isolated as a slightly off-white powder. ^{1}H-

NMR (300 MHz, $CDCl_3$) δ: 7.48 (m, 10H), 6.75 (m, 4H), 2.17 (s, 12H), 1.57 (s, 9H). ESI-MS (MH^+) calculated: 538.2, found 538.4.

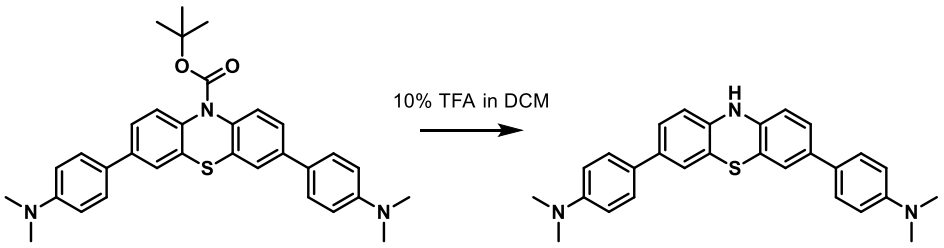

3,7-bis(4-dimethylaminophenyl)-phenothiazine

A 25 ml round bottom flask was charged with 100 mg of N-Boc-3,7-bis(4-dimethylaminophenyl)-phenothiazine, which was subsequently charged with DCM containing 10% TFA. The reaction was monitored by LC/MS. After 2 hours, the starting material had disappeared and was replaced with what appeared to be predominately product. The 10% TFA in DCM solution was pumped off, then brought back up in DCM. This was done three times. After the third time, the DCM was washed with saturated sodium bicarbonate, yielding a yellow brown product. ^{1}H-NMR (300 MHz, $CDCl_3$) δ: 7.63 (m, 10H), 7.46 (m, 4H), 2.17 (s, 12H), 1.57 (s, 9H). ESI-MS (MH^+) calculated: 438.2, found 438.1.

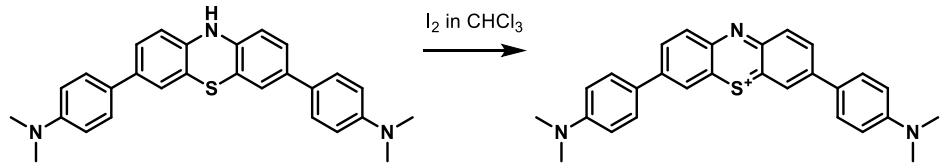

3,7-bis(4-dimethylaminophenyl)-phenothiazinium

A 10 ml round bottom flask was charged with 50 mg of 3,7-bis(4-aminophenyl)-phenothiazine, to which an excess of I_2 (10 equivalents) in $CHCl_3$ was added. The oxidation proceeded instantaneously by UV-VIS, but was allowed to proceed for an hour to ensure complete conversion. Product was isolated as a black solid via vacuum filtration and washed with DCM to remove excess iodine. ^{1}H-NMR (300 MHz, DMSO-D_6) δ: 8.72 (m, 2H), 8.48 (m, 2H), 8.16 (m, 6H), 6.97 (m, 4H), 3.18 (s, 12H). ESI-MS (M^+) calculated: 436.1, found 436.1.

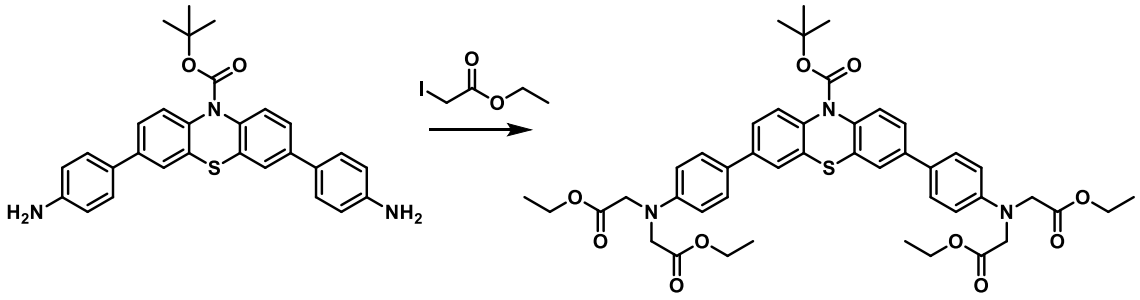

Tetraethyl-2,2',2'',2'''-((N-Boc-3,7-bis(4-aminophenyl)phenothiazine)tetraacetate)

100 mg of N-Boc-3,7-bis(4-aminophenyl)-phenothiazine were added to a 10 ml round bottom flask and subsequently dissolved in DMSO. A large excess of ethyl iodoacetate (250 µl, 10 equivalents) was added to the reaction mixture, which was set to 80°C and allowed to stir overnight. A range of alkylation patterns was observed by LC/MS, however, after 24 hours a majority of the starting material had become the tetraalkylated product. The reaction was then taken up in DCM, and washed three times with water, then once with brine. The solution was pumped down, yielding a slightly off white solid. This solid was then subjected to column chromatography, and eluted with a 0-5% methanol in DCM gradient. The obtained product was pure by NMR and mass spectrometry. ^{1}H-NMR (300 MHz, $CDCl_3$) δ: 7.48 (m, 10H), 6.68 (m, 4H), 4.24 (q, 8H), 4.18 (s, 8H). 1.27 (M, 21 H). ESI-MS (MH^+) calculated: 826.3, found 826.4.

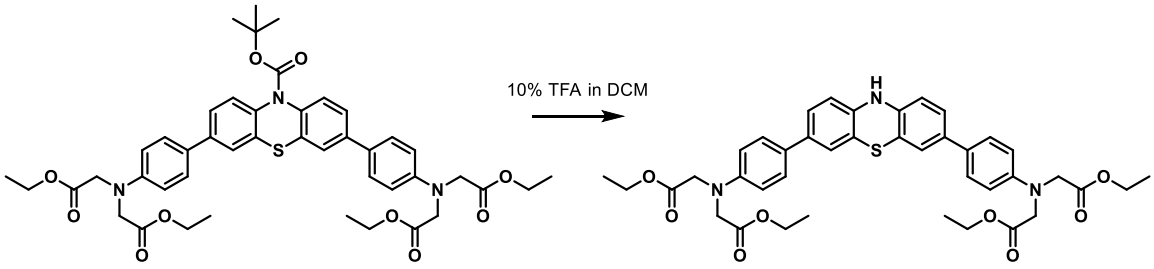

Tetraethyl-2,2',2'',2'''-((-bis(4-aminophenyl)phenothiazine)tetraacetate

A 25 ml round bottom flask was charged with 50 mg of N-Boc-3,7-bis(4-dimethylaminophenyl)-phenothiazine, which was subsequently incubated with DCM containing 10% TFA. The reaction was monitored by LC/MS. After 2 hours, the starting material had disappeared and was replaced with what appeared to be predominately product. The 10% TFA in DCM solution was pumped off, then brought back up in DCM. This was done three times. After the third time, the DCM was washed with saturated

sodium bicarbonate, yielding a yellow brown product. A clean ^{1}H NMR was not obtained, and this product was carried straight through into the oxidation step. ESI-MS (MH^+) calculated: 726.3, found 726.2.

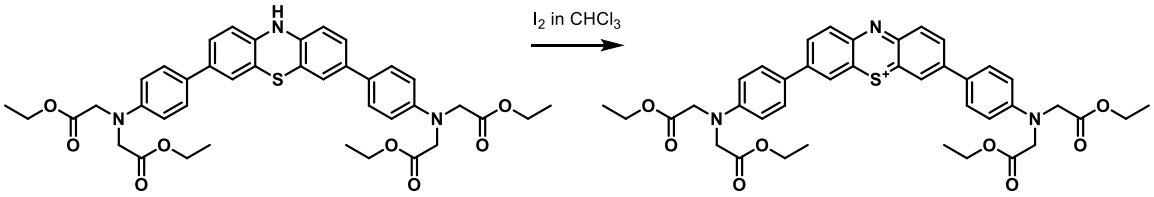

Tetraethyl-2,2',2'',2'''-((-bis(4-aminophenyl)phenothiazinium)tetraacetate

A 10 ml round bottom flask was charged with 25 mg of 3,7-bis(4-aminophenyl)-phenothiazine, to which an excess of I_2 (10 equivalents) in $CHCl_3$ was added. The oxidation proceeded instantaneously by UV-VIS, but was allowed to proceed for an hour to ensure complete conversion. Product was isolated as a black solid via vacuum filtration and washed with DCM to remove excess iodine. ^{1}H-NMR (300 MHz, DMSO-D_6) δ: 9.00 (s, 2H), 8.60 (d, 2H), 8.40 (d, 2H), 8.15 (d, 4H), 6.80 (d, 4H), 4.42 (s, 8H) 4.12 (q, 8H), 1.20 (m, 21H). ESI-MS (M^+) calculated: 724.3, found 724.3.

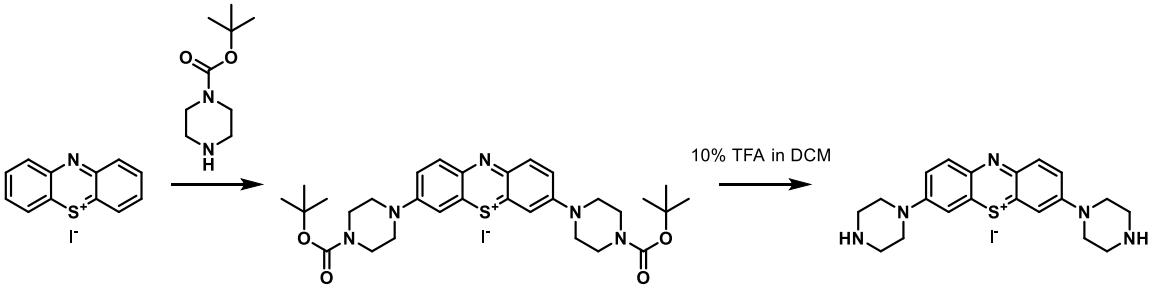

Generalized protocol for amine addition to oxidized phenothiazine (shown in the context of Boc-piperazine)

Amine (2 equivalents) was added to phenothiazinium iodide (1 equivalent) in methanol at room temperature. If the amine contained more than one amine, its second amine was Boc protected. The reactions were run under argon in the dark. After six hours the reaction was pumped down and evaluated for addition. In the event that only a single addition was observed, the product was taken up in DCM and base was added dropwise in the form of triethylamine (3 equivalents). Additional amine was then added to this solution (3 equivalents) and stirred overnight at room temperature. The organic layer was

then washed with water (3x), pumped down, and run on a 0-10% methanol in DCM column. When necessary, subsequent Boc deprotection was run with 10% TFA in DCM. ^{1}H-NMR for 3,7-dipiperazinyl-phenothiazinium (300 MHz, $CDCl_3$) δ: 8.08 (d, 2H), 7.90 (s, 2H), 7.76 (M, 2H), 4.15 (m, 8H), 3.48 (m, 8H). ESI-MS (MH^+) calculated: 366.2, found 366.3.

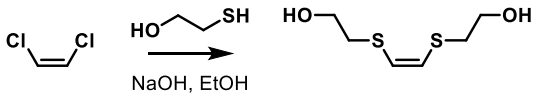

(Z)-2,2'-(ethene-1,2-diylbis(sulfanediyl))bis(ethanol)

To 0.8 grams (2.5 equivalents) of NaOH in ethanol was added 1.8 ml (2 equivalents) of β-mercaptoethanol in a 100 ml round bottom flask. This was stirred on ice for thirty minutes, at which point 1 gram of dichloroethylene was suspended in cold ethanol and added to the solution. The resulting solution was heated to 80°C and allowed to stir overnight. The reaction was monitored by TLC. After 18 hours, the starting material had disappeared by TLC and an orange solution remained. This solution was diluted into water, then extracted three times with ether. After pumping off the ether, the resulting oil was diluted directly onto a 70:30 ethyl acetate:hexanes column. The isolated product still contained β-mercaptoethanol starting material by NMR, so the column was run a second time to separate the desired product away from the impurity. ^{1}H-NMR (300 MHz, $CDCl_3$) δ: 6.17 (s, 2H), 4.87 (s, 2H), 3.69 (t, 4H), 2.84 (t, 4H). ESI-MS (MH^+) not obtained.

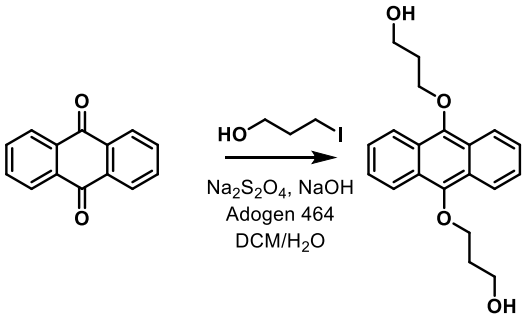

9,10-dialkoxyanthracenebispropanol

13 ml of H_2O was added to a 50 mL round bottom flask, then deoxygenated under vacuum and flushed with argon. Subsequently 13 mL of deoxygenated DCM was added. This combination was stirred and deoxygenated together for a second time. Next, 220 mgs of anthraquinone, 370 mg of $Na_2S_2O_4$ (2.1

equivalents), and 4 drops of Adogen 464 were added to the solution. This solution was stirred for 5 minutes, at which point 400 mg (10 equivalents) of NaOH were added. The solution turned red. After another 5 minutes, 1 gram (5 equivalents) of 3-iodopropanol was added. The reaction was followed by TLC, and allowed to stir overnight. After complete conversion of the starting material, the reaction was diluted into water and washed three times with DCM. The combined organic portion was pumped down, yielding an oil. This oil was purified on a 50:50 hexanes:ethyl acetate column, eluting as a yellow fraction. ^{1}H-NMR (300 MHz, $CDCl_3$) δ: 8.25 (m, 4H), 7.53 (m, 4H), 4.65 (t, 2H), 4.19 (m, 4H), 3.77 (m, 4H), 2.11 (m, 4H). ESI-MS (MH^+) not obtained.

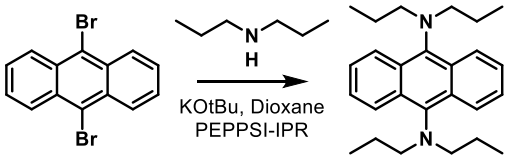

N,N,N',N'-tetrapropylanthracene-9,10-diamine

To 250 mg of 9,10-dibromoanthracene was added 200 mg (4 equivalents) of KOtBu in dioxane with a catalytic amount of PEPPSI-IPR catalyst in a 25 ml round bottom flask. This solution was heated gently to solubilization, at which point 250 μL of dipropylamine (4 equivalents) was added. The reaction was subsequently set to reflux overnight and monitored at intervals by TLC and LC/MS. Notably, a 30 min LC/MS run was required to observed product elution. The reaction was quenched by dilution in water, and the product extracted into DCM. The organic layer was washed three times with water, pumped down, and then loaded in DCM onto a 30% ethyl acetate in hexanes column. The desired product coeluted with an impurity, so a second hexanes column was run to obtained completely pure product. ^{1}H-NMR (300 MHz, $CDCl_3$) δ: 8.43 (m, 4H), 7.42 (m, 4H), 3.41 (m, 8H), 1.56 (m, 8H), .82 (m, 8H). ESI-MS (MH^+) calculated: 377.3, found 377.5.

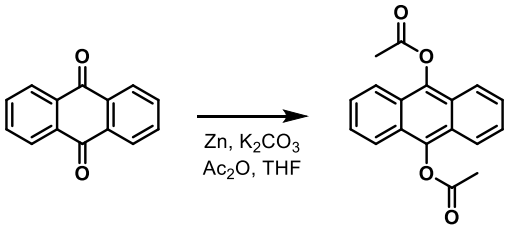

9,10-anthracenediacetate

To 500 mg of anthraquinone was added 1.6 grams of zinc dust (>10 equivalents) and 3.3 grams of potassium carbonate (10 equivalents) in a 100 ml round bottom flask. This was stirred in THF under argon, and subsequently 2.5 ml (10 equivalents) of acetic anhydride was added. This reaction was stirred for 3 hours, at which point complete conversion was observed by TLC. The reaction was worked up by filtering to remove suspended zinc dust, quenching with .1 M HCl for 1 hour, then extracting with DCM. After washing the organic layer three times, the solution was pumped down. Further purification was not required. ^{1}H-NMR (300 MHz, $CDCl_3$) δ: 7.95 (m, 4H), 7.53 (m, 4H), 2.64 (s, 6H). ESI-MS (MH^+) not obtained.

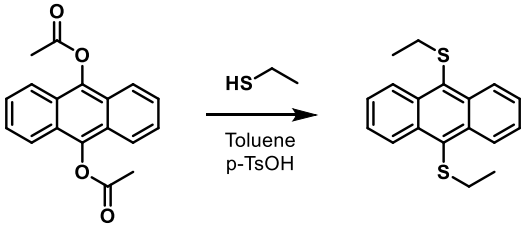

9,10-diethylthioanthracene

To 200 mgs of 9,10-anthracenediacetate in toluene in a 50 mL round bottom flask was added an excess of *p*-toluenesulfonic acid and ethane thiol. The reaction was set to reflux and allowed to proceed for 4 hours. Over this time, the reaction mixture went from clear to yellow. After 4 hours the reaction was diluted in ethyl acetate then washed with water three times. The organic layer was pumped down, taken up in a small amount of DCM, and loaded onto a DCM column. The eluted product was still contaminated with a small amount of ethane thiol, so a second column (0-2% ethyl acetate in hexanes)

was run. A high vac was used to remove final traces of ethane thiol. ^{1}H-NMR (400 MHz, $CDCl_3$) δ: 9.11 (m, 4H), 7.64 (m, 4H), 2.94 (q, 4H), 1.18 (t, 6H). ESI-MS (MH^+) calculated: 299.1, found 299.5.

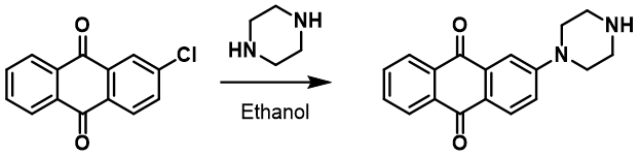

2-piperazinylanthraquinone

200 mg of 2-chloroanthraquinone was added to 700 mg of piperazine (10 equivalents) in a 25 ml round bottom flask. To this, ethanol was added, but not enough for complete solubilization of the 2-chloroanthraquinone at room temperature. The mixture was set to reflux, and transitioned from a yellow starting material to a dark red product. Ethanol was allowed to boil down. Upon cooling, the slurry was dissolved in DCM and washed three times with water. A 0-10% methanol in DCM column was run to isolate pure product. ^{1}H-NMR (300 MHz, $CDCl_3$) δ: 8.25 (m, 2H), 8.15 (d, 1H), 7.73 (m, 2H), 7.62 (d, 1H), 7.13 (dd, 1H), 3.44 (m, 4H), 3.03 (m, 4H). ESI-MS (MH^+) calculated: 293.1, found 293.2.

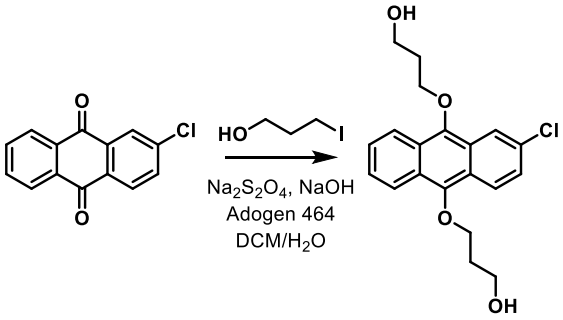

2-chloro-9,10-dialkoxyanthracenebispropanol

13 ml of H_2O was added to a 50 mL round bottom flask, then deoxygenated under vacuum and flushed with argon. Subsequently 13 mL of deoxygenated DCM was added. This combination was stirred and deoxygenated together for a second time. Next, 250 mgs of 2-chloroanthraquinone, 370 mg of $Na_2S_2O_4$ (2.1 equivalents), and 4 drops of Adogen 464 were added to the solution. This solution was stirred for 5 minutes, at which point 400 mg (10 equivalents) of NaOH were added. The solution turned red. After another 5 minutes, 1 gram (5 equivalents) of 3-iodopropanol was added. The reaction was followed by TLC, and allowed to stir overnight. After complete conversion of the starting material, the

reaction was diluted into water and washed three times with DCM. The combined organic portion was pumped down, yielding an oil. This oil was purified on a 50:50 hexanes:ethyl acetate column, eluting as a yellow fraction. ^{1}H-NMR (300 MHz, $CDCl_3$) δ: 8.26 (m, 4H), 7.55 (m, 3H), 4.66 (t, 2H), 4.18 (m, 4H), 3.76 (m, 4H), 2.11 (m, 4H). ESI-MS (MH^+) not obtained.

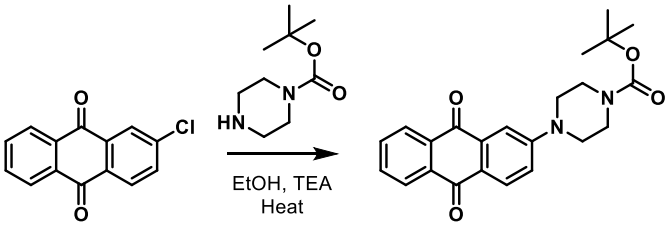

N-Boc-2-piperazinylanthraquinone

200 mg of 2-chloroanthraquinone was added to 1.5 g of Boc-piperazine (10 equivalents) in a 25 ml round bottom flask. To this, ethanol was added, but not enough for complete solubilization of the 2-chloroanthraquinone at room temperature. Triethylamine, 300 µl, was also added to facilitate the reaction. The mixture was set to reflux, and transitioned from a yellow starting material to a dark red product. Ethanol was allowed to boil down. Upon cooling, the slurry was dissolved in DCM and washed once with water, washed once with saturated ammonium chloride solution, and then three more timed with water. A 0-10% methanol in DCM column was run to isolate pure product. ^{1}H-NMR (300 MHz, $CDCl_3$) δ: 8.16 (m, 2H), 8.04 (d, 1H), 7.87 (m, 2H), 7.52 (d, 1H), 7.32 (dd, 1H), 3.5 (m, 8H), 1.42 (s, 9H). ESI-MS (MH^+) calculated: 393.2, found 393.4.

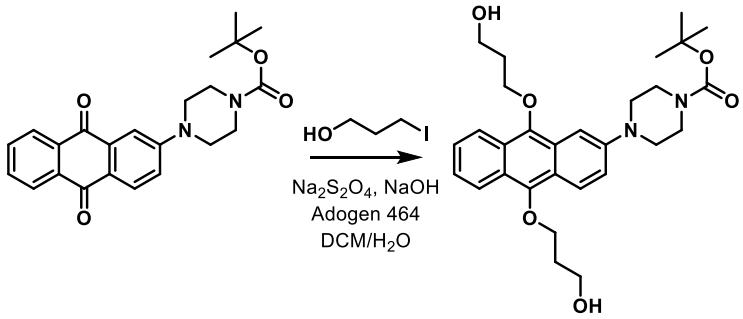

N-Boc-2-piperazinyl-9,10-dialkoxyanthracenebispropanol

13 ml of H_2O was added to a 50 mL round bottom flask, then deoxygenated under vacuum and flushed with argon. Subsequently 13 mL of deoxygenated DCM was added. This combination was stirred

and deoxygenated together for a second time. Next, 400 mgs of N-Boc-2-piperazinylanthraquinone, 370 mg of $Na_2S_2O_4$ (2.1 equivalents), and 4 drops of Adogen 464 were added to the solution. This solution was stirred for 5 minutes, at which point 400 mg (10 equivalents) of NaOH were added. The solution turned red. After another 5 minutes, 1 gram (5 equivalents) of 3-iodopropanol was added. The reaction was followed by TLC, and allowed to stir overnight. After complete conversion of the starting material, the reaction was diluted into water and washed three times with DCM. The combined organic portion was pumped down, yielding an oil. This oil was immediately subjected to Boc deprotection. ^{1}H-NMR and ESI-MS (MH^+) not obtained.

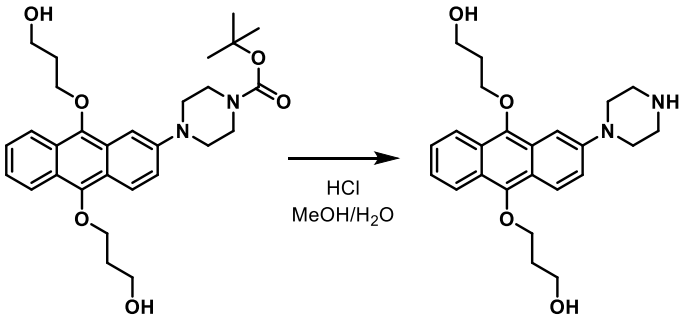

2-piperazinyl-9,10-dialkoxyanthracenebispropanol

Crude N-Boc-2-piperazinyl-9,10-dialkoxyanthracenebispropanol was taken up in methanol and diluted down in a combination of water and HCl (10%). Deprotection reaction proceeded slowly but cleanly. Product formation was observed by both TLC and LC/MS. After overnight deprotection, the reaction was worked up by dilution into a saturated sodium bicarbonate solution and extracted into DCM. Some side product formation was observed upon work up. Crude product was isolated and run on base-treated silica column using a 0-10% methanol in DCM gradient. ^{1}H-NMR (300 MHz, $CDCl_3$) δ: 8.19 (m, 3H), 7.44 (m, 4H), 4.29 (m, 4H), 4.12 (m, 4H), 3.72 (m, 4H), 3.39 (m, 4H), 3.17 (m, 2H), 2.27 (m, 2H). ESI-MS (MH^+) calculated: 413.2, found 413.4.

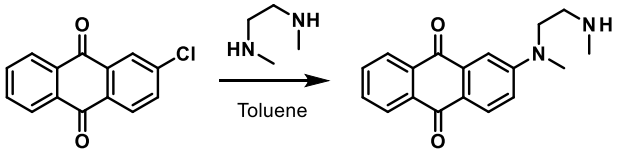

2-N,N'-dimethylethylenediamineanthraquinone

200 mg of 2-chloroanthraquinone was added to 700 mg of N,N'-dimethylethylenediamine (10 equivalents) in a 25 ml round bottom flask. To this, ethanol was added, but not enough for complete solubilization of the 2-chloroanthraquinone at room temperature. The mixture was set to reflux, and transitioned from a yellow starting material to a dark red product. Ethanol was allowed to boil down. Upon cooling, the slurry was dissolved in DCM and washed three times with water. A 0-10% methanol in DCM column was run to isolate pure product. ^{1}H-NMR (300 MHz, $CDCl_3$) δ: 8.24 (m, 2H), 8.13 (d, 1H), 7.71 (m, 2H), 7.44 (d, 1H), 6.97 (dd, 1H), 3.62 (t, 2H), 3.15 (s, 3H), 2.86 (t, 2H), 2.48 (s, 3H). ESI-MS (MH^+) calculated: 295.1, found 295.1.

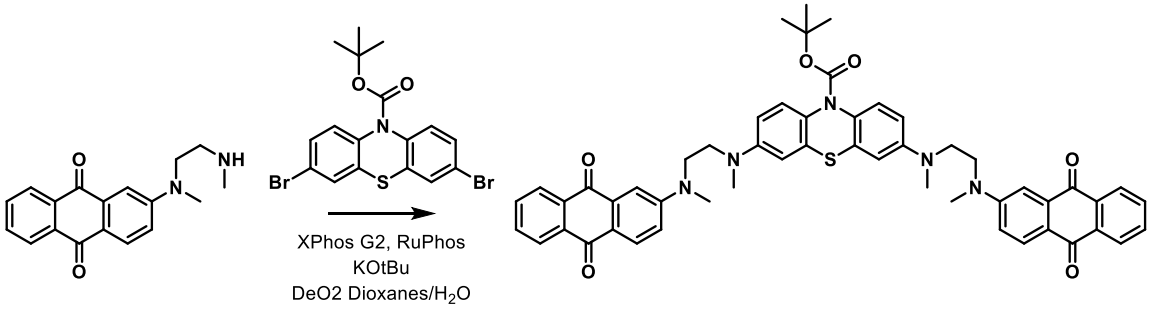

N-Boc-3,7-bis((2-((anthraquinone)(methyl)amino)ethyl)(methyl)amino)phenothiazine

In a 25 ml round bottom flask, 100 mg of N-Boc-3,7-dibromophenothiazine was dissolved in deoxygenated dioxanes and water (5:1 ratio). To this solution was added 500 mg (8 equivalents) of 2-N,N'-dimethylethylenediamineanthraquinone, 250 mg of KOtBu (10 equivalents), 10 mg of RuPhos, and a catalytic amount of XPhos Pd G2. The reaction was set to reflux, and allowed to proceed overnight. The reaction was observed by TLC, and by the removal of aliquots that were subjected to acid for Boc deprotection and subsequent MS analysis. After observing significant product formation, reaction was diluted in DCM and washed three times with water. The organic portion was pumped down, taken up in DCM, and then pumped down with silica to generate a powder for dry loading onto a column. A 0-10% DCM in methanol column was run, and a number of red and orange spots were isolated. Aliquots from these spots were subjected to Boc deprotection by TFA, and subsequent mass spectrometry analysis. Using this method, the doubly modified product was successfully identified as an orange compound, and separated from the singly modified product. Without TFA deprotection, the obtained mass spectrum was

uninterpretable. ^{1}H-NMR (300 MHz, $CDCl_3$) δ: 8.28 (m, 4H), 8.24 (d, 2H), 7.75 (m, 4H), 7.50 (d, 2H), 7.30 (m, 2H), 6.92 (d, 2H), 6.59 (m, 2H), 3.77 (m, 4H), 3.68 (m, 4H), 3.11 (s, 6H), 2.97 (s, 6H), 1.51 (s, 9H). ESI-MS (MH^+) not obtained.

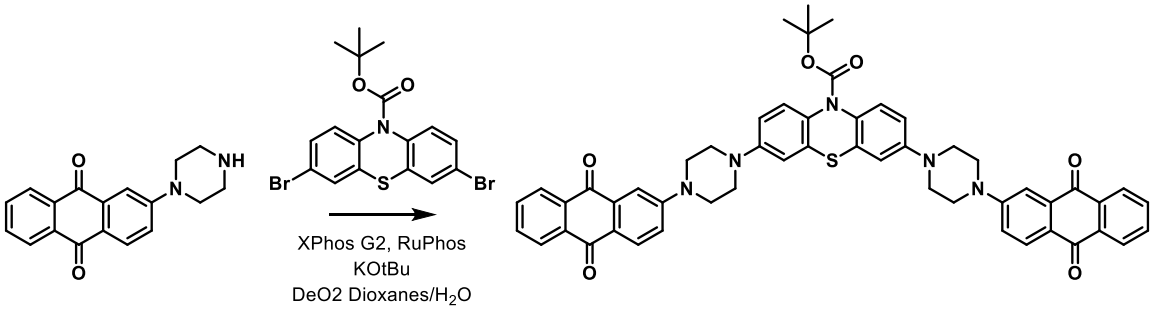

N-Boc-3,7-bis((2-piperazinylanthraquinone)phenothiazine

In a 25 ml round bottom flask, 100 mg of N-Boc-3,7-dibromophenothiazine was dissolved in deoxygenated dioxanes and water (5:1 ratio). To this solution was added 500 mg (8 equivalents) of 2-piperazinylathranquinone, 250 mg of KOtBu (10 equivalents), 10 mg of RuPhos, and a catalytic amount of XPhos Pd G2. The reaction was set to reflux, and allowed to proceed for 48 hours. The reaction was observed by TLC, and by the removal of aliquots that were subjected to acid for Boc deprotection and subsequent MS analysis. After observing significant product formation, reaction was diluted in DCM and washed three times with water. The organic portion was pumped down, taken up in DCM, and then loaded onto a silica gel column. Product was eluted with a 0-10% DCM in methanol gradient, and a number of red and orange spots were isolated. Aliquots from these spots were subjected to Boc deprotection by TFA, and subsequent mass spectrometry analysis. Using this method, the doubly modified product was successfully identified as an orange compound, and separated from the singly modified product. Without TFA deprotection, the obtained mass spectrum was uninterpretable. ^{1}H-NMR (300 MHz, $CDCl_3$) δ: 8.30 (m, 4H), 8.21 (d, 2H), 7.77 (m, 4H), 7.68 (d, 2H), 7.45 (m, 2H), 7.20 (m, 2H) 6.92 (m, 4H), 3.65 (m, 8H), 3.37 (m, 8H), 1.51 (s, 9H). ESI-MS (MH^+) not obtained.

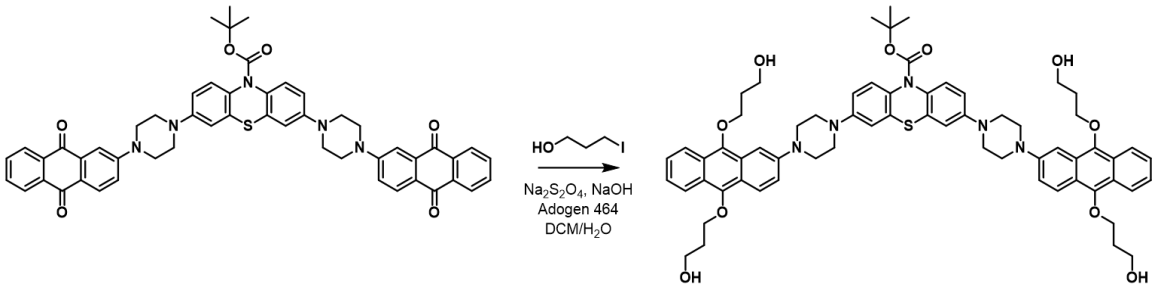

N-Boc-3,7-bis(2-piperazinyl-9,10-dialkoxyanthracenebispropanol)phenothiazine

13 ml of H_2O was added to a 50 mL round bottom flask, then deoxygenated under vacuum and flushed with argon. Subsequently 13 mL of deoxygenated DCM was added. This combination was stirred and deoxygenated together for a second time. Next, 200 mgs of N-Boc-3,7-bis((2-piperazinylanthraquinone)phenothiazine, 80 mg of $Na_2S_2O_4$ (2.1 equivalents), and 4 drops of Adogen 464 were added to the solution. This solution was stirred for 5 minutes, at which point 45 mg (10 equivalents) of NaOH were added. The solution turned red. After another 5 minutes, 100 mg (5 equivalents) of 3-iodopropanol was added. The reaction was followed by TLC and allowed to stir overnight. After complete conversion of the starting material, the reaction was diluted into water and washed three times with DCM. The combined organic portion was pumped down, yielding an oil. Purified the product using a 0-10% methanol in DCM column. ^{1}H-NMR (400 MHz, $CDCl_3$) δ: 8.26 (m, 4H), 7.54 (m, 4H), 7.47 (m, 4H), 7.42 (m, 4H), 6.98 (m, 4H), 4.38 (m, 8H), 4.21 (m, 8H), 3.58 (m, 8H), 3.46 (m, 8H), 2.35 (m, 8H). ESI-MS (MH^+) not obtained.

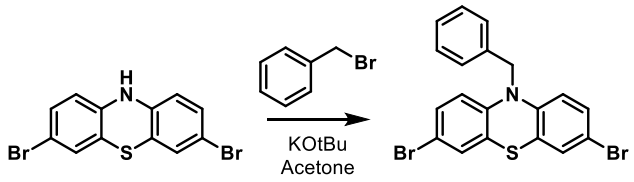

N-benzyl-3,7-dibromophenothiazine

A 100 ml round bottom flask was charged with 500 mg of 3,7-dibromophenothiazine and 200 mg (1.2 equivalents) of KOtBu, which were subsequently dissolved in acetone. A dark red solution was obtained. 350 μl (2 equivalents) of benzyl bromide was then added, and the color rapidly faded. Disappearance of the starting material was followed by TLC. After 1 hour, the product was precipitated

out via water addition and washed with cold water to remove impurities. The product was subsequently taken up in DCM and run through a silica plug to obtain pure product. ^{1}H-NMR (300 MHz, $CDCl_3$) δ: 7.41 (m, 2H), 7.33 (m, 3H), 7.24 (d, 2H), 7.11 (dd, 2H), 6.53 (d, 2H), 5.05 (s, 2H). ESI-MS (MH^+) not obtained.

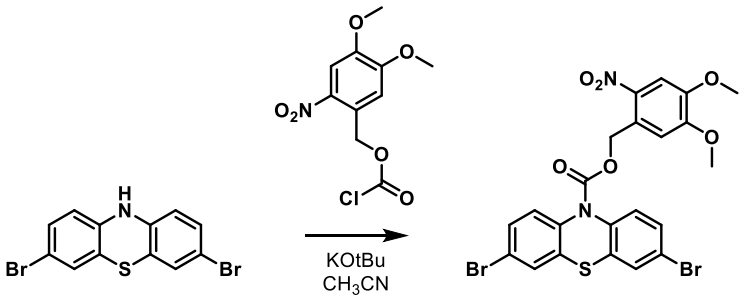

N-NVOC-3,7-dibromophenothiazine

A 25 ml round bottom flask was charged with 200 mg of 3,7-dibromophenothiazine and 60 mg (0.9 equivalents) of KOtBu, which were subsequently dissolved in acetone. A dark red solution was obtained. 150 mg (1 equivalent) of NVOC-chloride was then added, and the color rapidly faded. Disappearance of the starting material was followed by TLC. After 4 hours, the reaction was taken up in DCM and washed with water. The crude was then taken up in DCM and run on a DCM column. ^{1}H-NMR (300 MHz, $CDCl_3$) δ: 7.71 (s, 1H), 7.52 (m, 2H), 7.43 (m, 4H), 6.68 (s, 1H), 5.29 (s, 2H), 3.94 (s, 3H), 3.78 (s, 3H). ESI-MS (MH^+) not obtained.

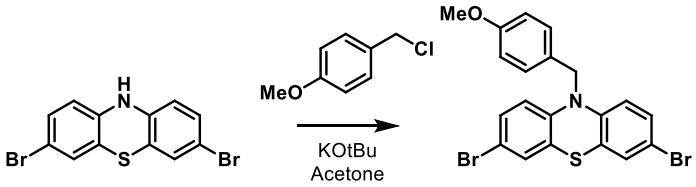

N-*p*-methoxybenzyl-3,7-dibromophenothiazine

A 25 ml round bottom flask was charged with 200 mg of 3,7-dibromophenothiazine and 250 mg (4 equivalents) of KOtBu, which were subsequently dissolved in acetonitrile. A dark red solution was obtained. 100 μl (1.25 equivalents) of *p*-methoxybenzyl chloride was then added, and the color faded. Disappearance of the starting material was followed by TLC. After 2 hours, the reaction was taken up in

DCM and washed with water. The crude was then taken up in DCM and run on a 0-50% DCM in hexanes column. ^{1}H-NMR and ESI-MS (MH^+) could not be obtained.

4.6 References

1 J. H. Kaplan, B. Forbush and J. F. Hoffman, *Biochemistry*, 1978, 17, 1929–1935.
2 J. Engels and E. J. Schlaeger, *J. Med. Chem.*, 1977, 20, 907–911.
3 P. Klán, T. Šolomek, C. G. Bochet, A. Blanc, R. Givens, M. Rubina, V. Popik, A. Kostikov and J. Wirz, *Chem. Rev.*, 2013, 113, 119–191.
4 J. M. Amatrudo, J. P. Olson, G. Lur, C. Q. Chiu, M. J. Higley and G. C. R. Ellis-Davies, *ACS Chem. Neurosci.*, 2014, 5, 64–70.
5 J. A. Peterson, C. Wijesooriya, E. J. Gehrmann, K. M. Mahoney, P. P. Goswami, T. R. Albright, A. Syed, A. S. Dutton, E. A. Smith and A. H. Winter, *J. Am. Chem. Soc.*, 2018, 140, 7343–7346.
6 T. Slanina, P. Shrestha, E. Palao, D. Kand, J. A. Peterson, A. S. Dutton, N. Rubinstein, R. Weinstain, A. H. Winter and P. Klán, *J. Am. Chem. Soc.*, 2017, 139, 15168–15175.
7 D. P. Walton and D. A. Dougherty, *J. Am. Chem. Soc.*, 2017, 139, 4655–4658.
8 M. J. Hansen, W. A. Velema, M. M. Lerch, W. Szymanski and B. L. Feringa, *Chem. Soc. Rev.*, 2015, 44, 3358–3377.
9 A. P. Gorka, R. R. Nani, J. Zhu, S. Mackem and M. J. Schnermann, *J. Am. Chem. Soc.*, 2014, 136, 14153–14159.
10 P. P. Goswami, A. Syed, C. L. Beck, T. R. Albright, K. M. Mahoney, R. Unash, E. A. Smith and A. H. Winter, *J. Am. Chem. Soc.*, 2015, 137, 3783–3786.
11 R. R. Nani, A. P. Gorka, T. Nagaya, T. Yamamoto, J. Ivanic, H. Kobayashi and M. J. Schnermann, *ACS Cent. Sci.*, , DOI:10.1021/acscentsci.7b00026.
12 C. Shirata, J. Kaneko, Y. Inagaki, T. Kokudo, M. Sato, S. Kiritani, N. Akamatsu, J. Arita, Y. Sakamoto, K. Hasegawa and N. Kokudo, *Scientific Reports*, 2017, 7, 13958.
13 A. P. Gorka and M. J. Schnermann, *Current Opinion in Chemical Biology*, 2016, 33, 117–125.
14 T. Yamamoto, D. R. Caldwell, A. Gandioso and M. J. Schnermann, *Photochemistry and Photobiology*, , DOI:10.1111/php.13090.
15 M. Scholz, R. Dědic, T. Breitenbach and J. Hála, *Photochemical & Photobiological Sciences*, 2013, 12, 1873–1884.
16 A. Gollmer, A. Felgenträger, W. Bäumler, T. Maisch and A. Späth, *Photochem. Photobiol. Sci.*, 2015, 14, 335–351.
17 T.-S. Hsieh, J.-Y. Wu and C.-C. Chang, *Dyes and Pigments*, 2015, 112, 34–41.
18 T.-S. Hsieh, J.-Y. Wu and C.-C. Chang, *Chemistry – A European Journal*, 2014, 20, 9709–9715.
19 S. D. P. Baugh, Z. Yang, D. K. Leung, D. M. Wilson and R. Breslow, *J. Am. Chem. Soc.*, 2001, 123, 12488–12494.
20 A. Rotaru and A. Mokhir, *Angewandte Chemie International Edition*, 2007, 46, 6180–6183.
21 S. Kim, M. Fujitsuka and T. Majima, *J. Phys. Chem. B*, 2013, 117, 13985–13992.
22 D. Arian, L. Kovbasyuk and A. Mokhir, *J. Am. Chem. Soc.*, 2011, 133, 3972–3980.
23 S. Sasaki, S. Suzuki, W. M. C. Sameera, K. Igawa, K. Morokuma and G. Konishi, *J. Am. Chem. Soc.*, 2016, 138, 8194–8206.
24 C. Nerungsi, P. Wanitchang, S. Sahasithiwat, K. Sadorn, T. Kerdcharoen and T. Thongpanchang, *Tetrahedron Letters*, 2010, 51, 6392–6395.
25 D. P. Andrews, G. G. McFadyen and G. S. Beddard, *Chemical Physics Letters*, 1998, 293, 343–351.

Chapter 5: Development of Heptamethine-Based Charge-Transfer Dyes for Long-Wavelength (NIR I/II) Photochemistry

5.1 Abstract

The ability to perform photochemistry at longer wavelengths would afford a range of new biological applications, enabled by the better penetration of light into the body. However, the development of long wavelength photochemistry in the near-infrared optical windows remains a significant challenge. Towards this end, the development of a new dye capable of generating singlet oxygen was explored. A heptamethine-based charge-transfer dye was designed based on previous evidence of triplet state formation in orthogonal charge-transfer partners, and the ability of this dye to generate a charge-transfer state was predicted computationally. This dye, IR-1061-pyridinium, was subsequently synthesized and evaluated for its ability to generate singlet oxygen. Although it was unstable to the irradiation conditions – making it difficult to determine the exact effects of irradiation – irradiation of the dye suggested singlet oxygen formation, prompting the development of a more stable derivative, IR-1061-acridinium. This dye was shown to be stable under irradiation conditions, and generated singlet oxygen upon irradiation at 1064 nm. Despite some limitations on these dyes, the observed reactivity marks a significant step in the development of long wavelength photochemistry, as no single photon photochemistry has previously been described above 900 nm.

5.2 Introduction

5.2.1 Near-Infrared Photochemistry

The rational design of new photochemical reactivity is challenging, but extremely important given the burgeoning number of photochemical applications. To complement a host of impressive work being done in the visible spectrum[1–6], novel photochemical reactivity based on near-infrared (NIR) light is required. Although the development of NIR-absorbing photoremovable protecting groups remains the primary goal in the Dougherty lab, an interim step – one that could potentially guide the development of future photoremovable protecting groups – would be the development of NIR singlet oxygen generators.

Singlet oxygen – the first excited state of O_2 – has significant therapeutic potential. It is already used in a variety of clinical applications, from photodynamic therapy[7] to corneal crosslinking[8], and new

applications continue to emerge. For most therapeutic applications, singlet oxygen is generated *in situ* via excitation of a photosensitizer. Although this affords unmatched spatiotemporal control over the reactive singlet oxygen molecules[9], it constrains applications to areas that can be accessed by light. Compared to visible light, NIR light offers several advantages, most notably significantly greater light penetration in the body.[10,11] Although a number of fluorophores are now being designed with this in mind[12,13], there are few small molecule NIR chromophores capable of generating singlet oxygen past 800 nm, and those that can do not absorb significantly above 800 nm.[11,14,15] In fact, no single photon chemistry has previously been observed above 900 nm. Different methods – such as two-photon excitation[16] and upconverting nanoparticles[17] – have been proposed to circumvent this issue, but a need remains for small molecules capable of directly generating singlet oxygen using NIR light.

5.2.2 Photochemistry of Charge-Transfer States

Inspiration for a class of chromophores with reactivity beyond 900 nm came from previous reports that demonstrated the ability of dyes containing an orthogonal charge-transfer partner to generate a triplet state.[18–20] Although charge-transfer dyes that mediate ISC are actively being explored, there is a lack of consensus on the required characteristics.[21] Interestingly, to this point few attempts have focused on the characteristic that made earlier systems unique: sterically confined charge transfer partners. A clear example of this phenomenon was demonstrated in a series of BODIPY derivatives synthesized and characterized by the Ziessel group. By comparing a standard BODIPY dye to one functionalized at the para position with an N-methylpyridinium cation (Figure 1A), the authors were able to realize a substantial increase in the triplet state quantum yield, from nearly zero in the former to approximately 0.75 in the latter.[19] The authors propose a mechanism by which the BODIPY dye is excited into a traditional singlet state (S_1), but rapidly relaxes to a charge-transfer state (CTS) involving the orthogonal N-methylpyridinium.[19] This charge-transfer state is long lived and preferentially relaxes into an excited

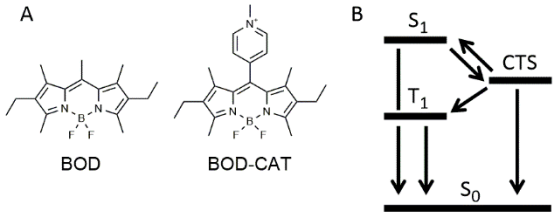

Figure 1: Charge-transfer state formation. A.) BODIPY derivatives used to elucidate intramolecular charge-transfer mechanism responsible for enhanced triplet state formation.[15] B.) Jablonski diagram proposed for orthogonal charge-transfer dyads.[16]

triplet state (T_1) (Figure 1B).[19] Although the authors' goal was to explore the mechanism of triplet formation, their results suggested that singlet oxygen sensitization was occurring under atmospheric conditions. This phenomenon has been reported using dyes that absorb ultraviolet and visible light, but it has never been expanded to near-infrared absorbing substrates.[18–20]

5.3 Results and Discussion

5.3.1 Computational Evaluation of Heptamethine Charge-Transfer Dyes

Heptamethine dyes present an opportune starting point for charge-transfer capable NIR dyes. A diverse class of chromophores, their solubility and absorption spectra can be significantly modified by altering the backbone termini. Furthermore, many contain an accessible backbone chlorine that can be used for introduction of a charge-transfer partner. Of the heptamethine dyes, the thiopyrilium dye IR-1061 was chosen for initial experiments due to its NIR absorption spectrum and precedence of modification at its backbone chlorine.[22] To rationally select an appropriate charge-transfer partner for IR-1061, we turned to computation.

In a previous report, the 9-mesityl-10-methylacridinium charge-transfer dyad was evaluated using density functional theory (DFT), and the ground state frontier orbitals were shown to be disjoint – with one localized to the acridinium and the other to the orthogonal mesityl.[20] To determine if this ground state calculation could have predictive power, we ran an analogous set of calculations on the previously mentioned BOD-CAT and its non-methylated derivative BOD-PY (Figure 2A) using the B3LYP functional and 6-31G** basis set. In BOD-PY, which does not exhibit a charge-transfer state, both the HOMO and the LUMO resided on the BODIPY core. However, in BOD-CAT, which does exhibit a charge-transfer state, the LUMO had shifted to the orthogonal N-methylpyridinium charge-transfer partner. This result, along with the 9-mesityl-10-methylacridinium calculations, suggested that disjoint

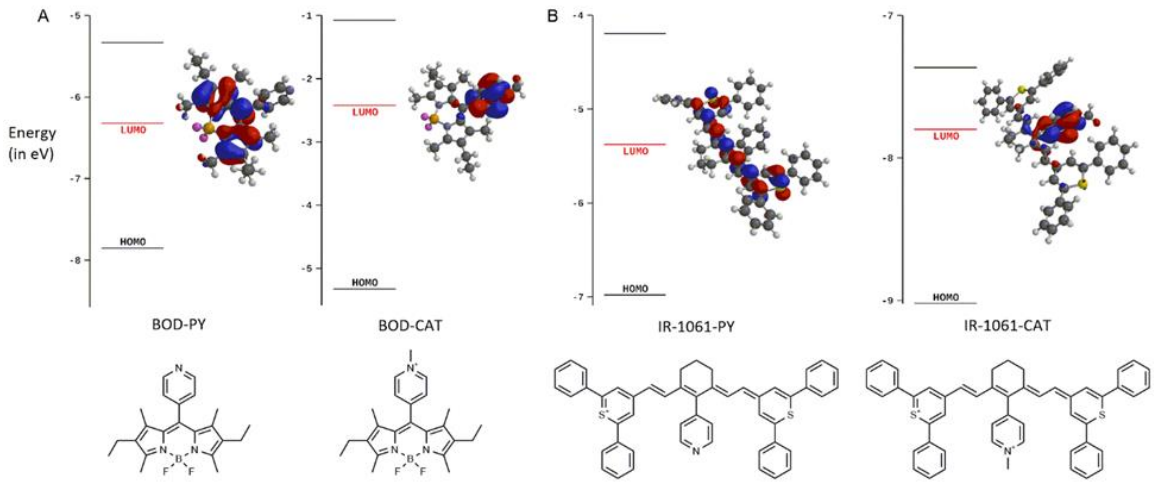

Figure 2: Charge-transfer state computational predictions. For all molecules the HOMO resides on the primary chromophore and the LUMO is shown. A.) Comparison of BOD-PY and BOD-CAT demonstrating a LUMO shift upon methylation. B.) A comparison of IR-1061-PY and IR-1061-CAT showing a similar orbital shift.

ground state frontier molecular orbitals were a characteristic of long-lived charge-transfer dyads, and thus the nature of frontier molecular orbitals could be used to quickly screen potential charge-transfer partners. We recognize that more sophisticated calculations would be required to develop a truly predictive screen, but we felt that this simpler set of calculations would be able to guide our experimental efforts.

We began by evaluating a set of IR-1061 derivatives analogous to the BODIPY derivatives: IR-1061-PY and IR-10161-CAT (Figure 2B). In IR-1061-PY, both the HOMO and the LUMO remained on the heptamethine backbone, suggesting that no charge-transfer would occur. In IR-1061-CAT, the LUMO shifted to the N-methylpyridinium, generating a disjoint set of frontier molecular orbitals and suggesting that charge-transfer was possible. These results mirrored those for the BODIPY system and suggested that pyridinium might be a good starting point for an IR-1061 charge-transfer dye. To complement these results, an N-C linked dyad, which we will refer to as IR-1061-pyridinium, was also evaluated. The frontier orbitals remained disjoint, however, the LUMO and the LUMO+1 were significantly closer in energy (Figure 3).

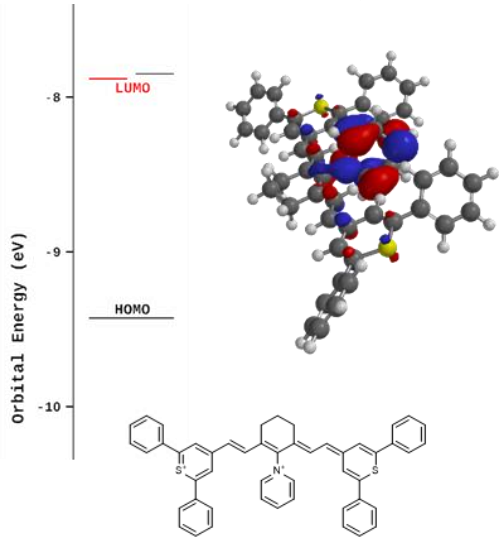

Figure 3: IR-1061-pyridinium orbital energies. Upon inverting the pyridine charge-transfer partner so that it is linked via an N-C bond instead of a C-C bond, similar orbitals are observed.

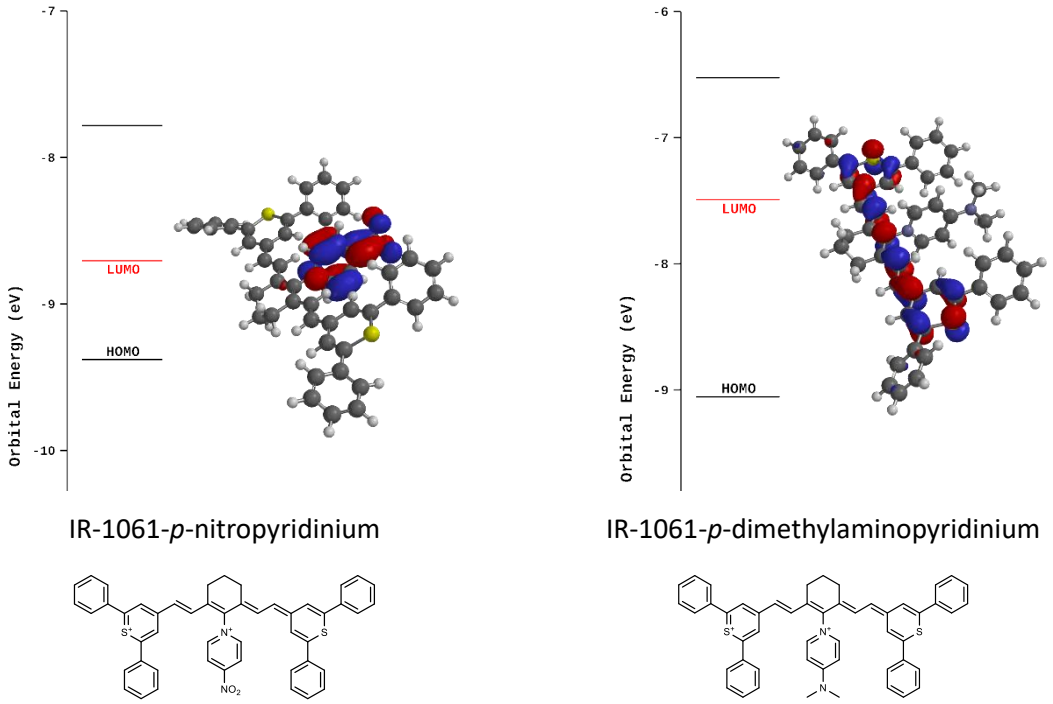

Figure 4: Representative IR-1061-pyridinium derivatives. Electron withdrawing groups (*p*-nitropyridinium) reinforce frontier orbital orthogonality while electron donating groups (*p*-dimethylaminopyridinium) do the opposite.

Since the N-C linkage in IR-1061-pyridinium provided an opportunity for functionalization at the pyridine 4-position, a number of derivatives were explored. Electron withdrawing groups tended to reinforce the observed disjoint character, whereas electron donating groups did the opposite, at times undoing the effect all together (Figure 4). Beyond pyridine derivatives, a range of results were observed with different charge-transfer partners, with acridinium standing out as a potential alternative to pyridinium (Figure 5).

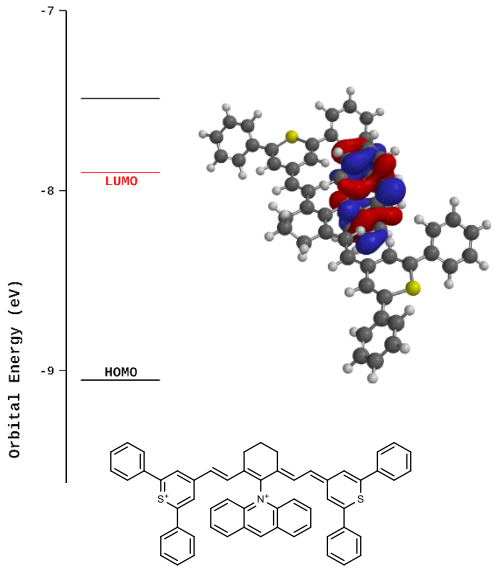

Figure 5: IR-1061-acridinium orbital energies. In IR-1061-acridinium the orthogonal orbital is heavily favored as the LUMO, suggesting the possibility of charge-transfer.

5.3.2 Synthesis and Characterization of IR-1061-pyridinium

From the range of charge-transfer partners computationally vetted, IR-1061-pyridnium was selected for initial photochemical studies due to its synthetic

accessibility (Figure 6). IR-1061-CAT was also considered, but its synthesis proved to be more challenging. The pyridine addition reaction was extremely sensitive to water, but gave good conversion using dry pyridine. Unfortunately, the product was too sensitive to isolate in pure form due to hydration that occurred under all evaluated purification conditions (Figure 7). Despite this inconvenience, the slightly impure dye was used as a proof of principle. For initial singlet oxygen generation experiments, the dye was dissolved in $CDCl_3$ – the solvent in which it had the highest solubility – and irradiated using a 1 watt/cm^2 980 nm laser in the presence of a singlet oxygen trap, diphenylisobenzofuran (DPBF). DPBF was selected as a trap because it is a standard in the field and because other popular detectors (such as singlet oxygen sensor green, SOSG) led to precipitation of IR-1061-pyridinium over time. After 30 minutes of irradiation, a significant decrease in the DPBF signal was observed relative to a dark control, suggesting that singlet oxygen sensitization was occurring (Figure 8A).

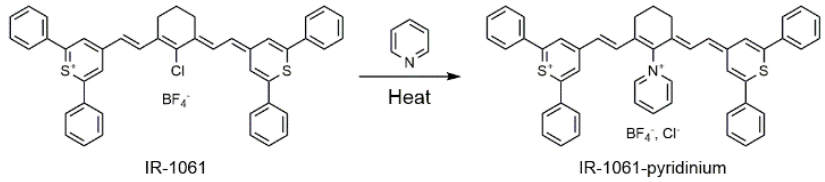

Figure 6: IR-1061-pyridinium synthesis.

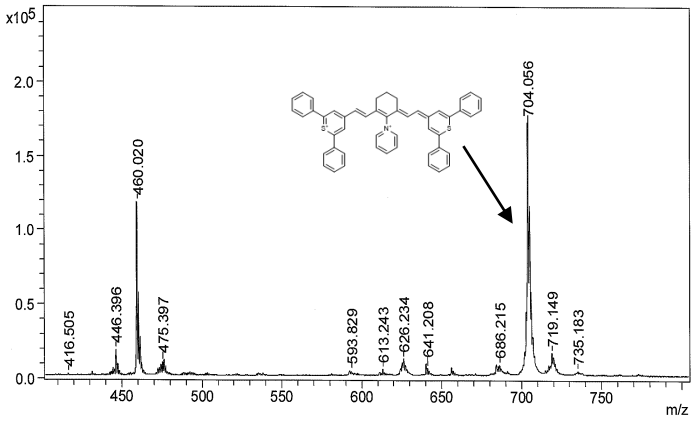

Figure 7: MALDI of slightly impure IR-1061-pyridinium. When isolated, the major impurity at 460 amu has no absorbance in the NIR.

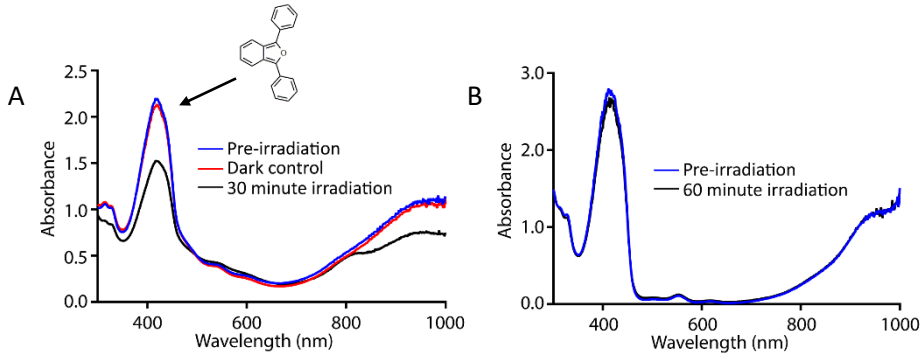

Figure 8: IR-1061-pyridinium singlet oxygen generation. A.) Irradiation of IR-1061-pyridinium with DPBF. The structure of DPBF is shown next to its absorbance peak. B.) Irradiation of IR-1061 with DPBF.

In comparison, the parent dye, IR-1061, was irradiated under the same conditions and no significant changes in DPBF signal were observed (Figure 8B). This suggested that the designed dye had novel reactivity at previously inaccessible wavelengths, but a more stable derivative was required to better characterize the reaction.

5.3.3 Synthesis and Characterization of IR-1061-acridinium

In an attempt to overcome the susceptibility of IR-1061-pyridinium to hydration, the pyridine charge-transfer partner was exchanged for acridine, which we suspected would shield the dye from water addition due to its additional bulk. Although high temperatures – and thus a solvent with a high boiling point – were required to synthesize the derivative (Figure 9), the product was more amenable to purification, ultimately yielding pure dye. The absorption spectra of IR-1061-acridinium in chloroform was taken, and notably had significant tailing in the NIR. This is reminiscent of spectra observed for other heptamethine dyes such as ICG, which demonstrate spectral shifting due to aggregation.[23] To determine whether or not this phenomenon was specific to chloroform, the absorption spectrum was taken in a range of solvents, (Figure 10). In most, the dye had a similar spectrum, however, significant peak broadening was observed in water.

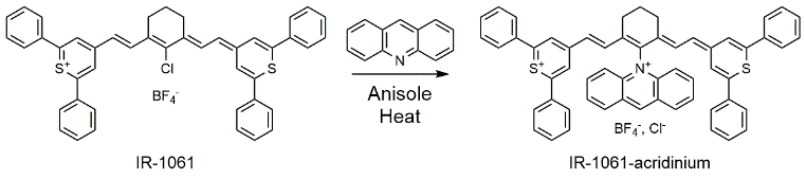

Figure 9: IR-1061-acridinium synthesis.

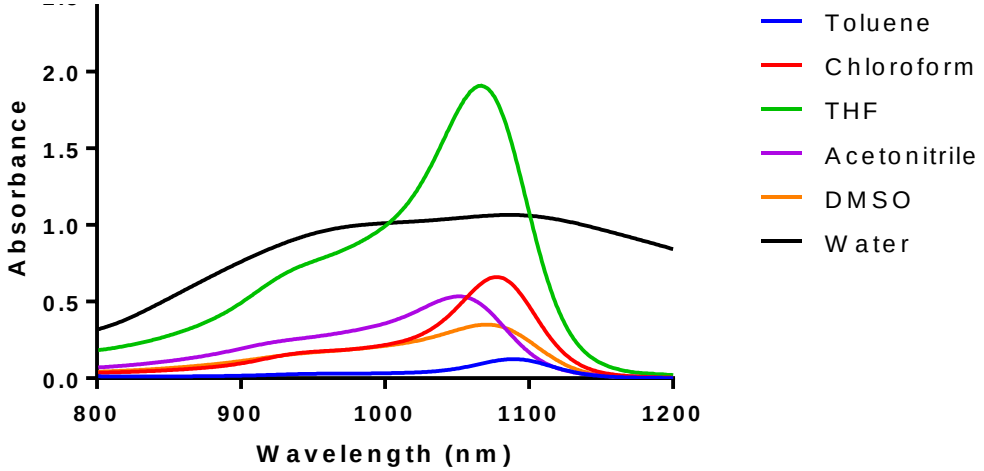

Figure 10: NIR absorbance of IR-1061-acridinium in multiple solvents. Spectra shown at a concentration of .025 mg/ml (27 μM). λ_{max} occurs at 1078 for chloroform, with a significant tail suggesting possible aggregation.[23]

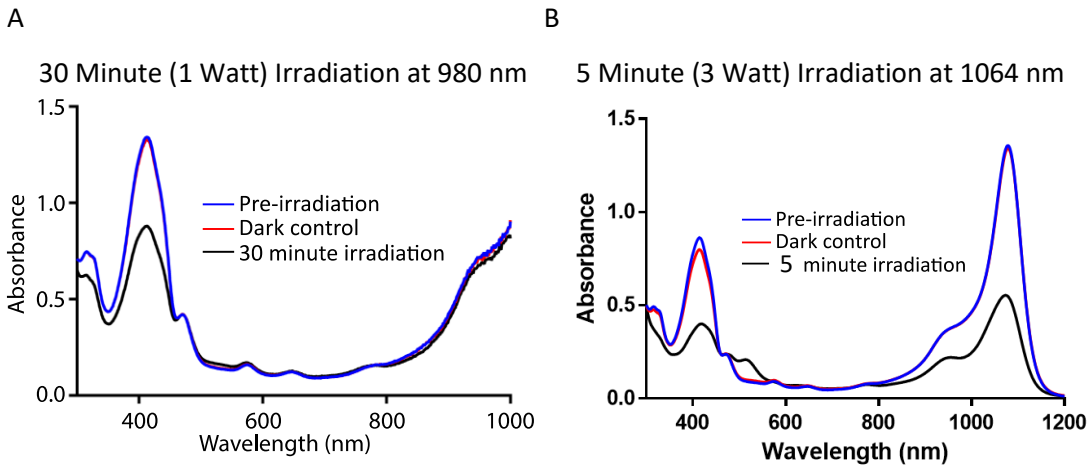

Figure 11: Irradiation of IR-1061-acridinium in $CDCl_3$. A.) Irradiation of IR-1061-acridinium with a 1 watt, 980 nm laser. B.) Irradiation of IR-1061-acridinium with a 3 watt, 1064 nm laser.

Like IR-1061-pyridinium, IR-1061-acridinium was irradiated in $CDCl_3$ in the presence of DPBF using a 1 watt/cm^2 980 nm laser (Figure 11A). As a comparison, a similar irradiation was carried out using a 1.8 watt/cm^2 1064 nm laser (Figure 11B). Under both irradiation conditions, a decrease in DPBF signal was observed, however, the time scales varied drastically. At 980 nm significant DPBF photobleaching was observed only after 30 minutes, but in just 5 minutes of irradiation at 1064 nm, near complete photobleaching of DPBF was observed, as well as significant bleaching of the dye. This destruction of the dye is to be expected in the presence of high concentrations of singlet oxygen, as heptamethine dyes have been used as photoremovable protecting groups on the basis of this phenomenon.[6] In an attempt to better define the efficiency of singlet oxygen generation, we obtained a relative quantum yield by comparing DPBF bleaching in the presence of IR-1061-acridinium and in the presence of phenalenone, a compound with a high quantum yield for singlet oxygen generation on irradiation at 365 nm in chloroform[24] (Figure 12). The results gave a relative quantum yield of 0.3%, which must be considered approximate given the substantially different wavelengths involved. Although this value is low, it provides a starting point for 1064 nm photochemistry and a benchmark for future generations of dyes.

Further characterization of the dye was pursued at 980 nm, where irradiation resulted in a more controlled reaction. To confirm that the process was singlet oxygen-mediated, irradiation of a freeze-

pump-thawed sample – devoid of oxygen – was carried out. This irradiation produced no change in DPBF signal (Figure 13), suggesting that the process is indeed singlet oxygen mediated.

To evaluate the scope of the reaction, the dye was irradiated in an array of (deuterated) solvents. In nonpolar solvents, such as toluene, no singlet oxygen generation was observed. In polar aprotic solvents, such as DMSO, irradiation of the dye led to decreased DPBF degradation as well as photobleaching. In water, DPBF degradation rates comparable to those seen in chloroform were accompanied by high levels of photobleaching (Figure 14). Strong acids and bases both led to dye instability and bleaching prior to irradiation, and introduction of protein (in the form of BSA) led to precipitation of the dye. Exchanging the counterion from BF_4^- to $BArF^-$ resulted in an increase in solubility, but also a marked decrease in photosensitization capability. These results suggest that both the dye and the photosensitization process are sensitive, requiring further optimization to produce a practical photosensitizer.

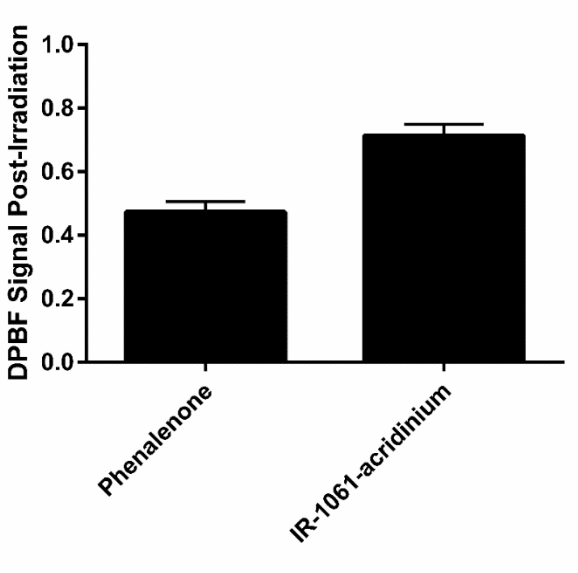

Figure 12: Quantum yield determination. Normalized decrease in DPBF signal following irradiation in the presence of phenalenone or IR-1061-acridinium. An approximately 200-fold greater photon flux was used to irradiate IR-1061-acridinium.

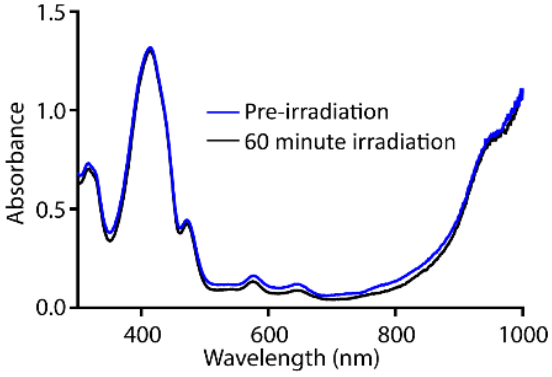

Figure 13: Irradiation of IR-1061-acridinium and DPBF in freeze-pump-thawed $CDCl_3$.

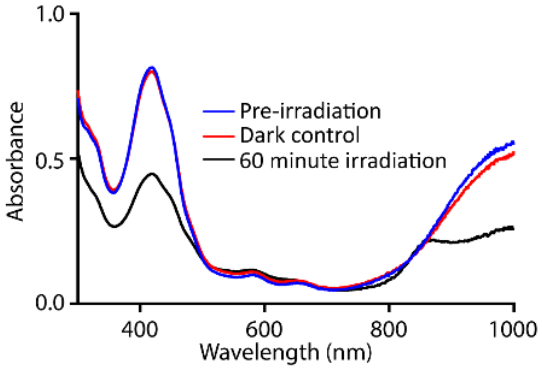

Figure 14: Irradiation of IR-1061-acridinium in D_2O. 7.5% DMSO-D_6 used for solubilization.

5.4 Conclusion

Generation of a dye capable of any photochemistry past 900nm is a significant achievement and marks a first in the field. These early studies provide a proof of concept for a new class of photoreactive compounds. Clearly, more optimization will be required to create a practically useful material. In addition, detailed mechanistic studies will be needed to confirm the proposed charge-transfer mechanism. The reactivity of both IR-1061-pyridinium and IR-1061-acridinium support the design principles used to conceptualize the dyes as well as the predictive value of the performed calculations. These dyes provide insight into a challenging problem and serve as an important step as the field works towards novel NIR photochemical reactivity.

5.5 Materials and Methods

5.5.1 Materials

IR-1061 tetrafluoroborate and dry pyridine were purchased from Sigma Aldrich. Acridine was purchased from Alfa Aesar. Sodium BArF was purchased from AK Scientific. Deuterated solvents were purchased from Cambridge Isotopes and used as received, with the exception of deuterated chloroform, which was filtered through a neutral alumina plug prior to use to neutralize and dry the solvent. Commercial reagents and solvents were purchased from Sigma-Aldrich, VWR, and Thermo-Fisher Scientific and used as received. Reactions involving air or moisture sensitive reagents were run under argon, with samples purged of air prior to use. Flash chromatography was performed using neutral silica gel from Merck (230-400 mesh). TLC analysis was performed with plates from Merck (60 A pore size, F_{254}, 0.25 mm).

5.5.2 Instrumentation

Irradiations at 980 nm were performed using a 1 watt/cm^2 infrared diode laser at 980 nm coupled to a PSU-III-FDA power supply. Both the laser and the power supply were purchased from CNI lasers. Irradiations at 1064 nm were performed using an Nd:YAG laser at 1.8 W/cm^2. Absorbance spectra were obtained using an Agilent CARY 60 UV-Vis for spectra below 1000nm, and a Cary 5000 UV-VIS-NIR for spectra above 1000 nm. Mass spectrometry characterization was performed via MALDI using a

BRUKER MALDI/TOF Autoflex Speed and a Waters LCT Premier XE Electrospray TOF. ^{1}H NMR spectra were obtained using a Varian 600 MHz Spectrometer. Chemical shifts are reported in parts per million (ppm, δ) referenced to the residual ^{1}H resonance of the solvent. Splitting patterns are designated as follows: s, singlet; br, boad; d, doublet; dd, doublet of doublets; t, triplet; q, quarted; m, multiplet.

5.5.3 Calculations

Computation was performed using the SPARTAN interface with calculations performed using the B3LYP functional and the 6-31G** basis set. These calculations were performed in accordance with previous calculations performed on the 9-mesityl-10-methylacrindium dyad.[20] Higher levels of computation (using the MO6 functional and larger basis sets) were performed on the BODIPY dyads to check for differences, and none were observed. Given the large size of the IR-1061 dye and the lack of significant differences in higher level calculations, we felt that B3LYP and 6-31G** were the most appropriate selection.

5.5.4 Irradiation Experiments

Dye was dissolved in deuterated solvent at a concentration that would produce an absorbance near 1 at 980 nm. This was calculated using extinction coefficients determined by absorbance measurements of the dye alone. The IR-1061-acridinium irradiation in water was an exception, as the concentration was kept lower to ensure solubility. Dye solution was split into two aliquots and added to two 1 cm by 1 cm quartz cuvettes purchased from Starna. The absorption spectra were taken for both cuvettes (to ensure the pre-irradiation sample looked the same in both cases), and subsequently one cuvette was irradiated while the other was kept in the dark. A stir bar was used to ensure proper mixing during irradiation. After irradiation, the absorbance of both solutions was again evaluated. Figures shown without a dark control still had one, however, no significant change was observed in the irradiated sample so the dark control trace was unnecessary and therefore not included. For the 1064 nm irradiation, the dye was dissolved at a slightly higher concentration to an absorbance of approximately 1.5 at 1064 nm and irradiated for 5 minutes. At this point significant photobleaching of the dye was observed, so additional irradiation was not performed.

The freeze-pump-thaw (FPT) experiment was carried out as follows. Dye was dissolved in deuterated chloroform and added to a FPT apparatus. Three consecutive freeze-pump-thaw cycles were carried out to a pressure of less than 200 mm Hg, at which point the solution was transferred under vacuum to the arm of the apparatus containing a fused 1 cm by 1 cm quartz cuvette (Starna). Irradiation and subsequent absorption measurements were carried out in the sealed cuvette.

5.5.5 Relative Quantum Yield Calculation

Phenalenone (Sigma-Aldrich), a highly efficient singlet oxygen generator with a known singlet oxygen quantum yield of 0.97 in chloroform[24] was used to benchmark the efficiency of IR-1061-acridinium singlet oxygen generation in chloroform. A solution of phenalenone at an absorbance of 0.30 at 365 nm was generated that also contained DPBF at an absorbance of approximately 1.0. This solution was irradiated for 30 seconds using a 365 nm variable power LED (3-300 mW, Thor labs) at 30 mW/cm^2. The percent decrease in DPBF signal at 415 nm was calculated, taking into account any background from phenalenone. This was done in triplicate. A similar experiment was then run using IR-1061-acridinium. A solution containing the dye at an absorbance of 0.30 at 1064 and DPBF at an absorbance of approximately 1.0 was irradiated for 30 seconds using a 1064 nm Nd:YAG laser with a power output of 1.8 W/cm^2. The percent decrease in DPBF signal at 415 nm was then calculated, taking into account any background from IR-1061-acridinium. This was also done in triplicate.

The percent decrease attributed to phenalenone was calculated to be 53% and the percent decrease attributed to IR-1061-acridinium was calculated to be 29% (Figure S8). To take into account the difference in photon flux at these two wavelengths, the ratio of the photon flux was calculated, where the photon flux was described by the following equation: $PF = I*\lambda/(h*c*N_a)$. PF stands for photon flux, I is the irradiation intensity, λ is the irradiation wavelength, h is Planck's constant, c is the speed of light and N_a is Avogadro's number. The ratio of the photon flux was simplified to $PF_R = (I_{Phe}*\lambda_{Phe})/(I_{IR}*\lambda_{Ir}) = (0.03\ W/cm^2*365\ nm)/(1.8\ W/cm^2*1064\ nm) = 0.006$. Taking into account this difference in photon flux and phenalenone's known quantum yield of singlet oxygen generation of 0.97, this yields a relative quantum yield of about 0.003, or 0.3%.

5.5.6 Syntheses

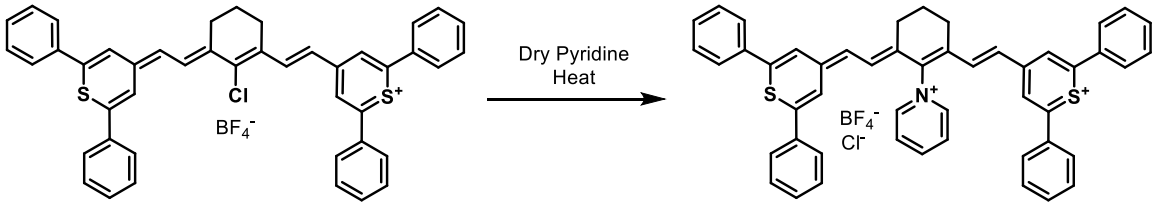

IR-1061-pyridinium

A 10 mL flame-dried round-bottom flask was charged with a stir bar and 25 mgs of IR-1061, to which 1 milliliter of dry pyridine was added. The reaction was heated to boiling under argon, and removed from heat once the solution transitioned from dark red to greenish-brown. At this point the compound was purified by silica gel chromatography using a 0-5% MeOH in DCM gradient. The product could not be cleanly purified due to decomposition during purification. All other attempted purification conditions gave the same result. Due to low solubility and contaminating species, an interpretable NMR was never obtained. However, a reasonably clean mass spectrometry trace was. Interestingly, the M-1 mass was observed, presumably due to loss of a proton to alleviate the dual positive charge. MALDI-MS (m-1) calculated: 704.24, found 704.06.

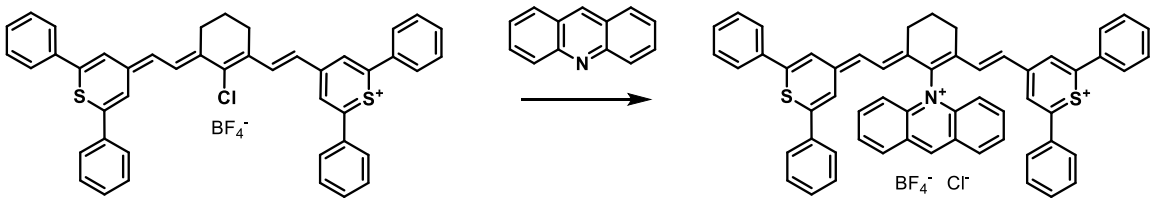

IR-1061-acridinium

A 10 ml round-bottom flask was charged with a stir bar, 25 mgs of IR-1061 (1 equivalent), and 60 mgs of acridine (10 equivalents). Two milliliters of anisole were added, and the reaction was heated to boiling under argon. It was removed from heat once the color changed from red to a yellow hued brown. Further heating led to formation of a green decomposition product. The reaction mixture was loaded onto a silica plug, and after eluting the anisole and any nonpolar compounds with DCM, a polar fraction containing the dye of interest was eluted with 5% MeOH in DCM. After pumping down, this polar fraction was resuspended in DCM and loaded onto a silica gel column, which was eluted with a 0-2%

MeOH in DCM gradient. 20 mgs of pure product were collected as a brown-yellow compound, giving a percent yield of 64%. ^{1}H-NMR (600 MHz, $CDCl_3$): 7.75 (m, 2H), 7.68-7.60 (m, 12H), 7.52-7.42 (m, 14 H), 6.99 (t, 2H) 6.91 (d, 2H), 6.65 (t, 2H), 6.59 (d, 2H), 6.28 (m, 1H), 2.84 (t, 2H), 2.56 (t, 2H), 1.95 (m, 2H). ESI-TOF-MS (m-1) calculated: 804.275, found 804.277.

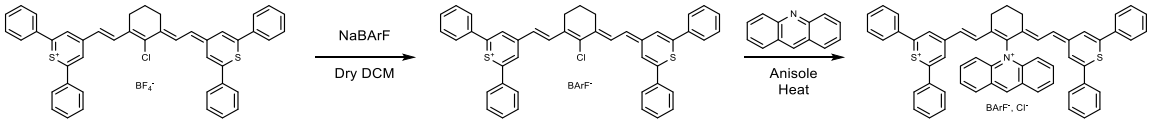

IR-1061-acridinium BArF

IR-1061 BArF was synthesized and purified in the manner described by Shi et al.[22] Following isolation, 25 mgs of IR-1061 BArF (1 equivalent) was added to a 10 ml round-bottom flask along with a stir bar and 29.3 mgs of acridine (10 equivalents). Two milliliters of anisole were added, and the reaction was heated under argon. It was removed from heat once the color changed from red to a yellow hued brown. Further heating led to formation of a green decomposition product. The reaction mixture was taken up in DCM and extracted three times with water and once with brine. The DCM fraction was pumped to near dryness, then resuspended in DCM and loaded onto a silica gel column. The product was eluted with a 0-1% MeOH in DCM gradient. 12 mgs of pure product were collected as a brown-yellow compound, giving a percent yield of 43%. NMR and mass spec data matched that of IR-1061-acridinium tetrafluoroborate, although significant peak broadening was observed on the MALDI with the BArF counterion. ^{1}H-NMR (600 MHz, $CDCl_3$): 7.75 (m, 2H), 7.68-7.60 (m, 12H), 7.52-7.42 (m, 14 H), 6.99 (t, 2H) 6.91 (d, 2H), 6.65 (t, 2H), 6.59 (d, 2H), 6.28 (m, 1H), 2.84 (t, 2H), 2.56 (t, 2H), 1.95 (m, 2H). MALDI-MS (m-1) calculated: 804.3, found 804.5.

5.6 References

1 J. M. Amatrudo, J. P. Olson, G. Lur, C. Q. Chiu, M. J. Higley and G. C. R. Ellis-Davies, *ACS Chem. Neurosci.*, 2014, **5**, 64–70.
2 J. A. Peterson, C. Wijesooriya, E. J. Gehrmann, K. M. Mahoney, P. P. Goswami, T. R. Albright, A. Syed, A. S. Dutton, E. A. Smith and A. H. Winter, *J. Am. Chem. Soc.*, 2018, **140**, 7343–7346.
3 T. Slanina, P. Shrestha, E. Palao, D. Kand, J. A. Peterson, A. S. Dutton, N. Rubinstein, R. Weinstain, A. H. Winter and P. Klán, *J. Am. Chem. Soc.*, 2017, **139**, 15168–15175.
4 D. P. Walton and D. A. Dougherty, *J. Am. Chem. Soc.*, 2017, **139**, 4655–4658.
5 M. J. Hansen, W. A. Velema, M. M. Lerch, W. Szymanski and B. L. Feringa, *Chem. Soc. Rev.*, 2015, **44**, 3358–3377.

6 A. P. Gorka, R. R. Nani, J. Zhu, S. Mackem and M. J. Schnermann, *J. Am. Chem. Soc.*, 2014, **136**, 14153–14159.
7 P. Agostinis, K. Berg, K. A. Cengel, T. H. Foster, A. W. Girotti, S. O. Gollnick, S. M. Hahn, M. R. Hamblin, A. Juzeniene, D. Kessel, M. Korbelik, J. Moan, P. Mroz, D. Nowis, J. Piette, B. C. Wilson and J. Golab, *CA Cancer J Clin*, 2011, **61**, 250–281.
8 F. Raiskup-Wolf, A. Hoyer, E. Spoerl and L. E. Pillunat, *Journal of Cataract & Refractive Surgery*, 2008, **34**, 796–801.
9 Y. Luo and D. Kessel, *Photochemistry and Photobiology*, 1997, **66**, 479–483.
10 A. S. Chuong, M. L. Miri, V. Busskamp, G. A. C. Matthews, L. C. Acker, A. T. Sørensen, A. Young, N. C. Klapoetke, M. A. Henninger, S. B. Kodandaramaiah, M. Ogawa, S. B. Ramanlal, R. C. Bandler, B. D. Allen, C. R. Forest, B. Y. Chow, X. Han, Y. Lin, K. M. Tye, B. Roska, J. A. Cardin and E. S. Boyden, *Nat. Neurosci.*, 2014, **17**, 1123–1129.
11 J. Atchison, S. Kamila, H. Nesbitt, K. A. Logan, D. M. Nicholas, C. Fowley, J. Davis, B. Callan, A. P. McHale and J. F. Callan, *Chem. Commun.*, 2017, **53**, 2009–2012.
12 J. Li and K. Pu, *Chem. Soc. Rev.*, 2019, **48**, 38–71.
13 Q. Miao and K. Pu, *Advanced Materials*, 2018, **30**, 1801778.
14 L. Luan, L. Ding, W. Zhang, J. Shi, X. Yu and W. Liu, *Bioorganic & Medicinal Chemistry Letters*, 2013, **23**, 3775–3779.
15 X. Miao, W. Hu, T. He, H. Tao, Q. Wang, R.-F. Chen, L. Jin, H. Zhao, X. Lu, Q. Fan and W. Huang, *Chem. Sci.*, 2019, **10**, 3096-3102.
16 P. K. Frederiksen, S. P. McIlroy, C. B. Nielsen, L. Nikolajsen, E. Skovsen, M. Jørgensen, K. V. Mikkelsen and P. R. Ogilby, *J. Am. Chem. Soc.*, 2005, **127**, 255–269.
17 S. Han, B. W. Hwang, E. Y. Jeon, D. Jung, G. H. Lee, D. H. Keum, K. S. Kim, S. H. Yun, H. J. Cha and S. K. Hahn, *ACS Nano*, 2017, **11**, 9979–9988.
18 A. C. Benniston, A. Harriman, P. Li, J. P. Rostron, H. J. van Ramesdonk, M. M. Groeneveld, H. Zhang and J. W. Verhoeven, *J. Am. Chem. Soc.*, 2005, **127**, 16054–16064.
19 A. Harriman, L. J. Mallon, G. Ulrich and R. Ziessel, *Chemphyschem*, 2007, **8**, 1207–1214.
20 S. Fukuzumi, H. Kotani, K. Ohkubo, S. Ogo, N. V. Tkachenko and H. Lemmetyinen, *J. Am. Chem. Soc.*, 2004, **126**, 1600–1601.
21 J. Zhao, K. Chen, Y. Hou, Y. Che, L. Liu and D. Jia, *Org. Biomol. Chem.*, 2018, **16**, 3692–3701.
22 Y. Shi, A. J.-T. Lou, G. S. He, A. Baev, M. T. Swihart, P. N. Prasad and T. J. Marks, *J. Am. Chem. Soc.*, 2015, **137**, 4622–4625.
23 M. L. Landsman, G. Kwant, G. A. Mook and W. G. Zijlstra, *J Appl Physiol*, 1976, **40**, 575–583.
24 R. Schmidt, C. Tanielian, R. Dunsbach and C. Wolff, *Journal of Photochemistry and Photobiology A: Chemistry*, 1994, **79**, 11–17.